# Geology and Geochemistry of Waste Rock Piles in the Hillsboro Mining District, Sierra County, New Mexico

by

Erik A. Munroe

A thesis submitted in partial fulfillment
of the requirements for the degree of

Master of Science
In
Geology

Department of Earth and Environmental Sciences
New Mexico Institute of Mining and Technology, Socorro, NM
August, 1999

## ACKNOWLEDGEMENTS

I would like to acknowledge Dr. Virginia McLemore, Dr. Andrew Campbell, and Dr. Peter Mozley for their help, suggestions, and insight into the intricacies of this project. I especially thank Dr. McLemore for her continued effort and constructive criticism given to increase the caliber of this master's thesis. Special thanks to Dr. William X. Chavez for his guidance, support, and knowledge of reflected light microscopy.

I thank Lynn Branvold, Barbara Popp, and Tianguang Fan for assistance with sample analysis using the FAAS instrument. XRF data was obtained by Dr. Philip Kyle and Chris McKee using the Phillips PW 2400 instrument which was purchased with funds from NSF grant EAR-9316467. I thank Dr. Nelia Dunbar for technical help as well as insight into analytical approaches using the electron microprobe SX-681. Funding for electron microprobe analyses came from NSF grant STI – 9413900. I also thank Kathy Glesener, Dave McCraw, Becky Titus and Jan Thomas in the New Mexico Bureau of Mines and Mineral Resources (NMBMMR) cartography department for drafting figures. Dr. Abe Gundelier and Ruben Archuleta helped a great deal with sample preparation procedures in the Metallurgical laboratory. I thank Dr. Virgil Lueth and Robert Eveleth for their help with mineralogy and mineral occurrences in the Hillsboro mining district. I also thank Ruben Crespin and Jeanne Deardorff for their help in borrowing NMBMMR vehicles to do field work. Finally, I'd like to thank Glen Jones and Mark Mansell for their technical computer support. This project was funded by the NMBMMR, Charles Chapin, Director and State Geologist. Additional funding was obtained from the Budding grant,

the Graduate Student Association, and Dr. Daniel Lopez, President of the New Mexico Institute of Mining and Technology.

I especially thank my friends Shari Bauman, Peter Rinkleff, Shannon Lindaas, Dennis McMahon, Roseanna Neupauer, Sarah Wilson, Erwin Melis, Matt Herrin, Chris and Tanya Young, Jim Watrus, Harland Goldstein, and Tom Silverman who have been with me through thick and thin. I also especially thank my Mom and Dad (Antje and John), my brother Cliff, and my grandmother Nancy for help and continued support with all my endeavors.

"The strongest argument of the detractor (of mining) is that the fields are devastated by mining operations... They argue that the woods and groves are cut down, for there is a need of an endless amount of wood for timbers, machines and the smelting of metals. And when the woods and groves are felled, then are exterminated the beasts and birds, very many of which furnish a pleasant and agreeable food for man. Further, when the ores are washed, the water which has been used poisons the brooks and streams, and either destroys the fish or drives them away."

Georgius Agricola, 1556, De Re Metallica, translated by Hoover, 1950

# TABLE OF CONTENTS

## LIST OF FIGURES

## LIST OF TABLES

## LIST OF APPENDICES

# LIST OF ABBREVIATIONS AND TERMS

In this study numerous acronyms were incorporated into the text. For simplicity the acronyms and abbreviations are defined in alphabetical order.

AMD = acid mine drainage
ARD = acid rock drainage
BLM = Bureau of Land Management
BSE = back-scatter mode for electron microprobe
EAM = prefixes for stream sediment samples
FAAS = Flame Atomic Absorption Spectroscopy
GFAA = graphite furnace atomic absorption
$K_{sp}$= solubility product constant
LLD = lower level of determination
NMBMMR = New Mexico Bureau of Mines and Mineral Resources
QA/QC = quality assurance and quality control
RC drilling = reverse circulation drilling
XRD = X-ray diffraction spectrometry
XRF = X-ray Fluorescence Spectrometry

## ABSTRACT

In New Mexico, there are more than 100,000 abandoned mine waste rock piles with variable mineralogical and geochemical compositions. To better understand the environmental consequences of metal mobility in regions of minimal precipitation, a mineralogical and geochemical study was implemented for four mine waste rock piles and their drainage systems in the Hillsboro mining district.

A sampling strategy was developed to geochemically characterize four mine waste rock piles representing four different mineral deposits: a placer gold waste rock pile (Site A), a Laramide polymetallic vein waste rock pile (Site B), a carbonate-hosted Pb-Zn waste rock pile (Site C), and a carbonate-hosted Ag-Mn waste rock pile (Site D). In addition, another Laramide polymetallic vein waste rock pile (Site E) was studied to compare physical and chemical characteristics specifically with Site B. To determine the appropriate grain size range to be sampled, six grain size fraction ranges (2-1 mm, 1-0.5 mm, 0.5-0.25 mm, 0.25-0.125 mm, 0.125-0.063 mm, and < 0.063 mm) were analyzed by FAAS and XRF. The < 0.25 mm grain size fraction (encompassing the three smaller grain size fraction ranges) was used to sample the mine waste rock piles because it was determined to typically contain the highest metal concentrations. Using grid patterns unique to each of the waste rock piles, three homogenized samples were obtained using sampling densities of 15, 30, and 45 sample cells. Chemical analyses by FAAS and XRF determined that these mine waste rock piles can be adequately geochemically characterized by homogenizing samples collected from a grid pattern containing 15-30 samples.

An examination of metal mobility from the waste rock piles indicate that metals are moving as mineral grains, suspended material, and dissolved material. Chemical metal mobility is higher in the Laramide polymetallic vein waste rock piles (Site B and Site E) relative to the carbonate-hosted waste rock piles (Site C and Site D). This may be a result of pyrite-bearing waste rock piles (Site B and E) generating sulfuric acid that can increase metal availability to the environment. Site C and D, however, have less chemical movement due to the abundance of calcite. Physical movement of material from these sites is the primary cause for metals in down gradient stream sediments.

Secondary mineral rinds play a major role in the release of metals to the environment. Iron sulfate, iron oxide, and iron oxyhydroxide form rinds on the chalcopyrite and pyrite. Pyrite oxidation rinds preferentially partition arsenic. Oxidation rind thickness varies depending on mineralogy, mineral residence time in the waste rock pile, and hydrothermal history associated with the different deposits. Strong precipitation events may flush out metals partitioned in the outer rinds of oxidized sulfide grains. However, hydrothermal oxidation of some mineral grains like galena may be "armored" by cerussite. This leads to a significant decrease in the lead concentration available for chemical transport in the environment. Dissolved material may precipitate soluble salts onto grains in waste rock piles and stream sediments.

Agitation tests indicate copper and zinc are preferentially partitioned in the suspended material during a simulated precipitation event. Primary clays present in the stream sediments were smectite, illite, and illite/smectite mixed layer clays. Metal movement in a semi-arid environment is governed by local drainage characteristics, mineralogy, and grain size.

# 1.0 INTRODUCTION

Waste rock piles are anthropogenically created landforms that are derived from open pit and underground mining methods. Surficial oxidation of sulfide minerals in these piles is a major cause of acid drainage and an increase in metal concentration down gradient from the mining areas. Waste rock piles can exhibit a diverse mineralogy and geochemistry. In addition to the mineral and chemical heterogeneities, the waste rock piles contain variable grain sizes. There are more than 100,000 abandoned waste rock piles in New Mexico of varying size and composition. One of the controversial problems facing scientists and regulatory agencies today is how to sample these waste rock piles quickly and economically in order to adequately assess and prioritize potential environmental hazards.

Many different methods have been employed for sampling waste rock piles in order to characterize them geochemically (U.S. Environmental Protection Agency, 1986; British Columbia Acid Mine Drainage Task Force, 1992; U.S. Environmental Protection Agency 1994; Herring and McLemore, in press). However, documentation of sampling procedures of tailings dumps are more common due perhaps to the relative homogeneous grain size, geochemistry, and relative ease of reprocessing the material (Sidle et al., 1991; British Columbia AMD Task Force, 1992; Boulding, 1994; Smith and Williams, 1996). Tailings dumps and waste rock piles are primarily comprised of different materials. Tailings dumps represent spent ore material which is normally crushed and milled and contains relatively homogeneous sand to silt grain sizes. On the other hand waste rock piles contain gangue minerals and are composed of variable grain sizes. Pyrite can be in high abundance in waste rock piles as well as tailings dumps. Heterogeneities are found

in tailings dumps characterized by a layering effect that often occurs after milled and/or leached material of varying grain size and mineralogy is emplaced. Table 1 identifies the different factors affecting acid generation between waste rock piles and tailings dumps.

Table 1. Comparison of factors affecting acid generation in waste rock piles and tailings dumps. From the U.S. Environmental Protection Agency (1994).

| **Acid Generation Factors Affecting:** | **Waste Rock Piles** | **Tailings Impoundments** |
|---|---|---|
| Sulfide Source | • variable in concentration and location<br>• conditions may vary from sulfide rich to basic over short distances | • conditions uniform, often with very high sulfide content |
| Particle Size | • average rock size typically greater than 20 cm (but highly variable) | • tailings may be 100% less than 0.2 mm |
| pH Variation | • highly variable conditions over short distances | • fairly uniform conditions with a few major horizontal zones |
| Initiation of Rapid Oxidation | • usually starts immediately after first rock is placed (in "trigger" spots) | • usually starts after tailings placement ceases at end of mine life |
| Oxygen Entry | • enters freely along highly conductive flow paths at base of pile and large open void spaces; "chimney and lung" effects | • restricted by water in void spaces and the lower conductivity of partially saturated void spaces |
| Temperature | • temperature in pile affected by convective flow of air from outside pile<br>• high oxidation rates result in high temperatures distributed convectively through pile | • temperature transmission mainly by conductance, generally slow<br>• low oxidation rates result in low localized temperature effects |
| Storage | • large storage of acid products due to evaporative concentration | • small storage of acid products |
| Seepage | • seepage rapid along preferential flow paths<br>• seasonal variations in flow path "flushes" out stored products resulting in concentration peaks | • seepage slow and uniform<br>• reduced flow path variation and stored product "flushing" |
| ARD Releases | • large infiltration resulting in large seepage from toe and to groundwater<br>• rapid release following generation, sometimes with both neutralized and acid ARD seeps | • large early top surface ARD runoff<br>• lower infiltration<br>• gradual transition in seeps from process water to neutralized ARD to low pH ARD |

One method of waste rock pile characterization has been the use of reverse circulation (RC) drilling to certain depths and with a given sampling density. Although

this technique characterizes much of the waste rock pile which can be extremely heterogeneous both chemically and physically, the financial cost incurred by the investigating organization can be very high. Additional drilling methods include the Becker Hammer and the air rotary rig with hammer bit (U.S. Environmental Protection Agency, 1994) which still have relatively high cost.

The purpose of this part of the study is to develop a more effective cost method of sampling waste rock piles using a hand shovel to no more than 25 cm depth. The procedure may be used as a first approximation of the geochemical signature to prioritize subsequent characterization drilling. This study functions, more importantly, as a sampling protocol to adequately characterize the waste rock piles geochemically.

Waste rock piles may generate acid rock drainage that can mobilize environmentally hazardous metals such as lead, arsenic, copper, and zinc (Ficklin, et al., 1994). Metal mobility has been well documented in temperate environments (Lawrence, 1990; Salomons, 1995; Trainor et al., 1996; Banks et al., 1997; Sanden et al., 1997; Whiting and Olsen, 1997; Zhixun and Herbert, 1997; Odor et al., 1998). However, in an arid to semi-arid environment, there is not as much precipitation available to generate ARD (acid rock drainage). Metal mobility is not as well understood in drier environments. There have been few studies on the mobility of metals away from waste rock piles in arid climates (Marcus, 1987; Rampe and Runnels, 1989). Thus, the second part of this study is an examination of the movement of metals from the waste rock piles into adjacent arroyos.

Metal mobility in an arid to semi-arid environment is governed by sporadic precipitation events characteristic of such a climate. Due to the typical cycle of sulfide

mineral dissolution and oxidation followed by water evaporation and deposition of secondary minerals, metal mobility factors become more complex in arid climates than temperate climates. The movement of metals away from sulfide grains is perpetuated as long as the sulfide host remains, thus renewing the source of sulfur for sulfuric acid production. Secondary mineral rinds on the surfaces of sulfide minerals are the first to be available to the environment and have the potential to produce sulfuric acid with the onset of precipitation. The amount of metal movement is dependent upon the pH and amount of solvent introduced, thickness and mineralogy of the sulfide oxidation rind, speed of evaporation, and the acid buffering capacity of country rock or sediment. These factors contribute to regulation of metal movement away from the waste rock piles and into adjoining arroyo stream sediments.

Stream sediments were sampled to determine the extent of metal mobility down drainage of the waste rock piles. Metals in stream sediments are mobilized by physical and chemical processes. Material is moved mechanically from the area disturbed by mining as suspended and bed load sediment during a precipitation event. Original mineralogy such as silicates make up a high percentage of the stream sediment sample, while original sulfides are present only in minor amounts. Physical and chemical metal movement in the stream sediment environment varies with the volume of water introduced to the system. Physical grain movement as well as dissolution, evaporation, and re-deposition of sulfates and chlorides are a factor in metal mobility in an arid climate. Furthermore, colloidal movement downstream also enhances the mobility of metals due to the high cation exchange capacity and high surface area characteristic of clays and some clay size particles (Moore and Reynolds, 1997). This enables metals to

adsorb to colloid surfaces and travel away from the waste rock pile source. Through this type of sampling, physical and chemical metal mobility in a semi-arid environment can be better evaluated.

The Hillsboro mining district was chosen for this study because: 1) metals have been mined for over 100 years, 2) there has been little or no reclamation of the mines in the district, 3) numerous geological and geochemical studies are available for background data (Lindgren et al., 1910; Wells, 1918; Harley, 1934; Bauer, 1950; Kuellmer, 1955; Reeves, 1963; Segerstrom and Antweiler, 1975; Hedlund, 1977; Alminas and Watts, 1978; Alminas et al., 1978a; 1978b; 1978c; Watts, 1978; Watts et al., 1978a; Watts et al., 1978b; Wynn, 1978; Hedlund, et al., 1979; Fowler, 1982; Hood et al., 1983; Lovering and Heyl, 1989; Norman et al., 1989; Gold Express Corporation, 1992; Ward, 1993; Korzeb and Kness, 1994; Korzeb et al., 1995; Bureau of Land Management, 1996; Bakkom and Salvas, 1997; Green and O'Neill, 1998; McLemore et al., 1999), 4) the district is readily accessible, 5) the Copper Flat porphyry-copper deposit may be reopened and an environmental study of the area will aid in determining current conditions and reclamation of the area.

## 2.0 MINING HISTORY

The Hillsboro mining district, located in the Animas Mountains in the eastern Black Range, New Mexico, has been mined intermittently over the last 120 years mainly for gold, silver, and copper (Fig. 1). The town of Hillsboro was founded in 1877, with the discovery of gold. Four types of deposits are found in the district: Laramide polymetallic vein, placer gold, porphyry-copper, and carbonate-hosted Ag-Mn and Pb-Zn replacement deposits. Underground mining began in 1877 for gold and silver from Laramide polymetallic veins. Copper was also recovered. Soon after the gold-bearing veins were found, placer gold was discovered in the Rattlesnake and Wicks Gulches (Harley, 1934). The placer gold deposits were found in ephemeral streams such as the Grayback, Hunkidori, and Greenhorn Gulches which drain the Copper Flat volcanic center (Hedlund, 1985). At the turn of the century, carbonate-hosted replacement deposits were mined for lead, zinc, manganese, and vanadium by underground and surface mining methods intermittently until the late 1950's.

A modest 200 tons of copper oxide ore, from the supergene enrichment zone of the porphyry-copper deposit, were produced from the Sternberg mine in Copper Flat from 1911-1931 (Harley, 1934). Underground mining was the main mode of extraction in the district until 1982, when open pit mining for copper began at Copper Flat. During the mine's short life span from March to June 1982, a total of 7.4 million pounds of Cu, 2,300 ounces Au, and 56,000 ounces Ag were produced from the Copper Flat porphyry-copper deposit (Alta Gold Co., Form 10K, 1999). Currently, Alta Gold Mining Company is applying for permits to continue mining the Copper Flat porphyry-copper. The Copper Flat deposit has proven and probable reserves of 50,210,000 tons of ore at a grade of

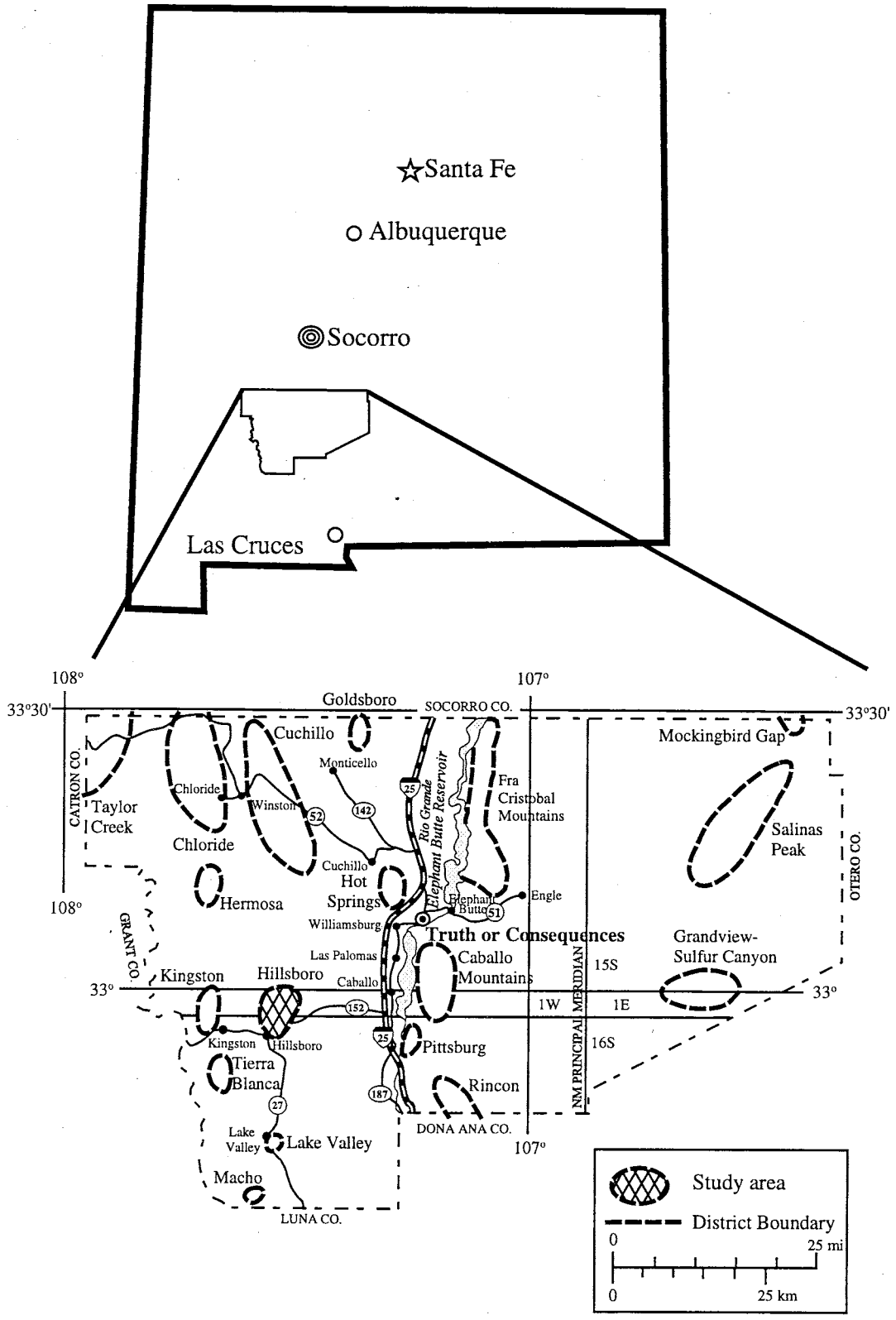


Figure 1. Location map of the Hillsboro Mining District, Sierra County, New Mexico

0.45% Cu, 0.004 oz/ton Au, 0.066 oz/ton Ag, and 0.015% Mo as of December 31, 1998 (Alta Gold Co., Form 10K, 1999). Contained metal is approximately 447,872,000 lbs. Cu, 223,900 oz Au, 3,299,500 oz Ag, and 14,762,000 lbs. Mo (Alta Gold Co., Form 10K, 1999). During the period 1877-1982 an estimated 270,000 ounces Au, from lode and placer gold, 134,000 ounces Ag, 154,000 pounds Pb, and 24.4 million pounds Cu were produced from the district (V.T. McLemore, unpublished data).

# 3.0 GEOLOGY

The Hillsboro area is dominated by Cretaceous andesite flows, breccias, volcanoclastic rocks and Paleozoic limestones and dolomites. Quartz monzonite intrusions with associated quartz latite and latite dikes intruded the andesite. The Copper Flat quartz monzonite, which intruded the andesite, is 75 Ma (McLemore et al., 1999). The Copper Flat porphyry-copper deposit consists of pyrite, chalcopyrite, minor sphalerite and galena, gold, and silver disseminated in the quartz monzonite stock and in quartz veinlets with molybdenite in the brecciated zone of the quartz monzonite stock (Hedlund, 1985). The Copper Flat quartz monzonite stock shows pervasive sericitic alteration of plagioclase and chloritic alteration of biotite, with pyritic alteration along veins and mineralized fractures (Lovering and Heyl, 1989). The Warm Springs quartz monzonite also intruded the andesite southwest of Copper Flat (Fig. 2), but is barren of mineralization and relatively unaltered. Quartz latite and latite dikes propagated radially from the Copper Flat porphyry-copper and intruded the andesite and the quartz monzonite. The quartz latite dikes and andesite host Laramide polymetallic vein deposits consist of pyrite, chalcopyrite, bornite, bismuthinite, tetradymite, sphalerite, galena, acanthite, chalcocite, limonite, and free gold (Hedlund, 1985). Propylitic alteration (epidote-chlorite-calcite-pyrite) commonly occurs in the andesite and local andesite breccias adjacent to the veins, but is only locally found in the quartz monzonite. Andesite exhibits intense propylitic alteration to chlorite, epidote, and carbonate alteration (Dunn, 1982, 1984; Lovering and Heyl, 1989) due to the veins. In the drainages to the east and west of Copper Flat volcano, placer gold deposits, consisting

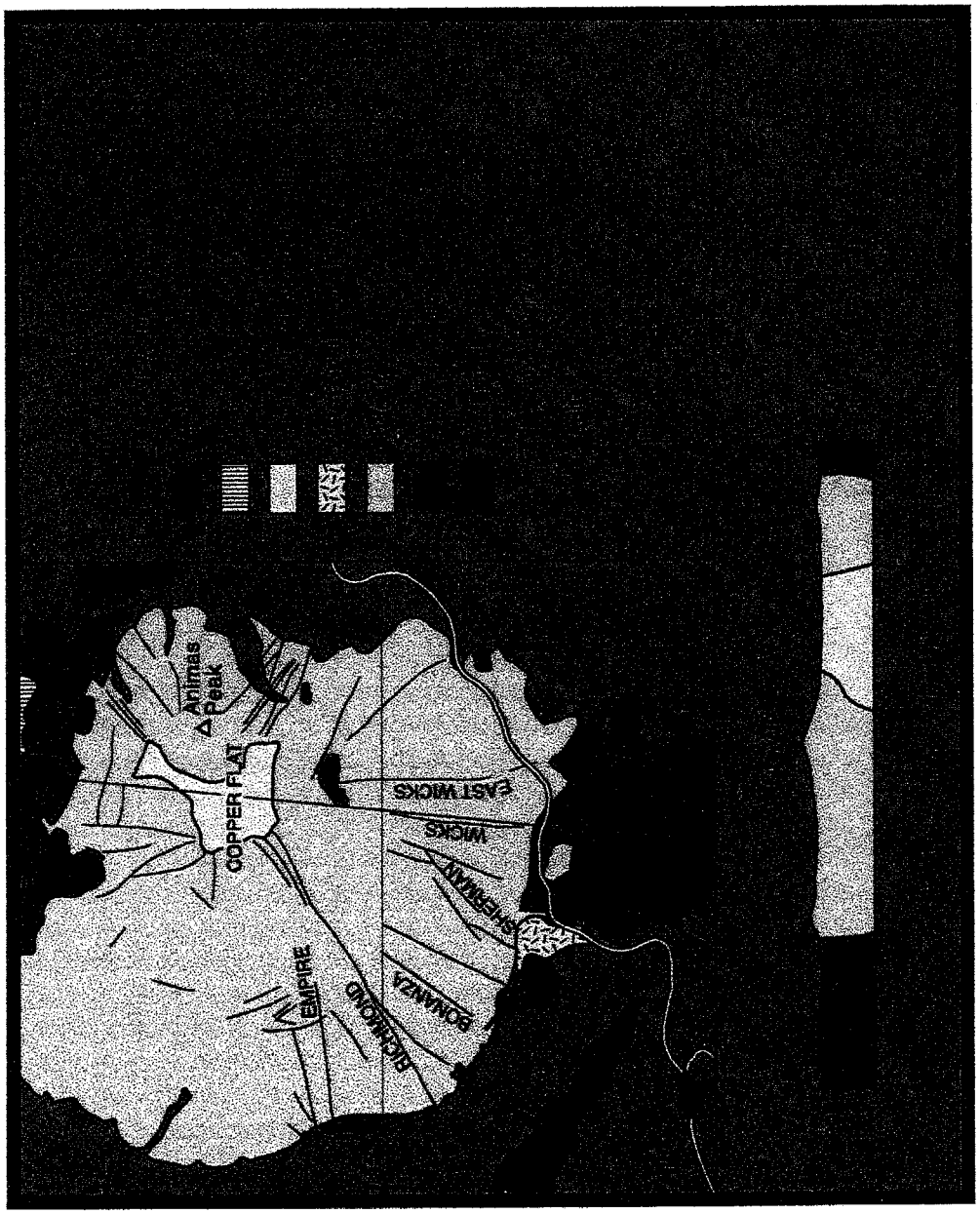


Figure 2. Geologic map of the Hillsboro mining district, modified from Hedlund (1985).

mainly of gold and electrum, formed by erosion and transport of material from the Copper Flat quartz monzonite and Laramide polymetallic vein deposits. Trace pyrite is found in these deposits. The majority of the carbonate-hosted replacement deposits are found in Ordovician El Paso Limestone and Silurian Fusselman Dolomite peripheral to the Copper Flat quartz monzonite intrusion. Fault veins and replacement deposits in the carbonate rocks contain, a mixture of plumbojarosite, argentojarosite, cerussite, anglesite, willemite, hemimorphite, hydrozincite, smithsonite and rare primary galena, sphalerite, and pyrite with subordinate wulfenite, vanadinite, endlichite, mottramite, malachite, azurite, linarite, and descloisite (Lovering and Heyl, 1989). The carbonate-hosted replacement deposits may have been formed by oxidizing fluids therefore minerals observed may be primary and not surface oxidation. The carbonate-hosted replacement deposits in the district also consist of smectite and illite/smectite mixed layer clays.

## 4.0 GEOCHEMICAL BACKGROUND STUDIES

A variety of geochemical data exists that provides information on the geochemistry of the mineral deposits in the Hillsboro mining district. Additional samples of host rocks and stream sediments provide information on background concentrations. Table 2 and 3 summarize the geochemical data available from past studies in the Hillsboro district.

Table 2. Geochemical analyses of samples from deposits, waste rock piles, and stream sediments, from previous work in the Hillsboro mining district. Korzeb et al. (1995) data are of single sample concentrations; McLemore et al. (unpublished data) are average concentrations for the listed deposit types; Alminas et al. (1978a,c) data are average Cu and Zn concentrations and Watts et al. (1978a) data are average Pb concentrations for stream sediments.

| Sample | Cu (ppm) | Pb (ppm) | Zn (ppm) | As (ppm) | sample # | Publication |
|---|---|---|---|---|---|---|
| laramide vein adit | 891 | 2072 | 2282 | 16 | 1 | Korzeb et al., 1995 |
| laramide vein adit | 3212 | 1226 | 985 | 46 | 1 | |
| carbonate-hosted Pb-Zn dump | 196 | > 10000 | > 20000 | 265 | 1 | |
| | | | | | | |
| Copper Flat copper-porphyry | 1806 | 34 | 170 | 2 | 24 | McLemore et al., unpublished data |
| carbonate-hosted deposit | 110 | 5151 | 12665 | 93 | 8 | |
| laramide vein deposit | 3428 | 770 | 863 | 120 | 194 | |
| jasperoid | 11 | 28 | 66 | 7 | 8 | |
| | | | | | | |
| below Bonanaza vein stream sed. | 1000 | 1000 | < 1000 | na | 1 | Alminas et al., 1978a,c |
| Grayback Gulch stream sed. | 5000 | 150 | < 1000 | na | 1 | |
| Ready Pay Gulch stream sed. | 150 | 1000 | 1000 | na | 1 | Watts et al., 1978a |

Table 3. Geochemical analyses of water samples from previous work in the Hillsboro mining district.

| Sample | pH | $HCO_3$ (mg/l) | $SO_4$ (mg/l) | Cu (ppm) | Pb (ppm) | Zn (ppm) | As (ppm) | Publication |
|---|---|---|---|---|---|---|---|---|
| Grayback Gulch upstream from pit lake (4/1/93) | 8.3 | 450 | 280 | < 0.01 | < 0.02 | < 0.01 | < 0.005 | BLM, (1996) |
| Grayback Gulch downstream from pit lake (3/31/93) | 7.7 | 376 | 1460 | 0.01 | < 0.02 | 0.01 | < 0.005 | |
| Copper Flat pit lake (2/12/93) | 5.6 | 7 | 2390 | 0.01 | < 0.01 | 1.8 | < 0.005 | |
| | | | | | | | | |
| Copper Flat pit lake (11/20/96) | 8.2 | 172 | 3275 | 0.71 | < 0.05 | 0.19 | na | Bakkom and Salvas, 1997 |
| Copper Flat pit lake (1/18/97) | 8.1 | 204 | 3265 | 0.61 | 0.01 | 0.35 | na | |

Note that the Laramide polymetallic vein and the carbonate-hosted replacement deposits contain varying Cu, Pb, Zn, and As concentrations. The stream sediment samples also show variation in Cu, Pb, and Zn concentrations throughout the district. Comparison of the BLM, (1996) and Bakkom and Salvas, (1997) data indicate decreasing metal concentration in water samples with time. Seasonal or monthly fluctuations in the pH and trace metal content of the pit lake may occur due to variable precipitation input.

## 5.0 CLIMATIC CONDITIONS

Hillsboro is situated on the eastern edge of the Black Range at 1599 m. April 12 is the average date of the last killing frost in spring, October 30 is the average date of the first killing frost in autumn, and the average length of the growing season is 201 days. The prevailing wind direction for each month of the year is westerly (U. S. Department of Agriculture, 1932).

Climatic conditions in the Hillsboro area are similar to other areas of southwestern New Mexico. The mean annual precipitation at the Hillsboro station is 327 mm (12.9 inches) with the highest rainfall amounts occurring during July, August, and September (BLM, 1996). The mean annual snowfall is 203 mm (8 inches) (BLM, 1996). Table 4 summarizes precipitation data in the Hillsboro area. High intensity, intermittent, short duration storms bring a majority of the rainfall to semi-arid environments.

Heavy run-off occurs due to the inablity of soil to absorb rain at the rate at which it falls. This may cause run-off to be locally concentrated in confined drainages. Run-off may increase the erosion of a waste rock pile, enabling higher chemical reactivity to occur due to increased surface area in direct contact with the rainfall. The remainder of the precipitation comes in the winter and early spring as light rain and snow that slowly percolates into the ground with the onset of warmer temperatures. Table 5 summarizes maximum and minimum temperature data for the Hillsboro area.

Table 4. Precipitation in the Hillsboro area from 1848 to 1993 (BLM, 1996).

| Month | Average Rainfall (inches) | Average Snowfall (inches) |
|---|---|---|
| January | 0.61 | 2.40 |
| February | 0.47 | 1.70 |
| March | 0.34 | 0.50 |
| April | 0.29 | 0.10 |
| May | 0.52 | 0.00 |
| June | 0.66 | 0.00 |
| July | 2.50 | 0.00 |
| August | 2.61 | 0.00 |
| September | 2.06 | 0.00 |
| October | 1.31 | 0.50 |
| November | 0.52 | 0.70 |
| December | 0.98 | 2.00 |
| Annual Average | 12.90 | 8.00 |
| Annual Maximum | 20.24 (1986) | 37.00 (1987) |
| Annual Minimum | 3.35 (1956) | 0.00 (1993) |

Table 5. Temperature (°F) in the Hillsboro area from 1953-1993 (BLM, 1996).

| Month | Maximum | Minimum |
|---|---|---|
| January | 54 | 24 |
| February | 60 | 28 |
| March | 66 | 33 |
| April | 74 | 40 |
| May | 82 | 47 |
| June | 91 | 55 |
| July | 91 | 61 |
| August | 88 | 59 |
| September | 83 | 52 |
| October | 74 | 42 |
| November | 63 | 31 |
| December | 55 | 25 |
| Annual Average | 73 | 41 |
| Annual Maximum | 75 (1956) | 44 (1957) |
| Annual Minimum | 71 (1991) | 39 (1987) |

# 6.0 FIELD PROCEDURES

## 6.1 SAMPLING

### 6.1.1 Rationale

Samples for this study were collected to characterize the waste rock piles, determine the level of metal movement in the environment, and determine geochemical baseline metal concentrations in the environment. Stream sediments were sampled to determine the amount of metal movement away from the waste rock piles. Water samples were taken from four sites within the district to determine a geochemical baseline for water present in the district.

Particle size fractions (2-1 mm, 1-0.5 mm, 0.5-0.25 mm, 0.25-0.125 mm, 0.125-0.063 mm, and < 0.063 mm) were analyzed to determine which grain size range or group of ranges contained the highest metal concentrations. The < 0.25 mm (250 micron) size fraction was used to sample the waste rock piles because it typically contained the highest metal concentrations which gives an estimate of the possible metal concentrations available to the environment (Table 12).

### 6.1.2 Methodology

Expensive drilling techniques can much better characterize physically and chemically heterogeneous waste rock piles. However, the financial cost can be very high. One of the difficulties in the current study is that stratigraphic layers were formed in Site B and E due mainly from the method of waste rock dumping onto the pile.

### 6.1.3 Preliminary characterization

First, samples were collected from the waste rock piles to determine the grain size distribution and obtain chemical compositions of different grain size fractions, to

determine the optimum size fraction to be collected. Material was collected across the mid-slope of each waste rock pile. The slope of each pile was divided into 5 zones from which 1/5 of a 5-gallon bucket was filled for each zone. A small stainless steel hand shovel was used throughout the sampling process. After the bucket was filled, the material was sieved to less than 2 mm and put into plastic sample bags. The greater than 2 mm fraction was also bagged and saved. In the laboratory, the less than 2 mm and the greater than 2 mm material, per waste rock pile, were weighed. After weighing, the less than 2 mm material was homogenized and split to a representative sample for chemical analysis of each grain size fraction (2-1 mm, 1-0.5 mm, 0.5-0.25 mm, 0.25-0.125 mm, 0.125-0.063 mm, and < 0.063 mm) while the greater than 2 mm material was archived. Samples were homogenized by cone and quarter methods and then split using a splitter.

### 6.1.4 Individual grid pattern sampling

One of the problems in sampling waste rock piles is determining how many samples to collect and where in the pile they should be collected. Initially, the Laramide polymetallic vein waste rock pile (Site B) was sampled with 45 individual samples from a sampling grid pattern tailored to the proportions of the site (Fig. 3). Each of the samples was analyzed individually (Table E.6, Appendix E). The less than 0.25 mm fraction was sampled at each location on the grid pattern. This grain size range was used because it typically contains the highest metal concentrations (see section 8.4 Chemical Analyses of Waste Rock Piles).

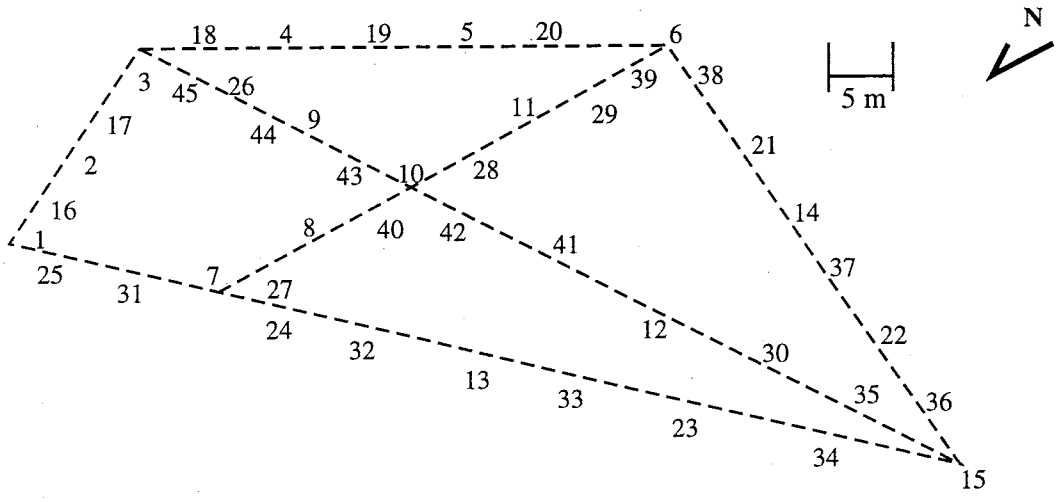


Figure 3. Sample locations for the Laramide polymetallic vein waste rock pile (Site B).

### 6.1.5 Grid pattern sampling

In the third stage of this project, each of the four waste rock piles was sampled using unique grid patterns which conformed to their respective dimensions. Each type of grid pattern was created to maximize surface area coverage of the waste rock piles. Samples were collected in three batches of 15 samples each. Average time to collect 15 samples was one hour and depended greatly on the terrain of the waste rock pile. Each set of samples was collected from a unique grid pattern system with no overlap in sample locations (Fig. 3-6). The less than 0.25 mm fraction was sampled from the waste rock piles. This grain size range was used because it typically yielded the highest metal concentrations (Table 12). Splits of samples were combined, homogenized, and analyzed in sets (i.e. 15, 30, and 45 samples) to determine the minimum number of samples necessary to adequately characterize the waste rock piles geochemically. An elongate/oval shaped sampling grid pattern was used for the placer gold waste rock pile (Site A, Fig. 4). A pseudo-trapezoidal sampling grid was superimposed on the Laramide polymetallic vein waste rock pile (Site B, Fig. 3). The short side of the trapezoid is at the top of the pile while the long side is at the toe of the pile. A crescent moon shaped grid pattern was used for the carbonate-hosted Pb-Zn waste rock pile (Site C, Fig. 5). Figure 6 shows a rectangular grid pattern used for the carbonate-hosted Ag-Mn waste rock pile (Site D). Sites A, B, C, and D were sampled in 15, 30, and 45 samples densities to obtain three homogenized samples.

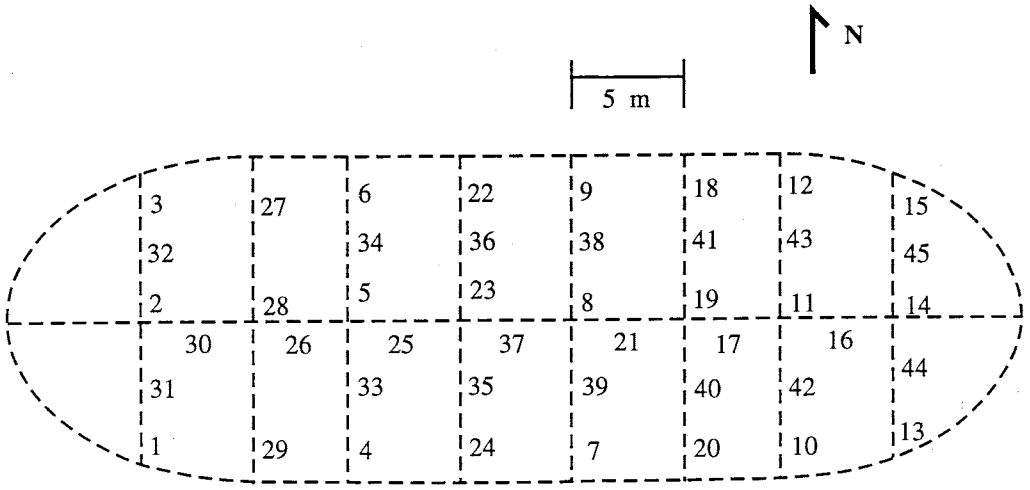


Figure 4. Sample locations for the placer gold waste rock pile (Site A).

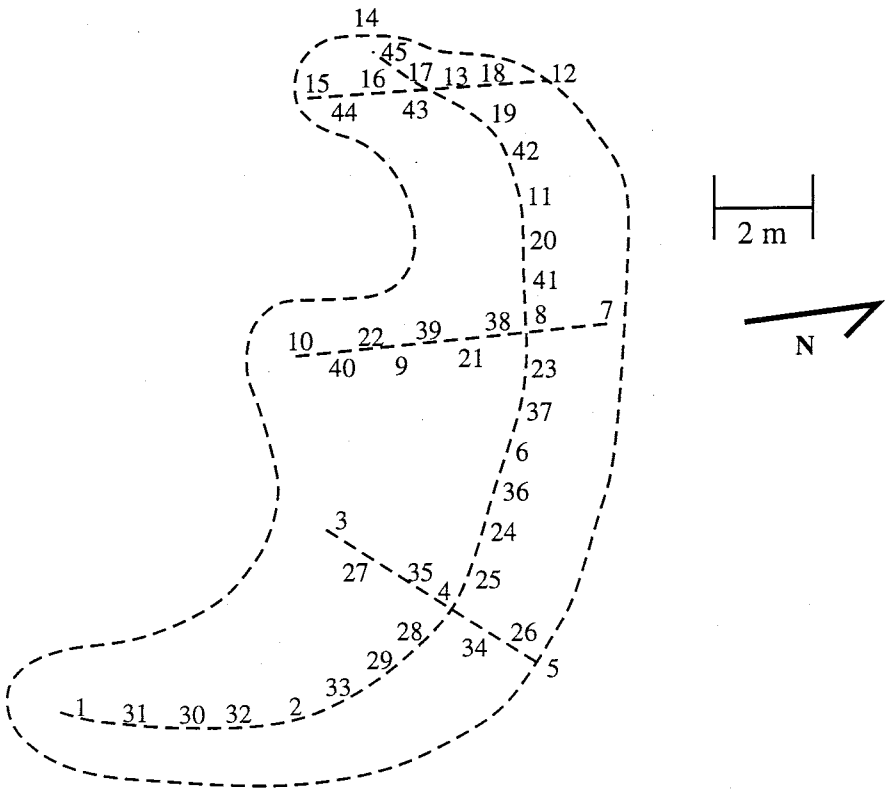


Figure 5. Sample locations for the carbonate-hosted Pb-Zn waste rock pile (Site C).

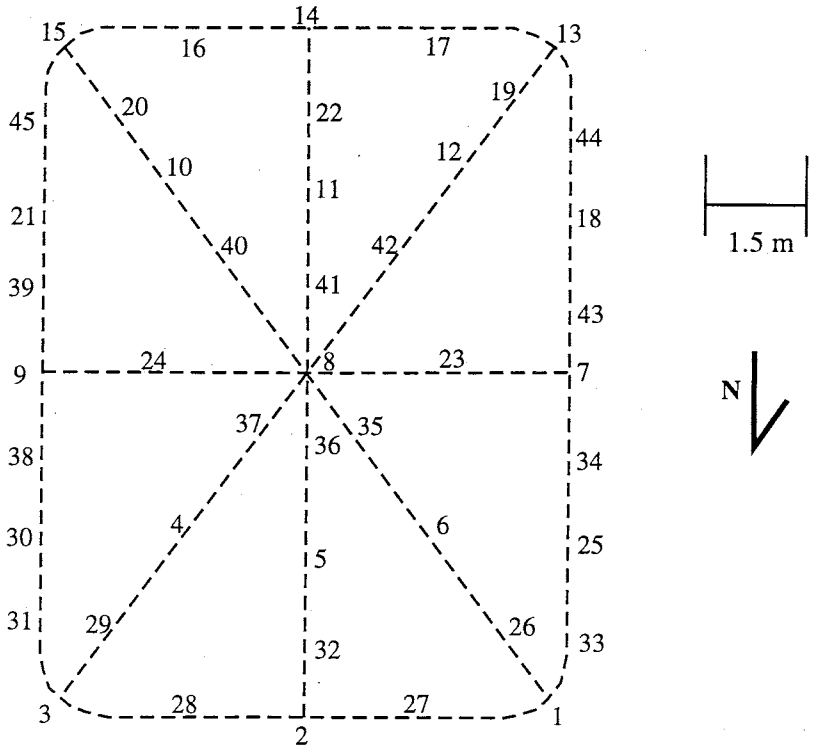


Figure 6. Sample locations for the carbonate-hosted Ag-Mn waste rock pile (Site D).

For each site (A, B, C, and D) three homogenized samples were prepared by thorough mixing. The samples were mixed at least four times by cone and quarter methods until there was no longer a color variation. Once a single color was obtained the sample was split to form three splits which weighed approximately 1000 grams each. Each of the homogenized samples were ground for chemical analysis using a stainless steel disc grinder to clay and silt size (< 63 microns). Figure 7 is a legend map for the sample location maps (Fig. 8, Fig. 9, Fig. 10). Waste rock piles (Sites A-E) are located in different parts of the district (Fig. 8, Fig. 9, Fig. 10).

### 6.1.6 Outcrop samples

Outcrop rock samples were taken in the form of chip samples and grab samples from the waste rock piles. Outcrops in the district were sampled in order to compile geochemical background data of unmineralized country rock. A chip sample constituted a sample taken horizontally or vertically for a given distance on an outcrop. A grab sample was any sample taken for chemical analyses and/or for thin section because of its hand sample properties (i.e. contained minerals or alteration of interest). All of the samples collected were chemically analyzed and thin sections were prepared. Chip samples were taken from the Black King manganese mine, the Petroglyph lead-zinc mine, and one of the Bonanza vein adits. A sampling bias was used for waste rock pile grab samples in order to obtain a representative suite of the petrology and mineralogy present on the waste rock piles. In addition, fresh unaltered rock samples were taken throughout the mining district to determine the elemental background concentrations.

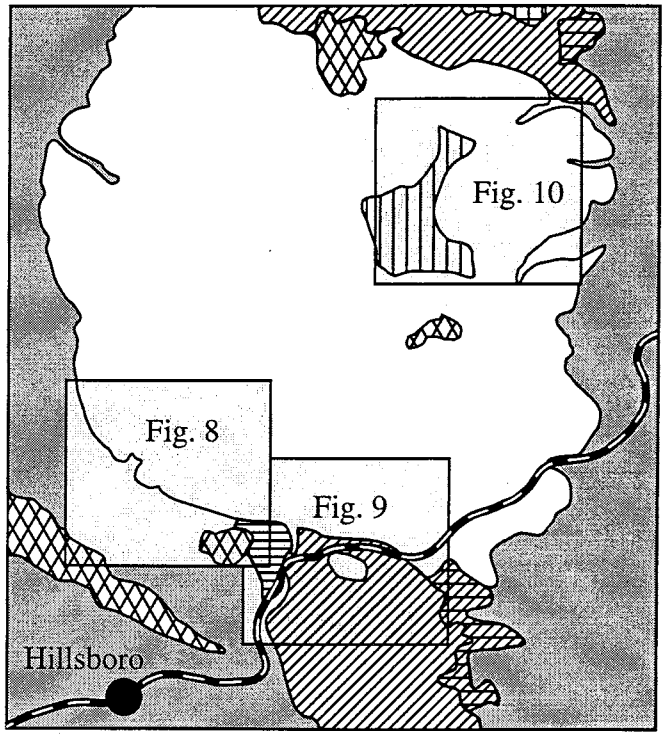


Quaternary alluvium and sediments

Tertiary sediments and interbedded basalt

Tertiary volcanics

Quartz diorite

Copper Flat quartz monzonite

Warm Springs quartz monzonite

Andesite

Paleozoic sediments

N

0 1 2 3 km

HWY 152

Figure 7. Location map legend of insets from Figures 8, 9, 10 in the Hillsboro mining district. The geology map is modified from Hedlund (1985).

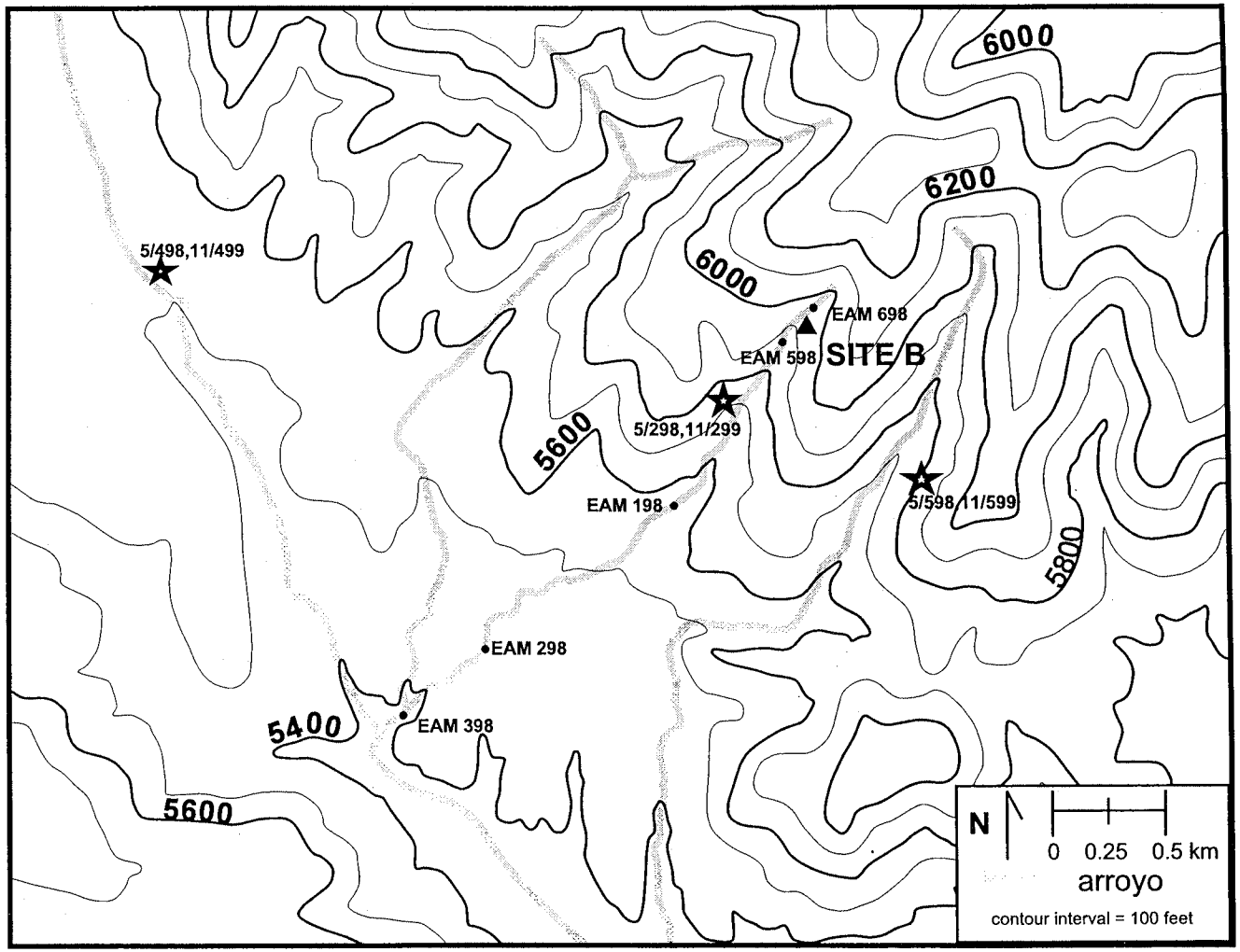


Figure 8. Sample location map (Site B). Black triangles indicate waste rock pile sampling sites, stars indicate district water sample sites, and dots indicate stream sediment samples.

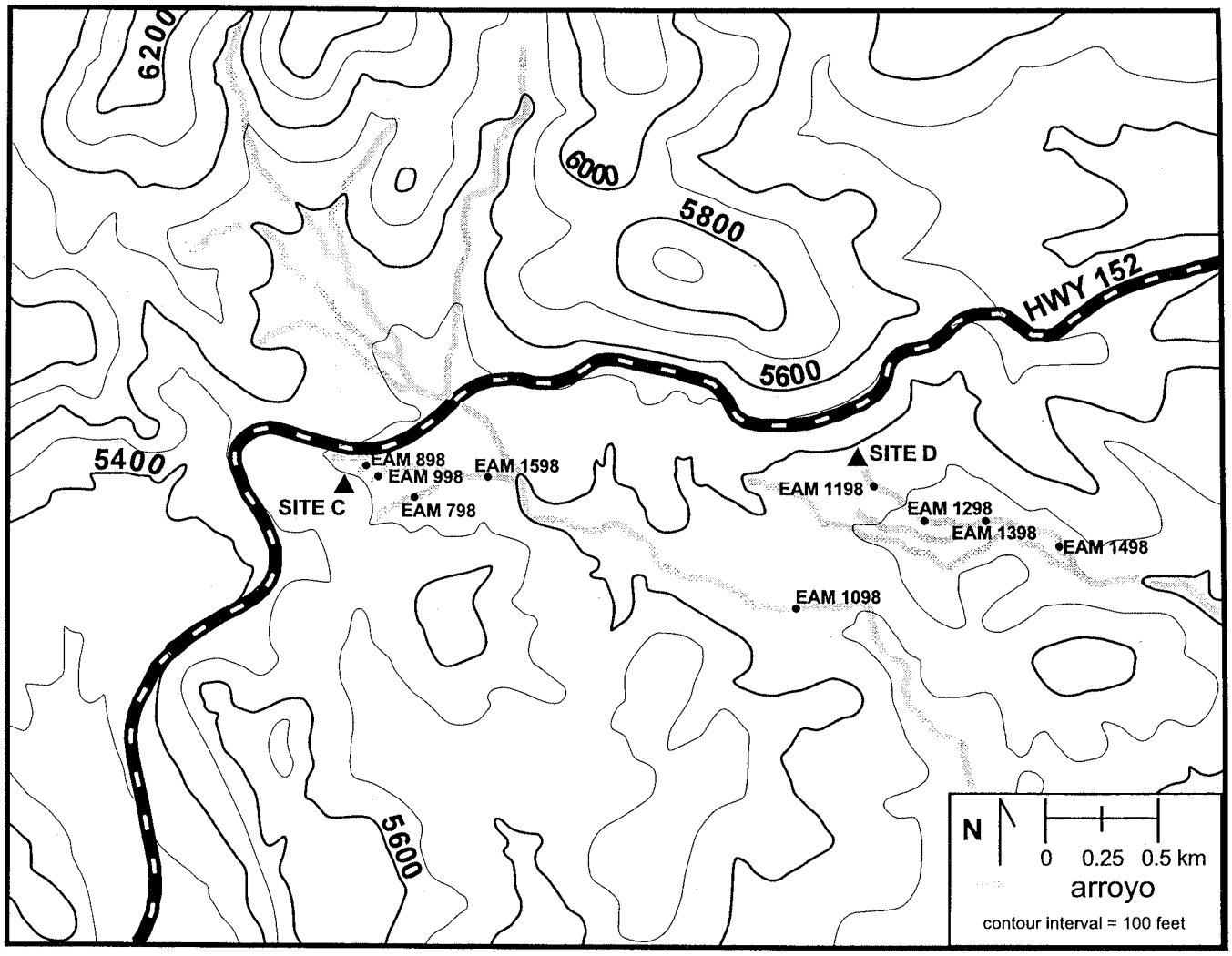


Figure 9. Sample location map (Site C, D). Black triangles indicate waste rock pile sampling sites and dots indicate stream sediment samples.

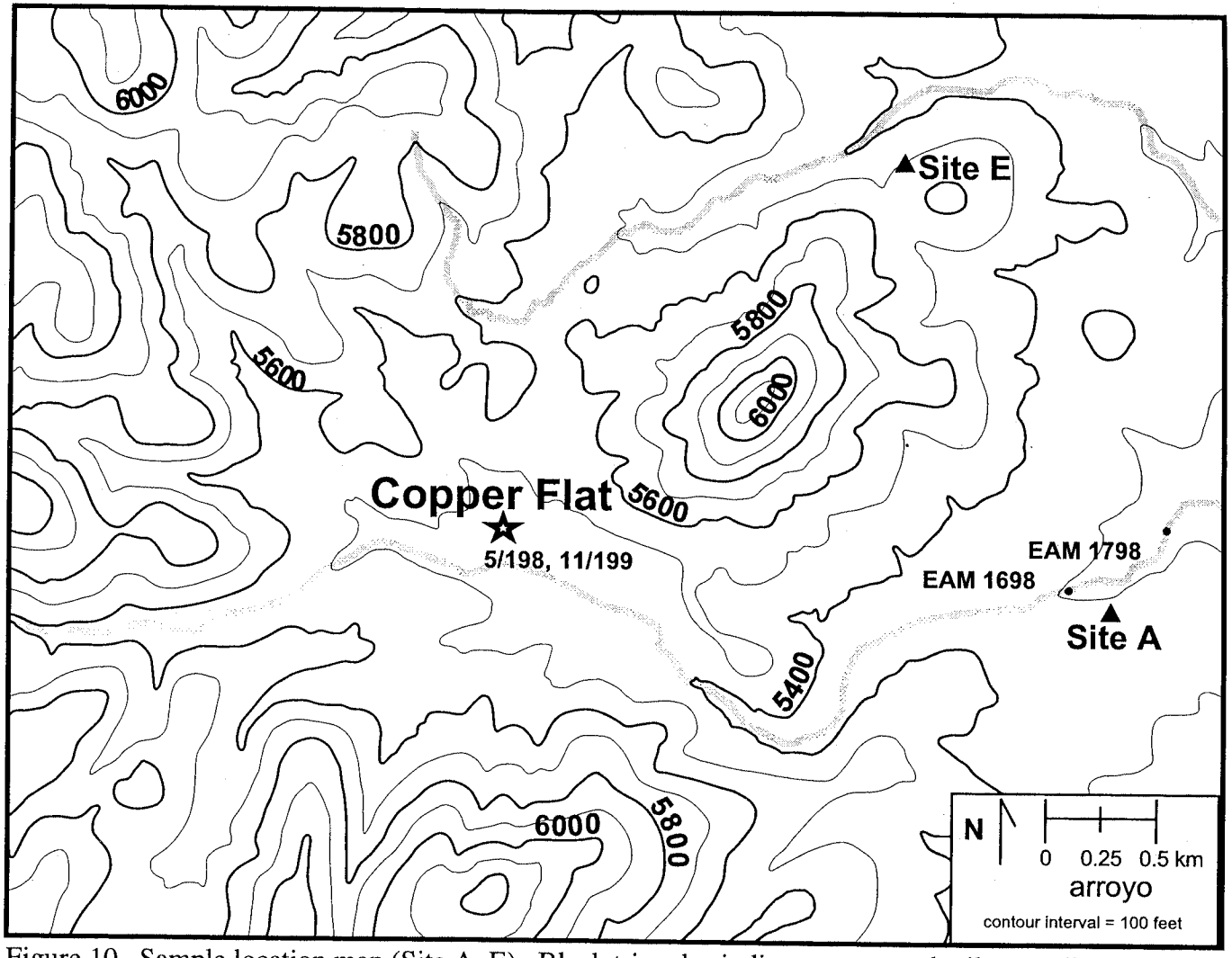


Figure 10. Sample location map (Site A, E). Black triangles indicate waste rock pile sampling sites, stars indicate district water sample sites, and dots indicate stream sediment samples.

### 6.1.7 Stream sediments

In order to ascertain the level of metal movement away from waste rock piles, stream sediment samples were collected in the active channels of arroyos draining catchments containing waste rock piles and mineralized areas (Fig. 8, Fig. 9, Fig. 10). Sample sites downstream of the waste rock piles were dependent upon accessibility, the location of the waste rock pile, and the drainage characteristics. Samples were collected in a narrow trench, the width of the active channel, using a stainless steel hand trowel and a 2 mm stainless steel sieve. Locations of plentiful stream sediment accumulation enabled the sampling depth of the trench to average 15 cm. Bedrock was present typically at 15-20 cm depth.

### 6.1.8 Water samples

Water samples were collected from four localities (Fig. 8, 10) to determine baseline water chemistry for specific areas in the mining district. Samples were collected from the Copper Flat open pit lake, a natural spring west of the Copper Flat Volcano, within an adit on the Bonanza vein, and within an adit on the Rattlesnake vein. Samples were collected in May and November 1998 and analyzed for major and trace element constituents. A detailed description of the water sampling procedure can be found in Appendix A.

# 7.0 LABORATORY PROCEDURES

## 7.1 ANALYTICAL METHODS

Different types of analytical techniques were used in this study to answer specific questions regarding waste rock pile sampling and metal mobility. Flame Atomic Absorption Spectroscopy (FAAS) was used to determine metal concentrations of all waste rock piles analyzed. X-ray Fluorescence Spectrometry (XRF) could not be used in samples where high Pb, Zn, and Mn concentrations were present due to instrumental interferences.

Transmitted and reflected light microscopy were used to determine mineralogy of translucent and opaque minerals. X-Ray Diffraction (XRD) was used to supplement and confirm mineralogical descriptions of stream sediment and waste rock pile samples. Opaque minerals of interest (i.e. pyrite, chalcopyrite, galena, and manganese oxides) and their secondary mineral rinds were identified and analyzed using the electron microprobe to determine the chemistry of the core versus that of the rind(s) in order to provide insight into metal mobility on a micro-scale. Finally, agitation tests for waste rock pile and stream sediment samples were employed to determine the metal concentrations present in suspension and in solution. Data from these tests give insight into metal availability to the environment with the onset of a short duration, high intensity precipitation events.

### 7.1.1 Mineralogical Analyses

#### 7.1.1.1 Petrographic techniques

Thin sections of grab samples from the waste rock piles and epoxy mounts of heavy mineral separates from waste rock piles were examined using transmitted and reflected light microscopy. Thin sections were professionally made while the epoxy

mounts were made and polished in-house. Additionally, mineralogy of the less than 2 mm fraction in the stream sediments and waste rock piles were identified using a binocular microscope.

#### 7.1.1.2 XRD techniques

X-ray diffraction (XRD) analysis was performed on whole rock, stream sediments, and less than 2 mm material from the waste rock piles to determine their mineralogy. Detailed sample preparation procedure can be found in Appendix B. To determine clay mineralogy, oriented clay slides were made with additional glycolated and heated runs. The oriented clay slides were run at 2-38° 2θ. Oriented slides were then glycolated for 24 hours and then run at 2-15° 2θ. After the glycolated slides were run, they were heated for 30 minutes at 350° C, run at 8.5-9.8° 2θ and at 2-15° 2θ. Unoriented or random powder mounts were prepared and analyzed to determine polytypes of different clays (Moore and Reynolds, 1997; standard NMBMMR procedures).

#### 7.1.1.3 Electron microprobe sample preparation procedure and analyses

Thin-sections of waste rock pile grab samples and epoxy mounts of the heavy mineral separates of the less than 2 mm grain size fraction from the waste rock piles were analyzed using the electron microprobe. Due to the high amount of calcium bearing minerals (i.e. calcite and gypsum) in some of the waste rock piles; sodium metatungstate was unable to be used to separate the heavy mineral fraction. Instead, approximately 1 kg of material from Sites A-E were run on a Willfley table and then panned to get the highest concentration of heavy minerals from each of the dumps. The heavy mineral concentrate was air-dried, mineralogically described using the binocular microscope, set

into epoxy, and polished. Once the samples were described mineralogically using transmitted and reflected light microscopy they were carbon coated prior to electron probe analysis. Qualitative and quantitative analyses were performed using the Cameca SX681 Electron Microprobe Spectrometer on Sites A-E. Heavy minerals were first viewed in backscatter (BSE). Quantitative analyses followed qualitative analyses that were used to determine chemical composition of the weathering rinds present on the heavy minerals.

Chemical analyses by electron microprobe techniques of the waste rock piles were used to determine mineralogy of some of the cores and rinds of mineral grains. Chemical percentages of the mineral grains were used to calculate specific mineral formulas whenever possible. Amorphous phases from weathering or hydrothermal alteration were only generally named because of their unique chemical content (i.e. iron sulfate).

### 7.1.2 Chemical Analyses

#### 7.1.2.1 FAAS and XRF techniques

Samples from Sites A, B, C, D, and E and the composite/homogenized samples from waste rock piles Sites A, B, C, and D were digested by dissolving 1 g of sample in aqua regia (15 ml HCl and 5 ml $HNO_3$). This procedure was repeated twice to dryness and then put into solution to a volume of 50 ml with 5% $HNO_3$. This dissolution process releases most metals bound in the sample, but the metals bonded in some silicate and other resistant minerals remain locked in the crystal lattice and are not completely recovered for analysis. Each sample was analyzed by FAAS using an Instrumentation

Laboratories Model Video 12 instrument, according to manufacturer's specifications (Ebdon, 1982).

In addition, samples from Sites A, B, and E were analyzed by X-ray Fluorescence Spectrometry (XRF) and compared with analyses by FAAS. XRF is a direct measure of the total metal concentration in the solid material and in some cases measures higher metal concentrations than FAAS. Trace element concentrations in Site C were unable to be determined by XRF due to interferences created by high concentrations of lead and zinc. Trace element concentrations for Site D were also unable to be determined by XRF because of high manganese concentrations (approx. 10%). Samples were analyzed using a Phillips PW2400 instrument. Standard pressed powder preparation procedures were followed to obtain trace element ($TiO_2$, $Fe_2O_3$, MnO, V, Cr, Ni, Cu, Zn, Ga, As, Rb, Sr, Y, Zr, Nb, Mo, Ba, Pb, Bi, Th, and U) analyses (Norrish and Chappel, 1977). All stream sediment samples were analyzed by XRF for trace elements except for those taken downstream from the manganese waste rock pile (Site D), which were analyzed by FAAS. The fresh unaltered rock samples were used for background concentration values.

Precision and accuracy were monitored throughout the study with FAAS and XRF analyses of duplicate, triplicate, and reference standard samples. Duplicates and triplicates monitored precision of the analytical method. Reference standards monitored the accuracy of the analyses. FAAS analyses typically are within ± 15% while the XRF analyses are within ± 2%. QA/QC data can be found in Appendix C.

#### 7.1.2.2 Water Analysis Techniques

Alkalinity, pH, and total dissolved solids were measured in the lab using standard laboratory techniques. Major ions and trace metals were measured using titration techniques and FAAS respectively.

### 7.2 WATER SAMPLE COLLECTION

Four separate samples were collected at each sample site to determine chemical analyses of different types of natural water in the district. The four sample types are: type "A" = unfiltered, unacidified (to measure dissolved major elements and ionic compounds plus suspended materials in water); type "B" = unfiltered, acidified (to measure dissolved trace metal components and suspended material in water); type "C" = filtered, acidified (to measure dissolved trace metal components in water); type "D" = filtered, unacidified (to measure dissolved major elements and ionic compounds in water).

### 7.3 AGITATION TESTS

Agitation tests were conducted on five waste rock piles and four stream sediments. These tests approximate dissolution as a result of excess rainfall. Tests were conducted to determine the metal concentrations present in solution and in suspension with the application of water to solid samples that were less than 2 mm in size and weighing approximately 75 g. Samples were mixed with deionized water, pH ranging between 5 and 6, for twenty minutes. The pH was measured throughout the duration of the tests. Previous laboratory procedures such as column leach tests and extraction techniques have been used to quantify metal concentrations in mine waste and mine rock samples (NMBMMR standard procedure; Lone Tree Mine, 1996; Browning-Ferris

Industries, 1991). Each sample was stirred with a magnetic stirrer in water for twenty minutes in order to mimic a short-duration, high intensity precipitation event whereby the sample media was inundated with water. These precipitation events are suspected of increasing the probability of metal transport downstream from the waste rock piles. The question of metal movement away from the waste rock piles was addressed with FAAS analyses of water samples with and without colloids. Water samples (30 ml) filtered with a 11 μm filter contained material in suspension which was acidified to a pH of 2, shaken for 2 hours, put through a 0.45 μm filter and analyzed by FAAS. This type of sample measured the metal content present in solution and adsorbed species to the colloids with the addition of acid. The other type of sample analyzed was an unacidified sample which determined the metal content present in solution. Water samples (30 ml) were filtered through the 11 μm and 0.45 μm filters and then analyzed by FAAS. These two types of samples helped determine the geochemical modes of metal movement. Procedures and sample preparations are described in Appendix D.

# 8.0 RESULTS

## 8.1 PHYSICAL CHARACTERISTICS

Physical characteristics of the waste rock piles sampled, such as grain size distribution, terrain, and the physical dimensions directly affect the geochemical behavior of each site. Knowledge of these parameters provides insight into overall metal availability from the waste rock piles in addition to their potential for wind and water erosion. Each of the waste rock piles sampled in the Hillsboro mining district are at different elevations, have different exposure to weather, and have different locations relative to ephemeral streams. Physical aspects of the waste rock piles are summarized in Table 6. Site A and Site D demonstrate similar grain size distributions in the greater than 2 mm fraction as well as in the less than 2 mm fraction (Table 7). By comparison, Site B and Site C have similar total weight percentages in the less than and greater than 2 mm fractions.

Table 6. Physical aspects of waste rock piles. Volume was calculated by Delunay triangulation method (calculated using Rock Ware Inc., 1995).

| Waste Rock Pile | Elevation (meters) above sea level | Width (meters) | Length (meters) | Average Height (meters) | Maximum Height (meters) | Average Slope (degrees) | Approx. volume ($meters^3$) |
|---|---|---|---|---|---|---|---|
| Site A | 1628.0 | 32.0 | 46.0 | 6.6 | 7.3 | 26.0 | 2969.5 |
| Site B | 1792.0 | 20.0 | 120.0 | 7.4 | 14.0 | 23.0 | 11582.0 |
| Site C | 1743.0 | 22.0 | 39.0 | 2.0 | 2.3 | 14.0 | 475.9 |
| Site D | 1664.0 | 6.0 | 33.0 | 1.8 | 2.5 | 18.0 | 52.8 |
| Site E | 1658.0 | 32.0 | 35.0 | 5.5 | 6.2 | 20.0 | 2267.1 |

Table 7. Grain size distribution of four waste rock piles displayed in total weight percentage.

| Grain Size | Site A Total Wt. % | Site B Total Wt. % | Site C Total Wt. % | Site D Total Wt. % |
|---|---|---|---|---|
| whole | 100.0 | 100.0 | 100.0 | 100.0 |
| > 2 mm | 57.7 | 75.4 | 74.6 | 51.4 |
| < 2 mm | 42.3 | 24.6 | 25.4 | 48.6 |
| 2-1 mm | 7.0 | 6.5 | 5.8 | 9.1 |
| 1-0.5 mm | 9.7 | 6.2 | 5.4 | 11.3 |
| 0.5-0.25 mm | 10.5 | 4.3 | 3.6 | 9.7 |
| 0.25-0.125 mm | 7.1 | 2.7 | 2.9 | 4.6 |
| 0.125-0.063 mm | 4.2 | 1.9 | 3.1 | 5.6 |
| < 0.063 mm | 3.8 | 3.0 | 4.6 | 5.3 |

## 8.2 BACKGROUND GEOCHEMICAL DATA

Samples of the major geologic units were analyzed to determine background concentrations of lead, arsenic, copper, and zinc. The background levels are important for comparison to local mining areas that may have relatively anomalous concentrations of metals. Not only does the background data give insight into what may be released to the environment, but it also gives an approximation of the acid neutralizing capacity of any given geologic formation (Table E.7, Appendix E). Table 8 displays trace element concentrations for the primary lithologies in the Hillsboro mining district. Although the major element analyses of the Fusselman Dolomite and El Paso Limestone lithologies are not represented (Table E.7 in Appendix E), they contain the highest and quickest acid buffering capacity of all the lithologies present in the district based on mineralogical composition.

Table 8. Selected average (where applicable) trace element concentrations of primary lithologies in the Hillsboro district. Chemical analyses were obtained by XRF.

| Lithology | Cu (ppm) | Pb (ppm) | Zn (ppm) | As (ppm) | # of samples |
|---|---|---|---|---|---|
| quartz latite | 59.6 | 18.8 | 71.6 | 2.2 | 5 |
| andesite | 104.2 | 21.0 | 444.8 | 4.5 | 6 |
| quartz monzonite | 151.8 | 15.3 | 42.0 | 1.5 | 4 |
| Fusselman Dolomite | 2.0 | 3.0 | 7.0 | 2.0 | 1 |
| El Paso Limestone | 15.0 | 13.0 | 52.0 | 2.0 | 1 |
| alkalai basalt | 47.0 | 6.0 | 86.0 | 1.0 | 1 |
| jasperoid | 30.0 | na | 144.0 | 6.0 | 2 |

Samples taken throughout the mining district of various host rock lithologies present in Hillsboro district showed distinct geochemistry. Quartz latite dikes contained lower base metal concentrations than the andesite which it intruded (Table 8). Copper is the highest metal concentration in the quartz monzonite. This pertains directly to the nature of the porphyry-copper deposit and its characteristics. The Fusselman Dolomite and the El Paso Limestone have relatively low trace element concentrations (Table 8). The alkali basalt which caps Black Peak in the district and a mesa to the west of the volcano contains moderate concentrations of trace metals, while the jasperoids contain anomalous levels of lead. See Appendix E for complete chemical analyses.

## 8.3 WASTE ROCK PILE MINERALOGY

Mineralogy of the waste rock piles was determined using XRD, binocular microscopy, reflected and transmitted light microscopy, and electron microprobe techniques. Mineral identification is important to understand the general mineral morphology and chemical constituents of the waste rock pile in order to prepare for specific element analyses on the electron microprobe. Acid rock drainage is controlled in

part by mineralogy that may affect metal availability and contamination to the environment. In addition, mineralogy is directly related to the chemical composition. Table 9 summarizes the mineralogy present in the waste rock piles sampled.

Table 9. Waste rock pile mineralogy. Identification of thin sections and heavy mineral concentrates with binocular and petrographic microscope and supplemented by XRD and electron microprobe. In order from greatest to least abundance.

| Waste Rock Pile | Mineralogy |
|---|---|
| Site A | plagioclase, quartz, pyroxene, biotite, chlorite, calcite, hematite, magnetite, ilmenite, malachite, sphene, pyrite, chalcopyrite, smectite, kaolinite |
| Site B | quartz, plagioclase, chlorite, calcite, sericite, pyrite, chalcopyrite, biotite, hematite, goethite, epidote, chalcanthite, bornite, actinolite-tremolite, sphene, jarosite, schwertmannite, smectite |
| Site C | calcite, microcrystalline quartz, cerussite, wulfenite, vanadinite, pyromorphite, mimetite, hematite, galena, sphalerite, chlorite, anglesite, smectite, illite/smectite mixed layer clays |
| Site D | psilomelane, calcite, hematite, wulfenite, cerussite, smectite |
| Site E | plagioclase, quartz, chlorite, calcite, sericite, biotite, hornblende, pyrite, chalcopyrite, hematite, goethite, cuprite, epidote, actinolite-tremolite, epidote, chalcanthite, garnet, gypsum |

The Copper Flat deposit contains pyrite, chalcopyrite, minor galena, gold, silver, molybdenite, sericite, electrum, chlorite, biotite, quartz, and plagioclase (Hedlund, 1985; Lovering and Heyl, 1989). Laramide polymetallic veins contain pyrite, chalcopyrite, bornite, bismuthinite, tetradymite, sphalerite, galena, acanthite, chalcocite, limonite, free gold, chlorite, epidote, and calcite (Hedlund, 1985; Dunn, 1982, 1984; Lovering and

Heyl, 1989). Carbonate-hosted replacement deposits contain plumbojarosite, argentojarosite, cerussite, anglesite, willemite, hemimorphite, hydrozincite, smithsonite, galena, sphalerite, pyrite, wulfenite, vanadinite, endlichite, mottramite, malachite, azurite, linarite, and descloisite (Lovering and Heyl, 1989).

Of interest is the negligible amount of chalcopyrite in Site E relative to Site B. Samples analyzed by the U.S. Bureau of Mines from an adit on the Bonanza vein (near Site B) contained 5517 ppm Cu average, while the samples near the El Oro mine (near Site E) contained 786 ppm Cu average (Korzeb et al., 1995).

### 8.3.1 Electron Microprobe

The electron microprobe was used to determine the composition of rinds on mineral grains in waste rock piles. Chemical analyses attained from quantitative points were used to determine the possible mineralogy. For all chemical analyses obtained from the electron microprobe refer to Appendix E.

#### 8.3.1.1 Placer Gold Waste Rock Pile (Site A)

Mineral grains from this waste rock pile exhibited rind textures of varying thicknesses. These include the hematite/ilmenite solid solution series. Minor clay rinds occur on the three grains analyzed. Chemical composition of the clay rind in Figure 11 are as follows: $SiO_2$ 38%, $Al_2O_3$ 19.5%, FeO 13%, MgO 9%, CaO 3%, and $K_2O$ 1% (a smectite mineral).

#### 8.3.1.2 Laramide Polymetallic Vein Waste Rock Pile (Site B)

This waste rock pile contains pyrite and chalcopyrite which appear to be the most reactive to oxidation. Chemical analysis of pyrite and its oxidation rind in Figure 12 shows there is a loss of sulfur and an increase in iron and arsenic in the rind (Table10).

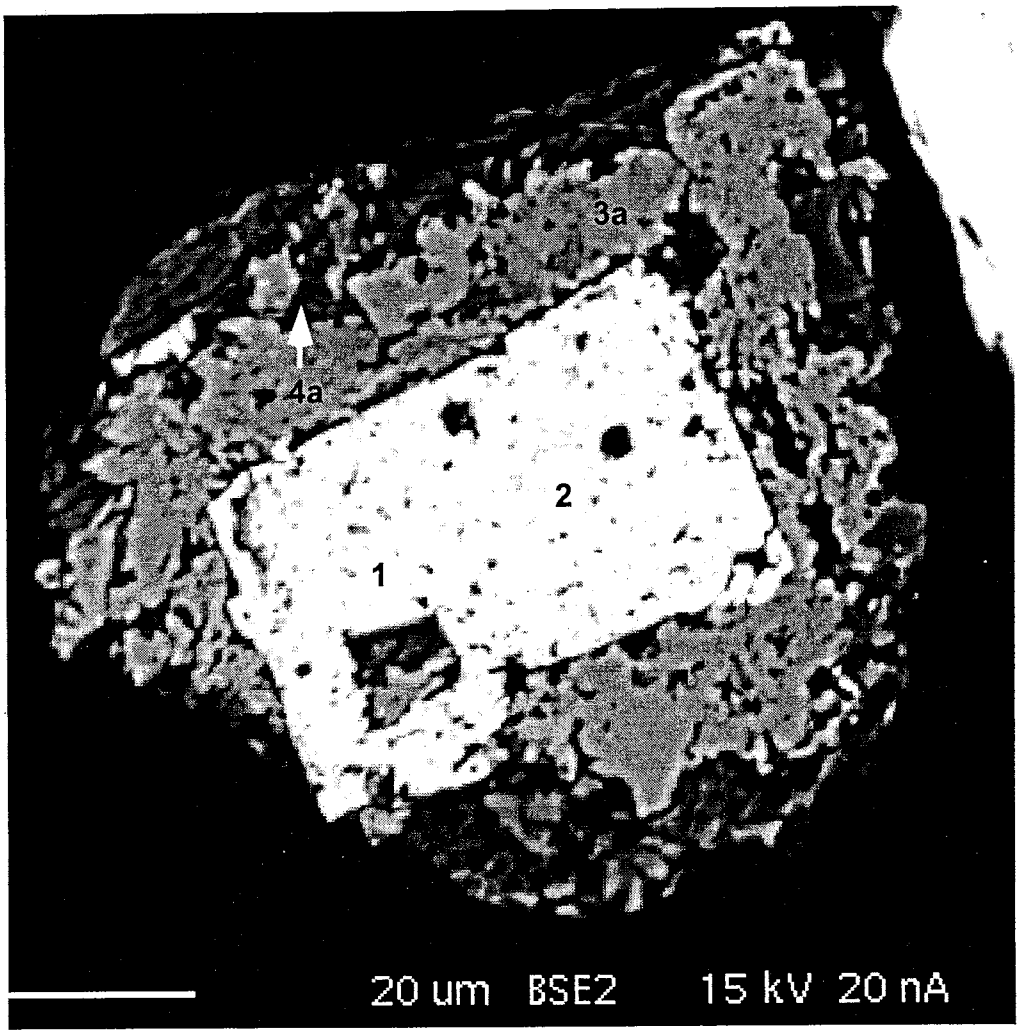


Figure 11. Back-scattered electron microprobe image of hematite core showing ilmenite rim and minor clay rind constituents in a heavy mineral separate grain mount from a placer gold waste rock pile (Site A). This is interpreted as a hydrothermal replacement of pyrite (points 1 and 2) by hematite followed by a later stage hydrothermal event to create the ilmenite rim (point 3a) which is then followed by minor clay rind formation (point 4a) from surficial weathering. Electron microprobe analyses for this image are designated by the numbers 1, 2, 3a, and 4a after the prefix (pic 10) in Appendix E, Table E.14a.

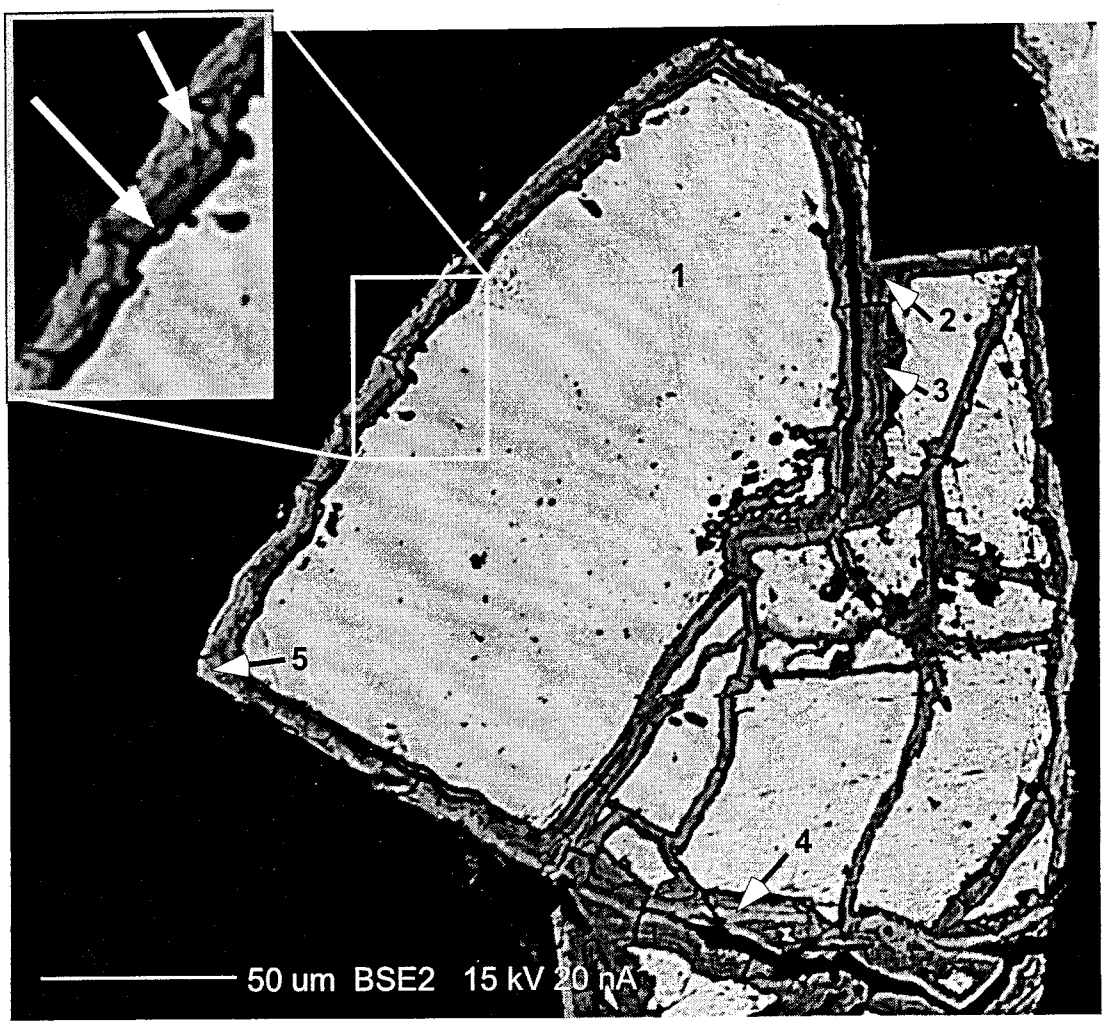


Figure 12. Back-scattered electron microprobe image of an oxidized pyrite grain with Fe-hydroxide and Fe-sulfate rinds of low and high atomic mean number from the Laramide polymetallic vein waste rock pile (Site B). The pyrite is in a heavy mineral separate grain mount. Brecciated parts of this grain are interpreted to have undergone hydrothermal fracturing and subsequent Fe-hydroxide and sulfate cementation. The pristine part of the grain is interpreted to have formed by weathering Electron microprobe analyses for this image are designated by the numbers 1, 2, 3, 4, and 5 after the prefix (pic 23) in Appendix E, Table E.14a.

The large initial loss in sulfur from the core to the first rind can be accounted for by the production of sulfuric acid during oxidation. The outer rind shows an increase in sulfur relative to the interior rind.

Table 10. Electron microprobe chemical analyses of pyrite grain (Fig. 12), pyrite ghost grain (Fig.13), chalcopyrite grain (Fig. 14), and two pyrite grains in Site E (Figs. 18 and 19)

| Location | Fe (%) | S (%) | As (%) | Cu (%) |
|---|---|---|---|---|
| Fig. 12 - pyrite core | 46.4 | 53.6 | trace | na |
| Fig. 12 - pyrite rind #1 | 66.1 | 1.4 | trace | na |
| Fig. 12 - pyrite rind #2 | 69.8 | 2.2 | 0.34 | na |
| Fig. 13 - ghost core | 69.7 | trace | trace | 0.9 |
| Fig. 13 - ghost rind | 66.8 | 0.3 | trace | 0.9 |
| Fig. 14 - core | 29.6 | 33.7 | trace | 33.1 |
| Fig. 14 - rind #1 | 57.5 | 0.3 | trace | 3.4 |
| Fig. 14 - rind #2 | 53.8 | 0.2 | trace | 3.2 |
| Fig. 18 - pyrite core | 46.9 | 53.2 | trace | na |
| Fig. 18 - pyrite rind #1 | 62.9 | 3.5 | 0.6 | na |
| Fig. 18 - pyrite rind #2 | 57.3 | 3.4 | 0.2 | na |
| Fig. 19 - pyrite core | 47 | 52.9 | trace | na |
| Fig. 19 - pyrite rind | 67.3 | 5.9 | trace | na |

Pyrite has been brecciated but continued to keep the cubic structure of the original crystal (Fig. 13). Minor sulfur is present in the pyrite ghost (Table 10). Effectively, the pyrite ghost has become $Fe_2O_3$ and $Fe(OH)_3$ with some remnant sulfur.

Chalcopyrite found in this waste rock pile showed weathering rinds of similar chemistry to that of the pyrites. Figure 14 shows a chalcopyrite grain and weathering rind (Table 10).

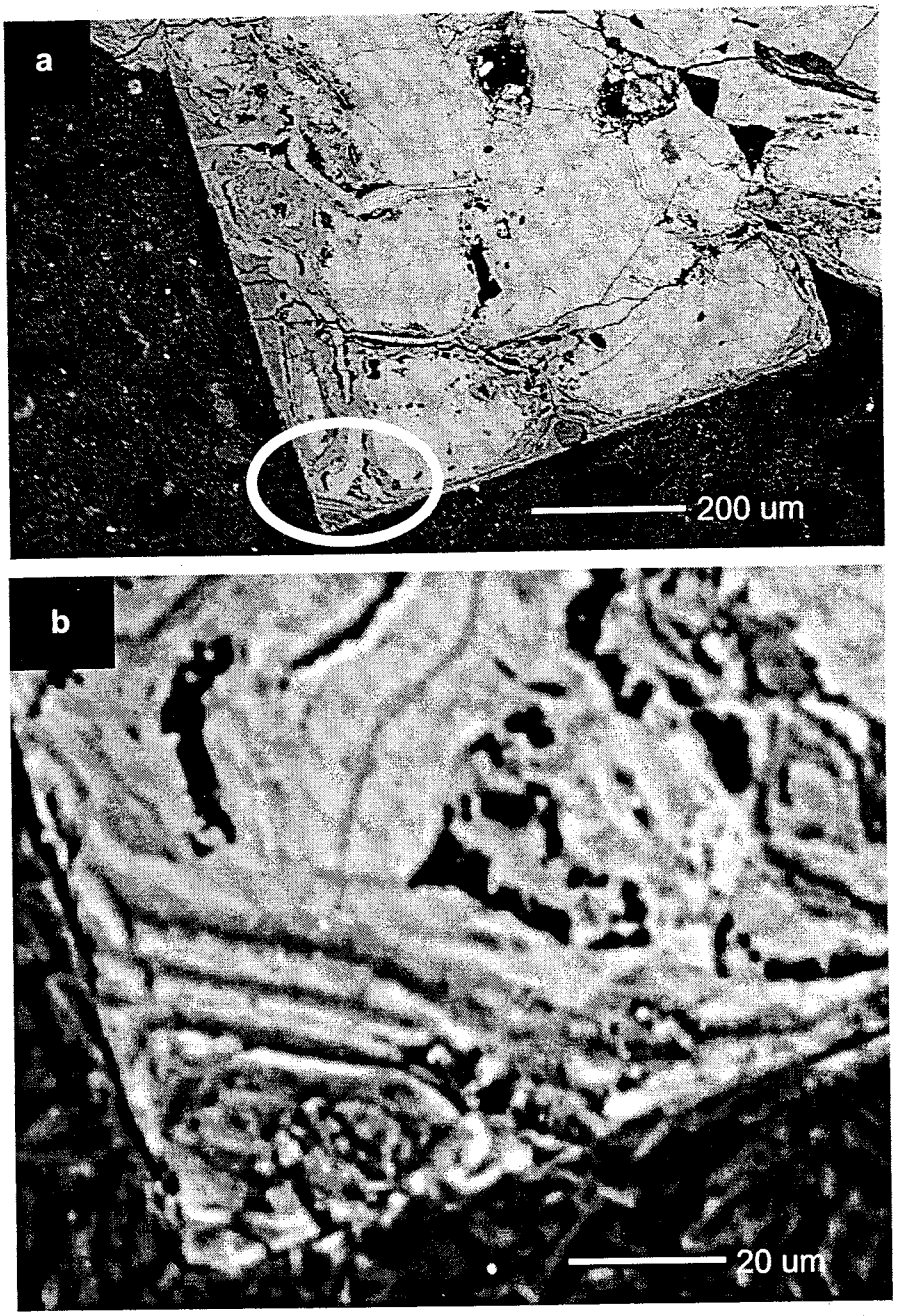


Figure 13. Figure a is a back-scattered electron microprobe image of heavily weathered or hydrothermally altered pyrite ghost from the Laramide polymetallic vein waste rock pile (Site B). Figure b is a back-scatter electron microprobe image magnification of Fe-hydroxide on the corner of the pyrite grain in Figure a. The pyrite grain was analyzed from a polished thin section.

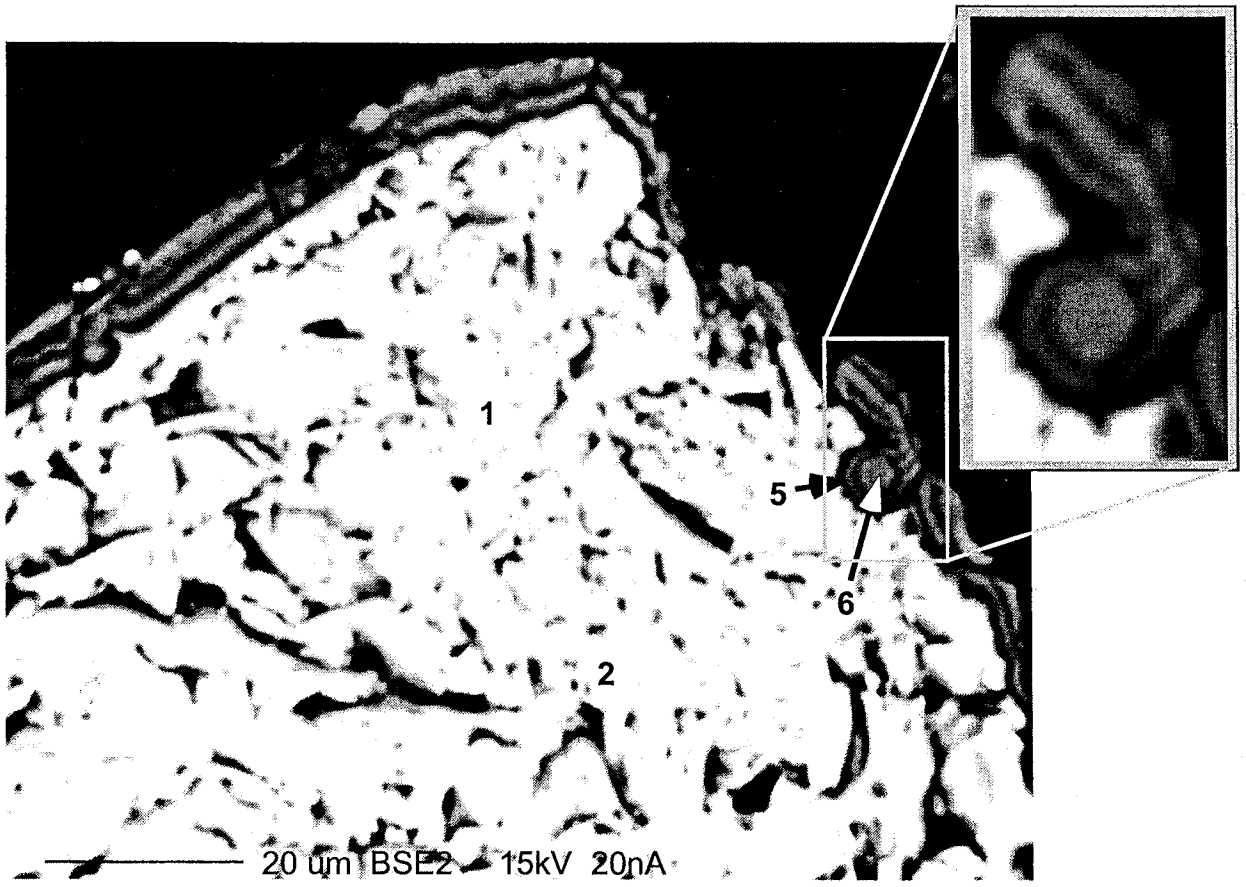


Figure 14. Back-scattered electron microprobe image of a chalcopyrite grain with 2 Fe/Cu-hydroxide rinds (high and low mean atomic number) from the Laramide polymetallic vein waste rock pile (Site B). The chalcopyrite is in a heavy mineral separate grain mount. I interpret the rind occurence is from weathering due to the pitted nature of the grain. Pitted features may be a result of slow destruction of the crystal lattice. Electron microprobe analyses for this image are designated by the numbers 1, 2, 5, and 6 after the prefix (pic 21) in Appendix E, Table E.14a.

### 8.3.1.3 Lead-Zinc Waste Rock Pile (Site C)

This waste rock pile contains a variety of lead-bearing minerals. Cerussite and galena are two minerals that contain oxidation rinds. Galena has two alteration phases, anglesite and cerussite most likely due to oxidation by hydrothermal fluids (Fig. 15). Table 11 shows chemical data gathered for a galena grain and its oxidation products.

Table 11. Electron microprobe analyses for galena and oxidation products (Fig. 15), and cerussite core and outer rind (Fig. 16).

| Location | Pb (%) | Zn (%) | S (%) | As (%) | Si (%) |
|---|---|---|---|---|---|
| Fig. 15 - galena | 86.6 | trace | 13.0 | trace | na |
| Fig. 15 - anglesite | 66.0 | trace | 5.9 | trace | na |
| Fig. 15 - cerussite | 78.4 | trace | nd | trace | na |
| Fig. 16 - core | 79.4 | na | na | na | 0.3 |
| Fig. 16 - rind | 78.5 | na | na | na | 0.3 |

Figure 16 shows a core and rind of similar chemistry but of very different textures. The core is composed of cerussite with pyromorphite inclusions while the rind is pure cerussite. The close similarities in the core versus the rind of the cerussite grain in Figure 16 can be seen with the comparison of quantitative points from each part of the grain in Table 11.

### 8.3.1.4 Silver-Manganese Waste Rock Pile (Site D)

This site is dominated by black manganese oxide minerals (mostly psilomelane). Samples exhibited some chemical differences within the grains, but also contained a thin clay weathering rind. The outermost rind of the lead-bearing manganese oxide grain (coronadite) contains some element constituents such as Si, Ca, Mg, and Al that are found in clay minerals (Fig. 17).

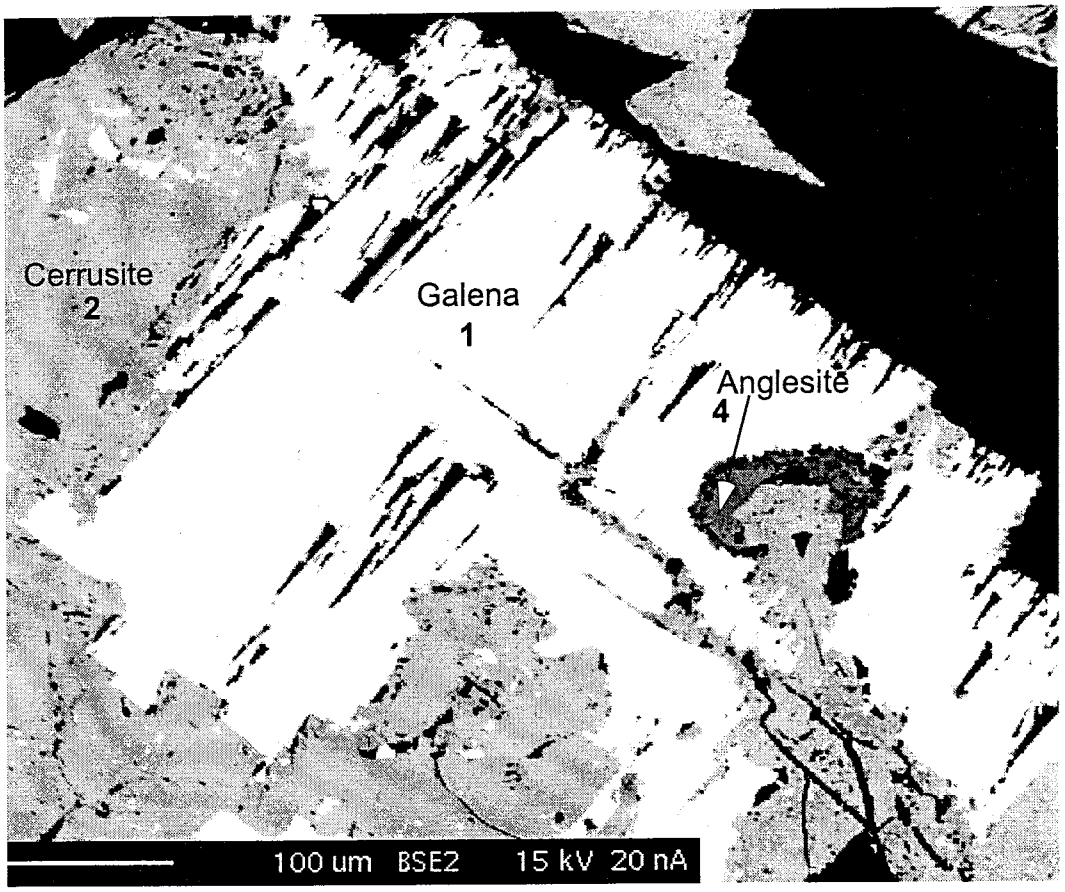


Figure 15. Back-scattered electron microprobe image of galena replaced and rimmed by cerussite and replaced by anglesite from the carbonate-hosted Pb-Zn waste rock pile (Site C). Due to the pervasive nature of the rind and its thichness, the galena grain is interpreted to have undergone hydrothermal alteration to anglesite and cerussite because the cerussite alteration appears to follow the crystal planes of the galena. Electron microprobe analyses for this image are designated by the numbers 1, 2, and 4 after the prefix (pic 13) in Appendix E, Table E.14b.

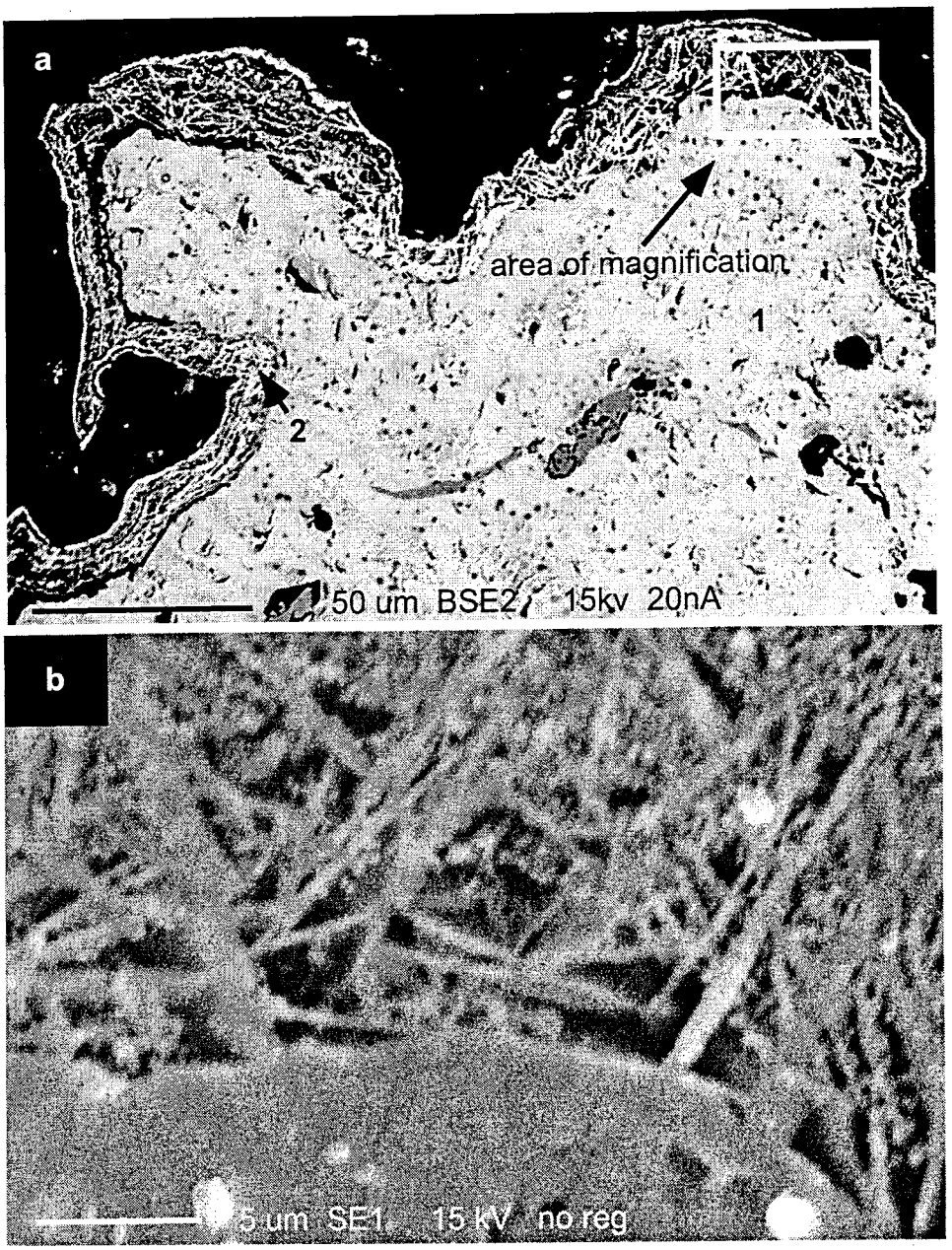


Figure 16. Figure a is a back-scattered electron microprobe image of cerussite core with pyromorphite inclusions and a cerussite rind from the carbonate-hosted Pb-Zn waste rock pile (Site C). The cerussite is in a heavy mineral separate grain mount. Figure b, a scanning electron microprobe image, shows a magnification of the different texture and crystal habit of cerussite in a rind. The rind appears to be a growth texture from the main core. I interpret the rind to be of hydrothermal origin due to its thickness and degree of crystallinity. Electron microprobe analyses for this image are designated by the numbers 1 and 2 after the prefix (pic 16) in Appendix E, Table E.14b.

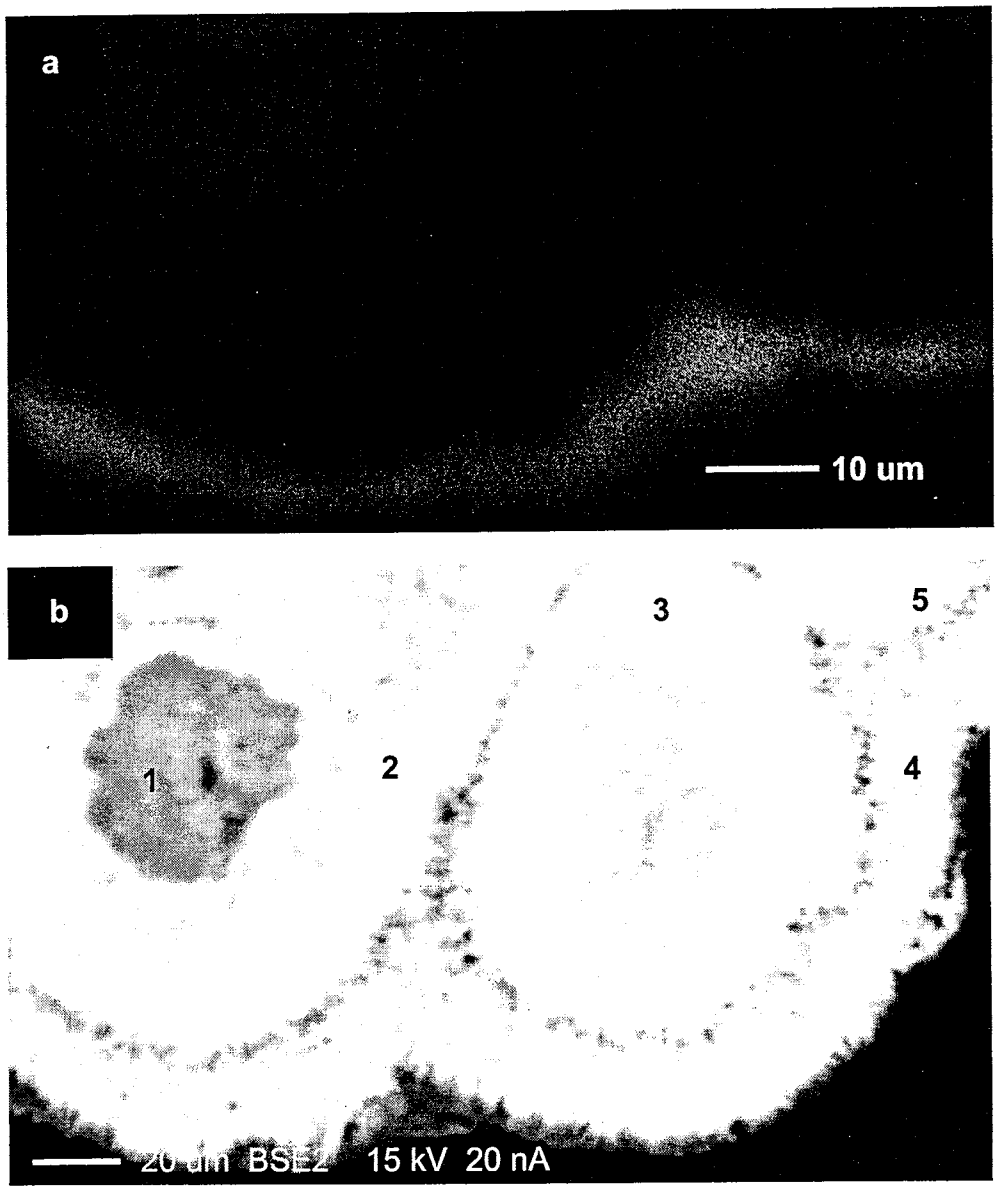


Figure 17. Figure a is a Si X-ray map of the clay rind at the bottom of Figure b. Figure b is a back-scattered electron microprobe image of manganese oxide with a botroidal texture, different chemical zones within the crystal, and clay weathering rinds from the carbonate-hosted Ag-Mn waste rock pile (Site D). This grain is from a heavy mineral separate grain mount. I interpret the silica rich rind around the manganese oxide is a clay formed from weathering due to the relative chemical inertness of the grain. Electron microprobe analyses for this image are designated by the numbers 1, 2, 3, 4, and 5 after the prefix (pic 19) in Appendix E, Table E.14a and 14b.

#### 8.3.1.5 Northern Laramide Polymetallic Vein Waste Rock Pile (Site E)

Pyrite oxidation rind textures are different at Sites E and B. A pyrite grain, typical of Site E, has a much thicker oxidation rind than pyrites found in Site B (Fig. 18). Fe, S, and As concentrations differ from oxidation rinds in Site B and Site E (Table 10). A pyrite grain from Site E has chalcopyrite inclusions (Fig. 19). Site E is a smaller volume waste rock pile than Site B but both contain similar mineralogies. Weathering rinds on these grains contain iron oxides, iron hydroxides, iron oxyhydroxides, and iron sulfates. Analysis of the grain and oxidation rind indicates several iron sulfate rinds of varying chemical composition may be forming during the oxidation of the pyrite grain (Fig. 18). Arsenic is preferentially concentrated in the weathering rinds. Pyrite oxidation shows a higher sulfur concentration most likely in the form of iron sulfate (Fig. 19). The rind thickness varies (Fig. 18, 19).

### 8.4 CHEMICAL ANALYSES OF WASTE ROCK PILES

#### 8.4.1 Grain Size Fractions

Chemical analyses by FAAS and XRF of six size fractions (2-1 mm, 1-0.5 mm, 0.5-0.25 mm, 0.25-0.125 mm, 0.125-0.063 mm, and < 0.063 mm) indicated the less than 0.25 mm grain size typically contained the highest metal concentration (Table 12). The less than 0.25 mm grain size contained the highest metal concentrations 50%, 87%, 87%, and 89% of the time for copper, lead, zinc, and arsenic respectively in the waste rock piles sampled. Chemical analyses for each of the waste rock piles are shown in Table 12. Six size fractions from the waste rock piles were analyzed for copper, lead, zinc and arsenic (Figs. 20, 21, 22, 23, 24, 25).

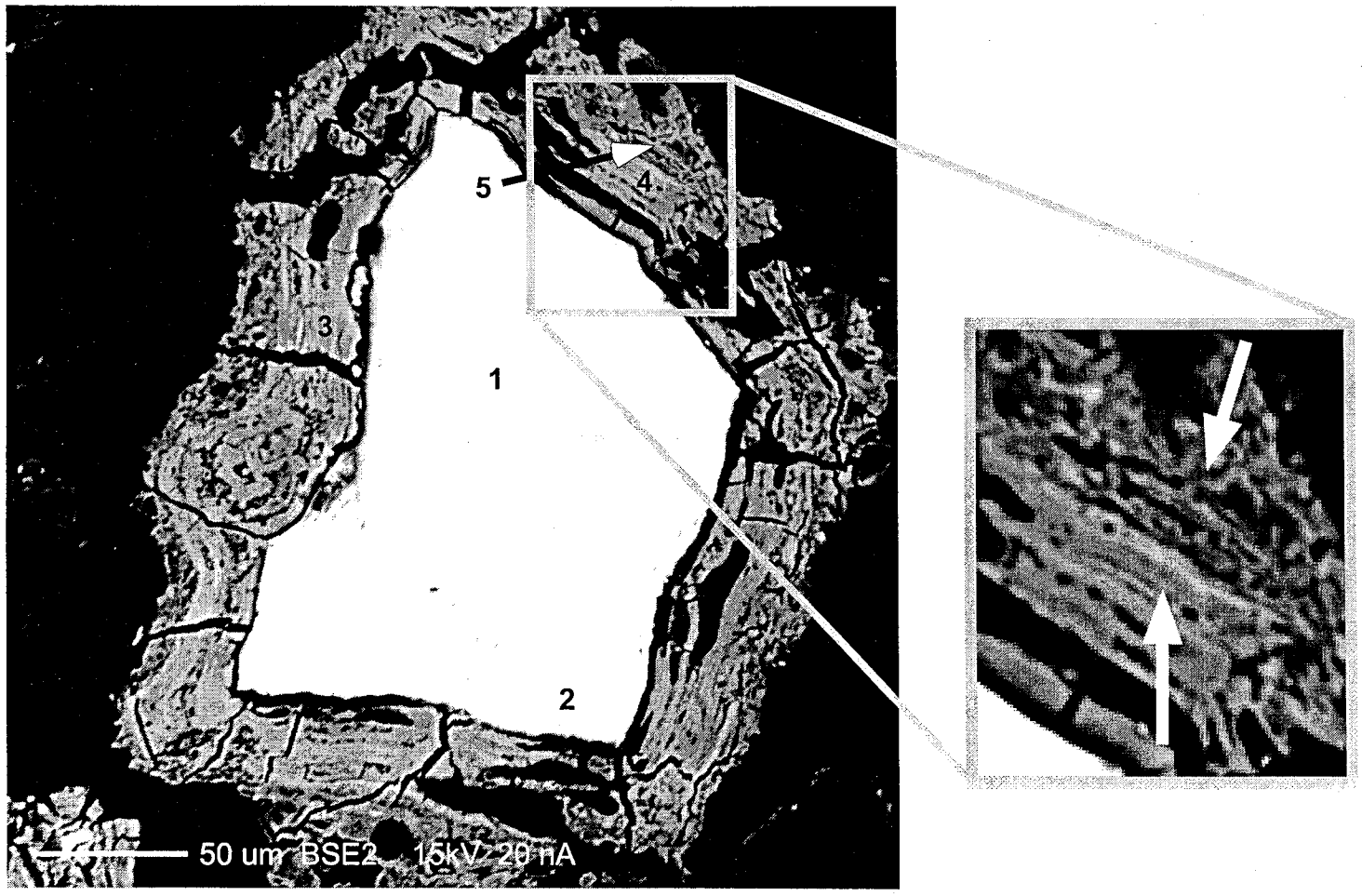


Figure 18. Back-scattered electron microprobe image of a pyrite grain with thick Fe-hydroxide and iron sulfate rinds from the northern Laramide polymetallic vein waste rock pile (Site E). The pyrite is from a heavy mineral separate grain mount. I interpret the rinds on the surface of the pyrite grain to have originally formed by hydrothermal alteration. I interpret that later weathering may have increased the thickness of the rind. Electron microprobe analyses for this image are designated by the numbers 1 - 5 after the prefix (pic 24) in Appendix E, Table E.14a.

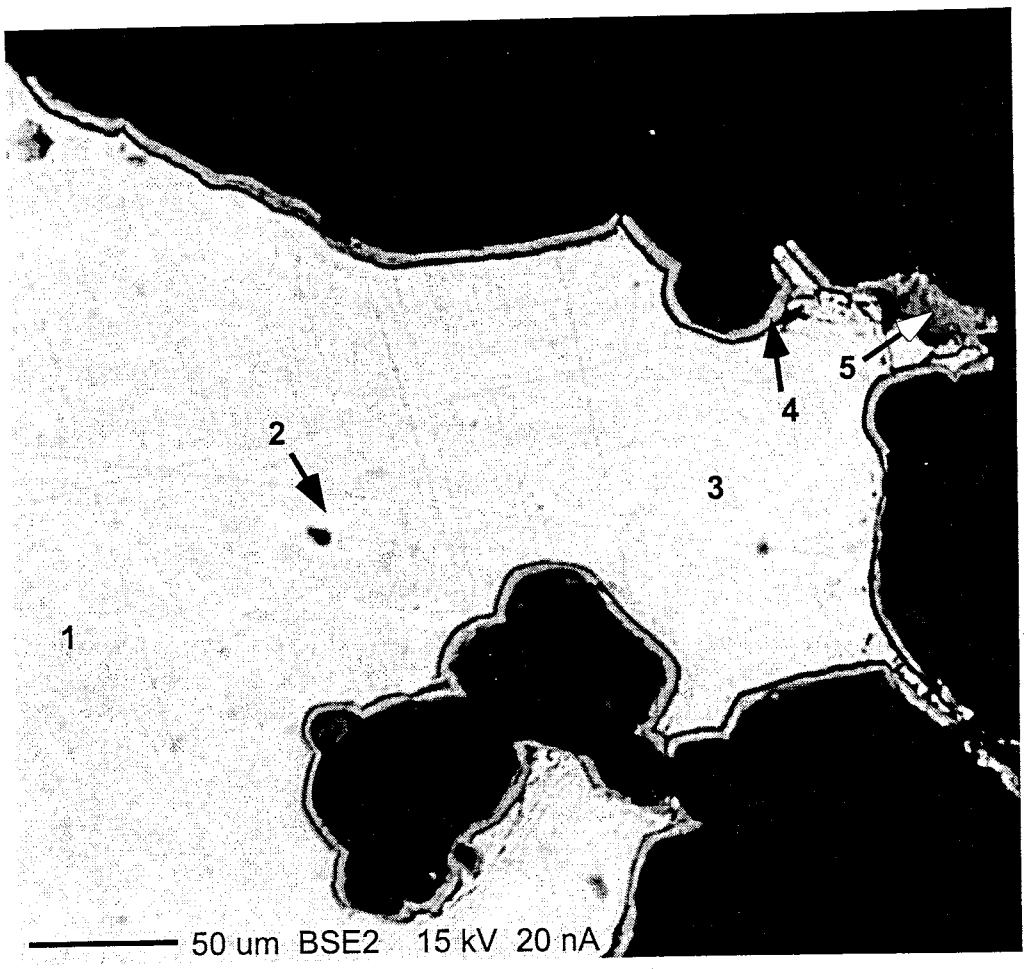


Figure 19. Back-scattered electron image of pyrite with "swiss chesse" hackly texture; also with thin Fe-sulfate rind from northern Laramide polymetallic vein waste rock pile (Site E). The pyrite is in a heavy mineral separate grain mount. Chalcopyrite inclusions are scattered throughout. I interpret the pyrite to have been in a part of the waste rock pile that may have produced more acid from other pyrite grains with rinds. The motteled texture may have been created by locally high sulfuric acid concentrations. Another interpretation is a late stage hydrothermal event. Electron microprobe analyses for this image are designated by the numbers 1 - 5 after the prefix (pic 26) in Appendix E, Table E.14a.

Samples from Site E were analyzed and compared to Site B (Figs. 26, 27). Analyses of the less than 0.25 mm grain size coincided with a relative low weight percentage of the total waste rock pile. Weight percent of the less than 0.25 mm grain size in Site A = 15.1%, Site B = 7.6%, Site C = 10.6%, and Site D = 15.5% were analyzed and show a chemistry of only a specific grain size range, representing less than 20% of the total waste rock pile weight.

Chemical analyses of different size fractions of the placer gold waste rock pile (Site A) yield a slight increase in copper concentration from the coarsest to the finest size fraction, and a peak for lead in the 0.25-0.125 mm and 0.125-0.063 mm size fraction ranges (Figs. 20,21). There is also an overall increase in zinc with a decrease in size fraction, with little change occurring for arsenic. Chemical analyses of different size fractions of the Laramide polymetallic vein waste rock pile (Site B) show a decrease in copper concentration with a decrease in grain size (Figs. 22, 23). Perhaps the main reason for this trend is the occurrence of chalcopyrite as the primary copper mineral in the Laramide polymetallic vein deposit. Chalcopyrite weathering is further supported by the chemical grain size analyses of Sites B and E. Copper is found in highest concentration in the 2-1 and 1-0.5 mm size fraction ranges at Site B because the waste rock pile may be younger and /or the initial mineralogy may be different from Site E (Fig.22). Lead increases with decreasing grain size while zinc and arsenic remain the same. However, arsenic values from XRF data show a gradual increase in concentration with decreasing grain size (Fig. 23). In the carbonate-hosted Pb-Zn waste rock pile (Site C), copper increases with decreasing grain size while lead, zinc, and arsenic concentrations peak at 0.25-0.125 mm range and then decrease towards the finest size

fraction (Fig. 24). The carbonate-hosted Ag-Mn waste rock pile (Site D) has similar copper and arsenic concentrations for all size fractions. Lead and zinc, however, follow the same trend as the carbonate-hosted Pb-Zn waste rock pile (Fig. 25). In the northern Laramide polymetallic vein waste rock pile (Site E), copper, lead, zinc, and arsenic concentrations increase with decreasing grain size (Figs. 26, 27). In Site E (the older waste rock pile) the highest copper concentration is found in the < 0.063 mm size fraction (Fig. 26).

Table 12. FAAS and XRF chemical analyses of six size fractions on five waste rock piles. Duplicate and triplicates for FAAS analyses were typically ± 15% while duplicate and triplicate XRF analyses were typically ± 2%. (na) designates concentrations unable to be determined by XRF.

| Waste Rock Pile | Particle Size | Cu (ppm) | | Pb (ppm) | | Zn (ppm) | | As (ppm) | |
|---|---|---|---|---|---|---|---|---|---|
| | | FAAS | XRF | FAAS | XRF | FAAS | XRF | FAAS | XRF |
| SITE A | 2-1 mm | 130.0 | 80.0 | 20.0 | 20.0 | 120.0 | 71.0 | 2.4 | 5.0 |
| | 1-0.5 mm | 130.0 | 87.0 | 20.0 | 21.0 | 75.0 | 77.0 | 2.3 | 4.0 |
| | 0.5-0.25 mm | 160.0 | 96.0 | 20.0 | 23.0 | 115.0 | 87.0 | 3.0 | 5.0 |
| | 0.25-0.125 mm | 140.0 | 102.0 | 20.0 | 25.0 | 145.0 | 110.0 | 2.1 | 5.0 |
| | 0.125-0.063 mm | 150.0 | 100.0 | 20.0 | 24.0 | 90.0 | 101.0 | 2.3 | 4.0 |
| | < 0.063 mm | 160.0 | 110.0 | 20.0 | 21.0 | 150.0 | 97.0 | 3.4 | 5.0 |
| | | | | | | | | | |
| SITE B | 2-1 mm | 1140.0 | 860.0 | 80.0 | 73.0 | 450.0 | 462.0 | 5.7 | 15.0 |
| | 1-0.5 mm | 1080.0 | 920.0 | 80.0 | 81.0 | 400.0 | 411.0 | 10.0 | 28.0 |
| | 0.5-0.25 mm | 900.0 | 790.0 | 80.0 | 94.0 | 380.0 | 392.0 | 11.0 | 34.0 |
| | 0.25-0.125 mm | 910.0 | 820.0 | 110.0 | 124.0 | 410.0 | 458.0 | 11.0 | 33.0 |
| | 0.125-0.063 mm | 780.0 | 810.0 | 120.0 | 160.0 | 440.0 | 464.0 | 9.3 | 35.0 |
| | < 0.063 mm | 760.0 | 760.0 | 180.0 | 218.0 | 440.0 | 477.0 | 9.4 | 35.0 |
| | | | | | | | | | |
| SITE C | 2-1 mm | 130.0 | 98.0 | 42450.0 | na | 70210.0 | na | 20.0 | na |
| | 1-0.5 mm | 160.0 | 186.0 | 72250.0 | na | 88780.0 | na | 33.0 | na |
| | 0.5-0.25 mm | 190.0 | 286.0 | 75710.0 | na | 95100.0 | na | 54.0 | na |
| | 0.25-0.125 mm | 220.0 | 365.0 | 73640.0 | na | 99170.0 | na | 83.0 | na |
| | 0.125-0.063 mm | 240.0 | 308.0 | 51010.0 | na | 64780.0 | na | 75.0 | na |
| | < 0.063 mm | 250.0 | 294.0 | 28140.0 | na | 43470.0 | na | 52.0 | na |
| | | | | | | | | | |
| SITE D | 2-1 mm | 120.0 | na | 1500.0 | na | 1710.0 | na | 4.0 | na |
| | 1-0.5 mm | 130.0 | na | 1700.0 | na | 1910.0 | na | 6.8 | na |
| | 0.5-0.25 mm | 110.0 | na | 1840.0 | na | 1950.0 | na | 6.7 | na |
| | 0.25-0.125 mm | 120.0 | na | 1770.0 | na | 1900.0 | na | 7.8 | na |
| | 0.125-0.063 mm | 120.0 | na | 1800.0 | na | 1810.0 | na | 8.9 | na |
| | < 0.063 mm | 90.0 | na | 1470.0 | na | 1520.0 | na | 6.7 | na |
| | | | | | | | | | |
| SITE E | 2-1 mm | 210.0 | 152.0 | 30.0 | 23.0 | 30.0 | 37.0 | 16.0 | 31.0 |
| | 1-0.5 mm | 220.0 | 161.0 | 30.0 | 26.0 | 30.0 | 40.0 | 30.0 | 49.0 |
| | 0.5-0.25 mm | 250.0 | 201.0 | 30.0 | 36.0 | 40.0 | 45.0 | 56.0 | 72.0 |
| | 0.25-0.125 mm | 290.0 | 232.0 | 40.0 | 41.0 | 40.0 | 52.0 | 73.0 | 97.0 |
| | 0.125-0.063 mm | 320.0 | 278.0 | 50.0 | 56.0 | 60.0 | 60.0 | 105.0 | 122.0 |
| | < 0.063 mm | 400.0 | 357.0 | 70.0 | 91.0 | 70.0 | 78.0 | 148.0 | 176.0 |

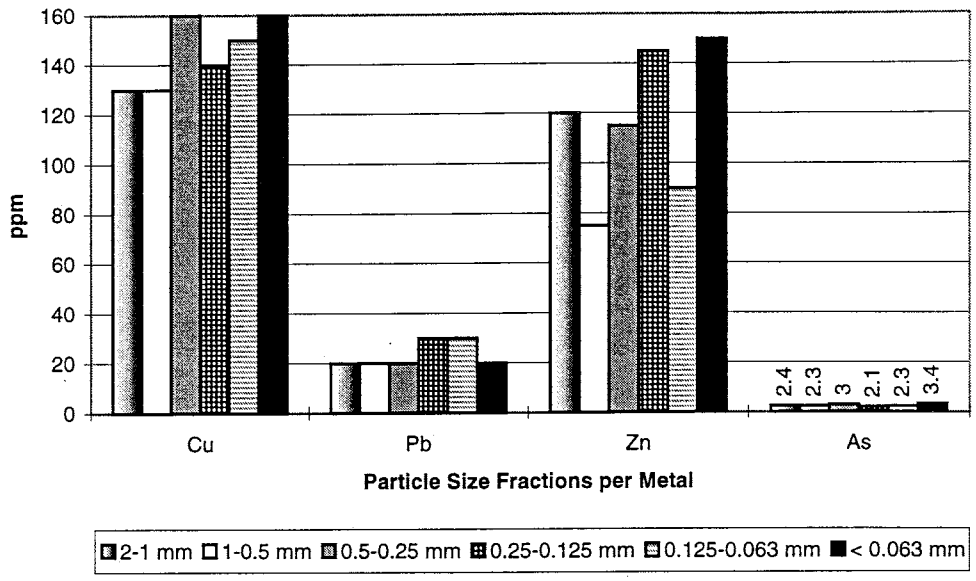


Figure 20. Chemical analyses of six size fractions of the placer gold waste rock pile (Site A) by FAAS. Note the increasing Cu and Zn concentrations with decreasing grain size.

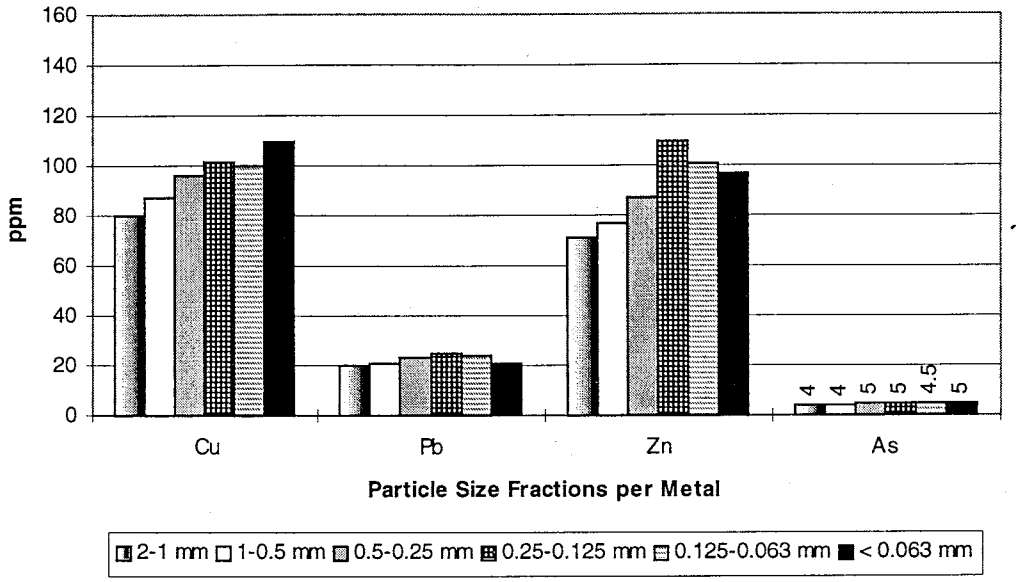


Figure 21. Chemical analyses of six size fractions of the placer gold waste rock pile (Site A) by XRF. Note that similar trends in concentration were obtained as by FAAS (Fig. 10).

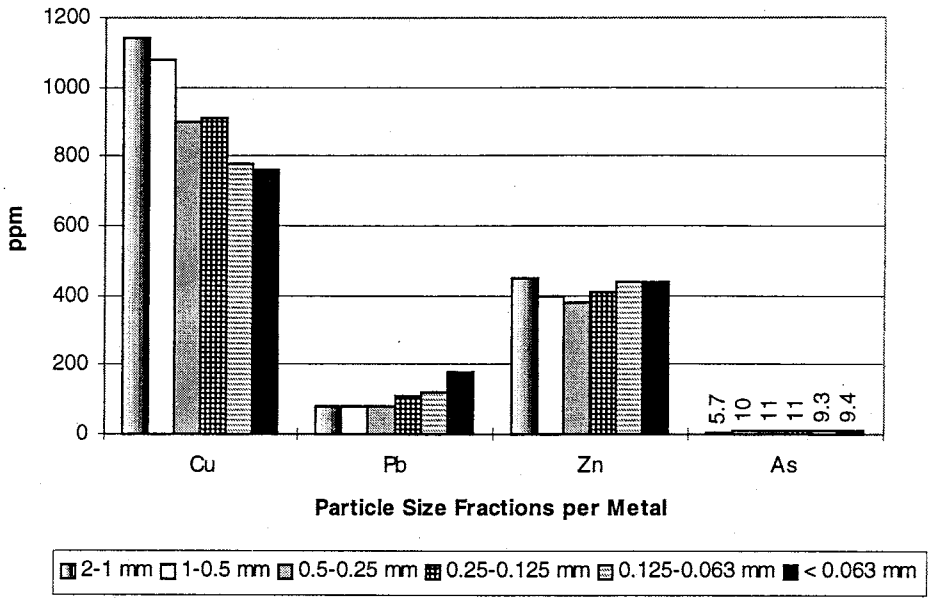


Figure 22. Chemical analyses of six size fractions of the Laramide vein waste rock pile (Site B) by FAAS. Note the decrease in concentration in Cu and increase in Pb with decreasing grain size.

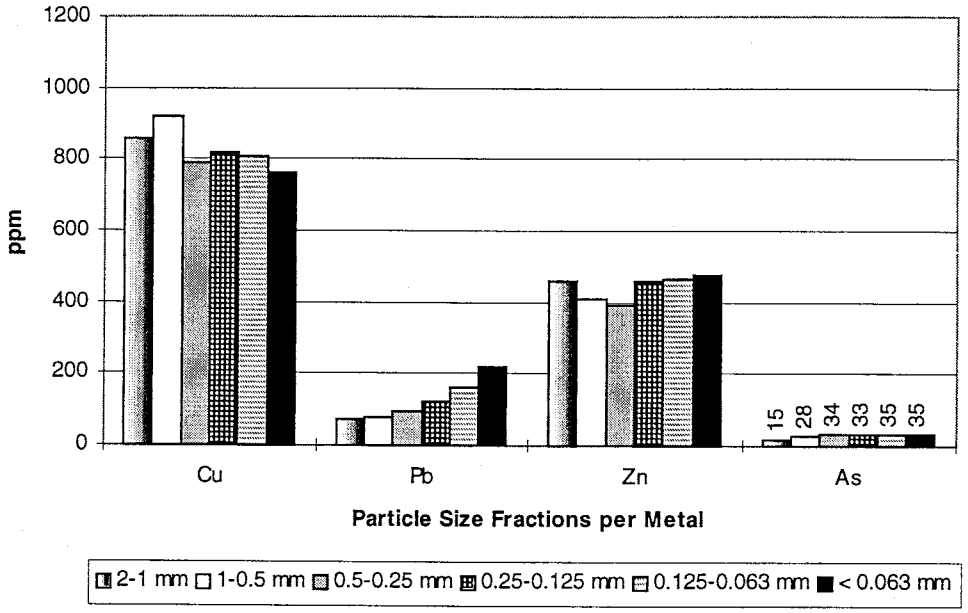


Figure 23. Chemical analyses of six size fractions of the Laramide vein waste rock pile (Site B) by XRF. Note that similar trends in concentration were obtained as by FAAS (Fig. 12).

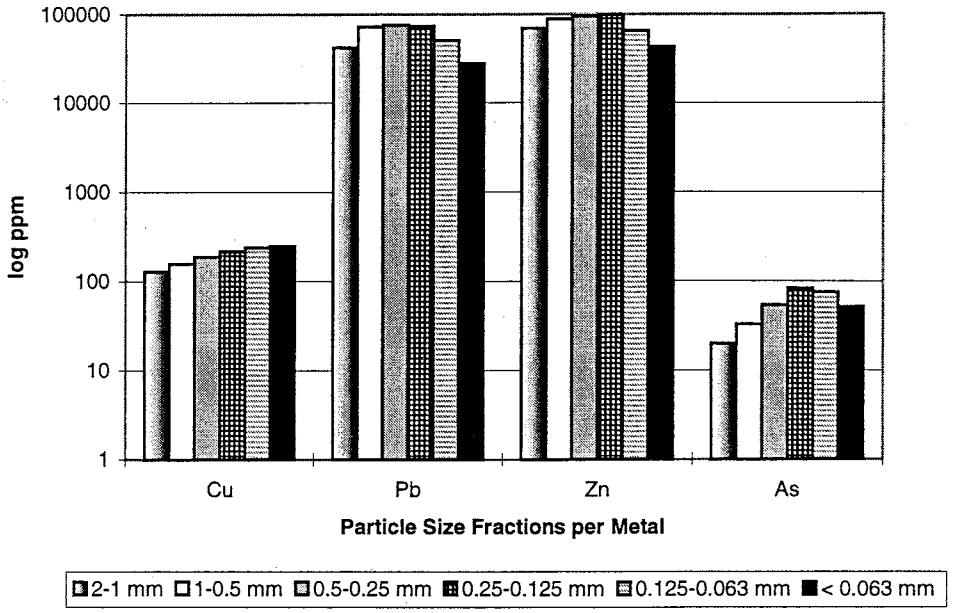


Figure 24. Chemical analyses of six size fractions of the carbonate-hosted Pb-Zn waste rock pile (Site C). Note the increase in Cu concentration with decreasing grain size and the peak in Pb, Zn, and As concentration at 0.25-0.125 mm grain size range.

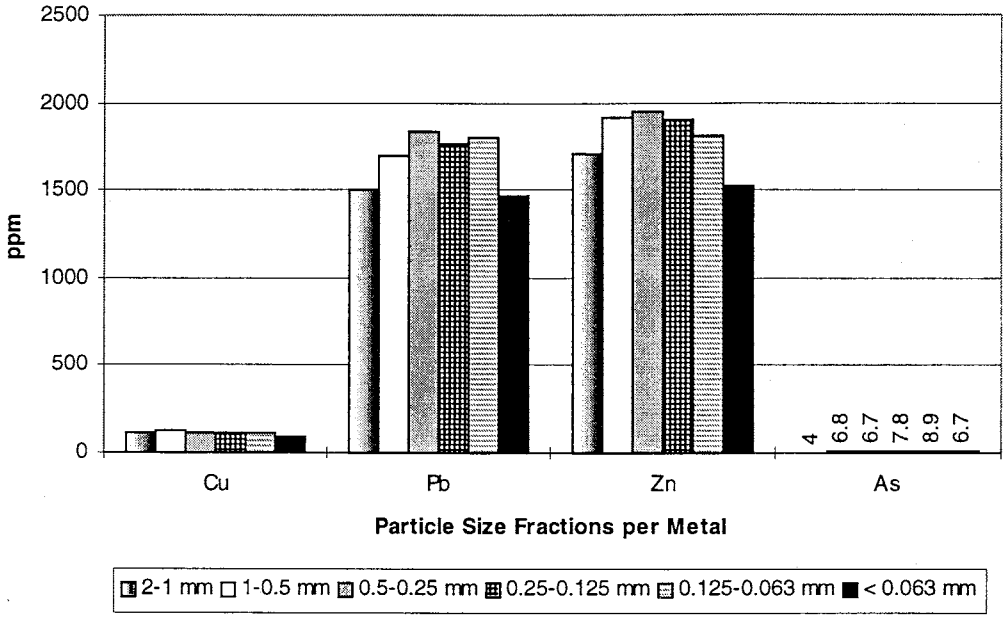


Figure 25. Chemical analyses of six size fractions of the carbonate-hosted Ag-Mn waste rock pile (Site D). Note the peak of Pb and Zn concentration at 0.25-0.125 mm grain size range.

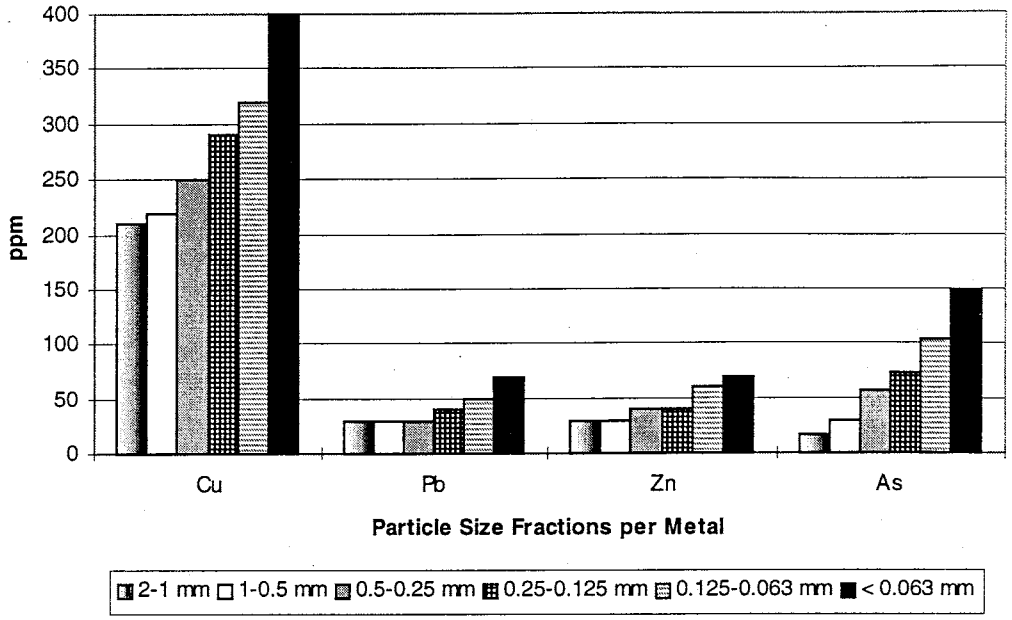


Figure 26. Chemical analyses using FAAS technique of six size fractions of the north Laramide vein waste rock pile (Site E). Note that all metal concentrations increase with decreasing grain size.

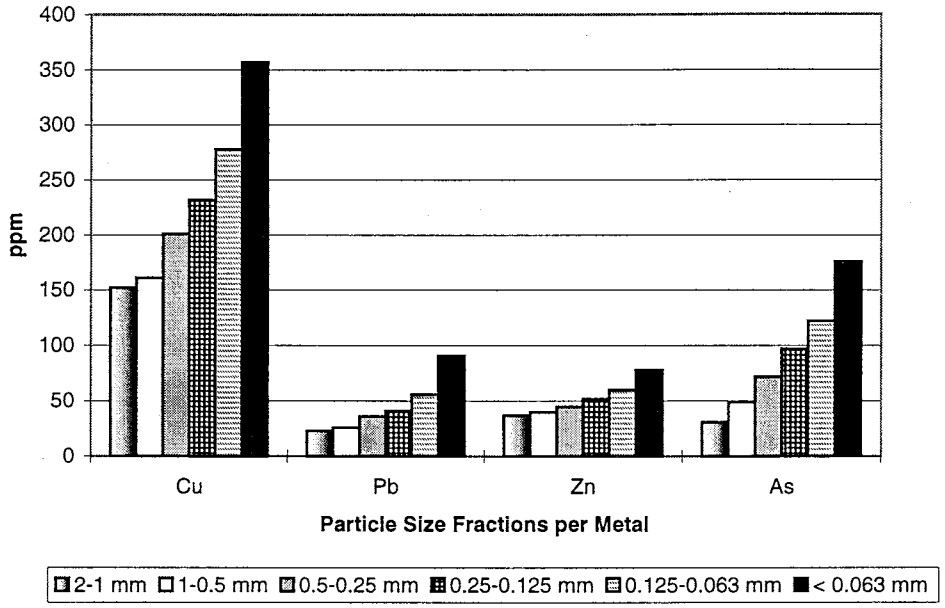


Figure 27. Chemical analyses using XRF technique of six size fractions of the north Laramide vein waste rock pile (Site E). Note that similar trends in concentration were obtained as by FAAS (Fig. 16).

### 8.4.2 Waste rock pile sampling densities

The geochemistry of each waste rock pile (Site A-D) is displayed as sampling density per given metal versus concentration (ppm) of copper in Figure 28, lead in Figure 29, zinc in Figure 30, and arsenic in Figure 31.

In most cases 15 to 30 sample cells per sampling pattern were found to adequately characterize the waste rock piles geochemically. This is supported by analyses from 45 individual samples in Site B for copper, lead, zinc, and arsenic (Figs. 32-35). Where the cumulative average coincides with the mean of the samples is the level of sampling which best characterizes the waste rock pile.

### 8.4.3 Waste rock pile heterogeneity

In addition to each of the grain size fractions, chemical heterogeneity is found within an entire waste rock pile. For example, 45 separate samples were analyzed by XRF for each of the sample sites on the grid of the Laramide polymetallic vein waste rock pile (Site B, Fig. 3). Copper concentrations range from 460-2700 ppm (Fig. 36, 37), lead from 73-730 ppm (Fig. 38, 39), zinc from 120-1400 (Fig. 40, 41), and arsenic from 4-76 ppm (Fig. 42, 43). Variations in metal concentrations indicate a heterogeneous waste rock pile. High copper and lead concentrations are located on the uphill side (samples 1, 16, 2, 17, and 3) and the top of the waste rock pile (samples 4, 5, and 20) which may indicate the original dumping pattern of the material (Figs. 37, 39). Zinc follows the trend of copper and lead but also shows high concentrations on the slope of the waste rock pile (samples 11, 28, 41, 42, and 13; Fig. 41). Arsenic concentrations are higher down gradient and down slope of high copper, lead, and zinc concentrations, as

designated by samples 31, 7, 9, 43, 10, 12, 14, and 33 which may indicate mobility within the waste rock pile (Fig. 43).

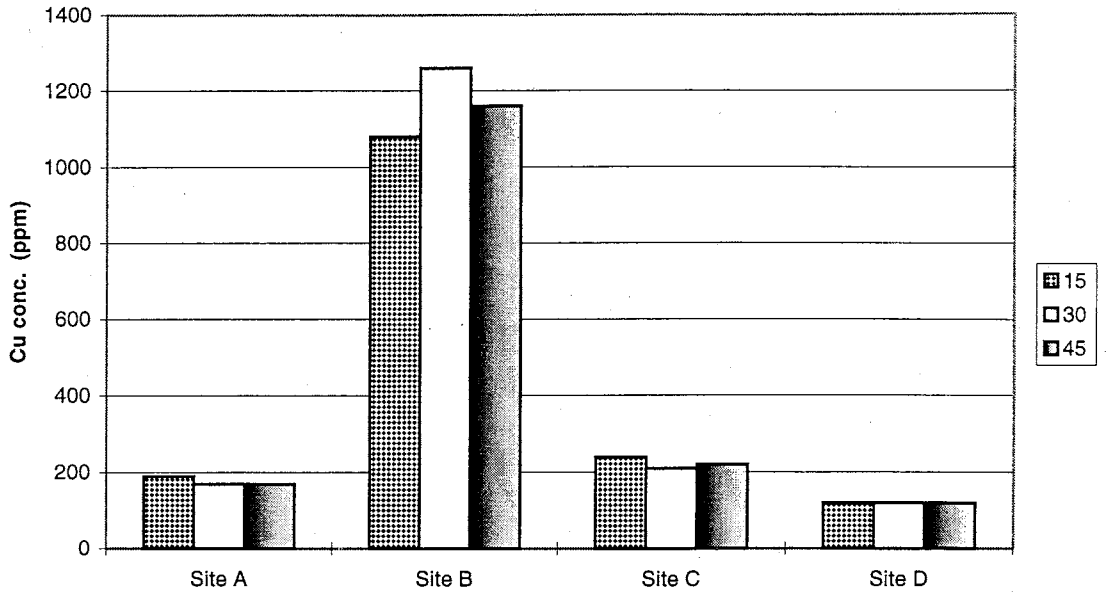


Figure 28. Copper concentrations (ppm) of homogenized samples representing three sampling densities (15, 30, 45) for Sites A-D. Note that metal concentrations are highest in the 15 or 30 samples per sampling grid pattern.

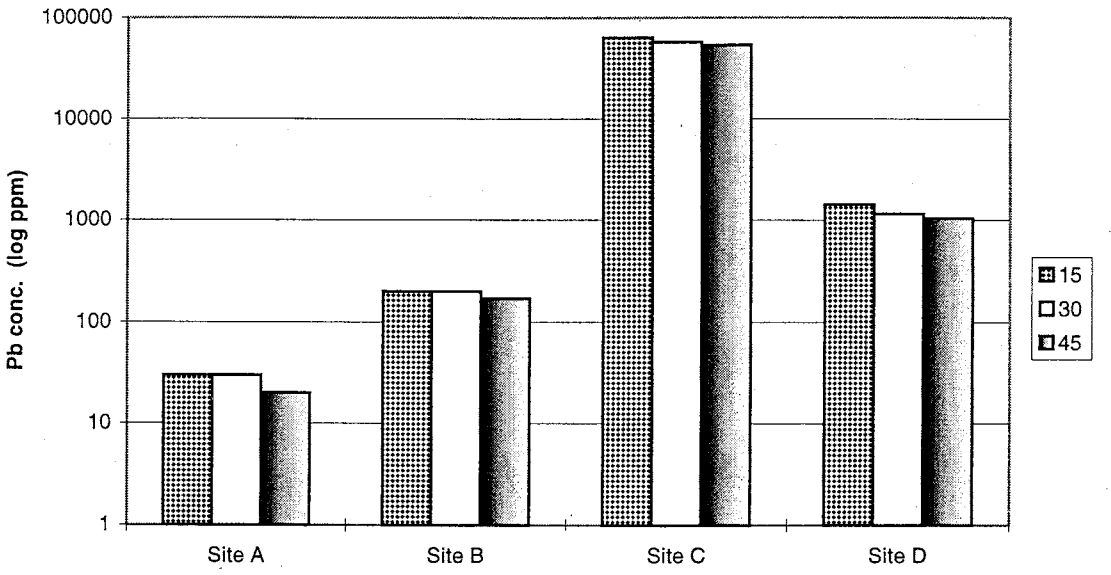


Figure 29. Lead concentrations (log ppm) of homogenized samples representing three sampling densities (15, 30, 45) for Sites A-D. Note that metal concentrations are highest in the 15 or 30 samples per sampling grid pattern.

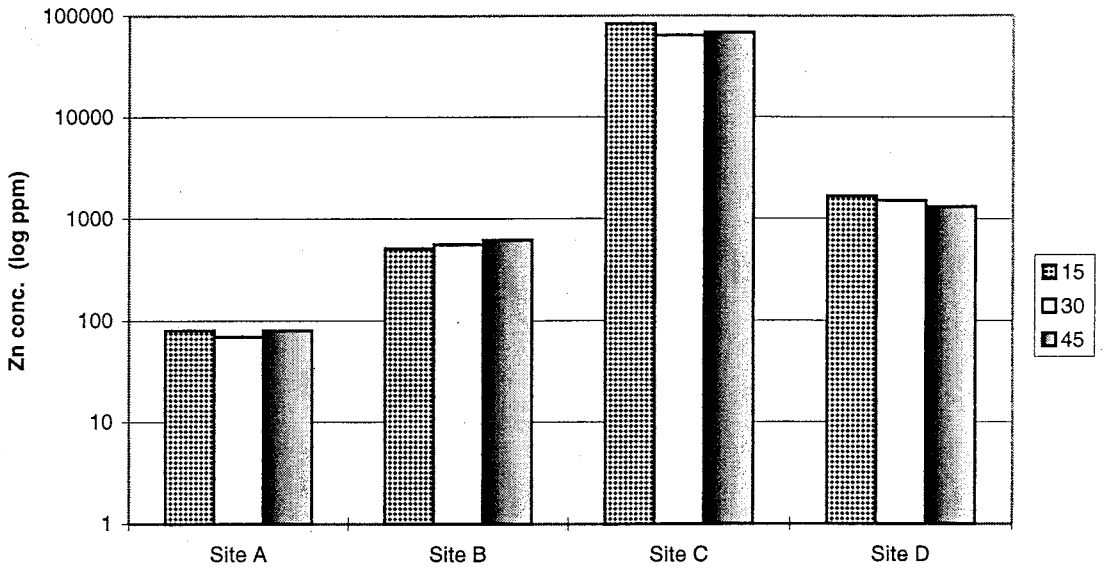


Figure 30. Zinc concentrations (log ppm) of homogenized samples representing three sampling densities (15, 30, 45) for Sites A-D. Note that typically the highest metal concentrations are obtained with 15 or 30 samples per sampling grid pattern.

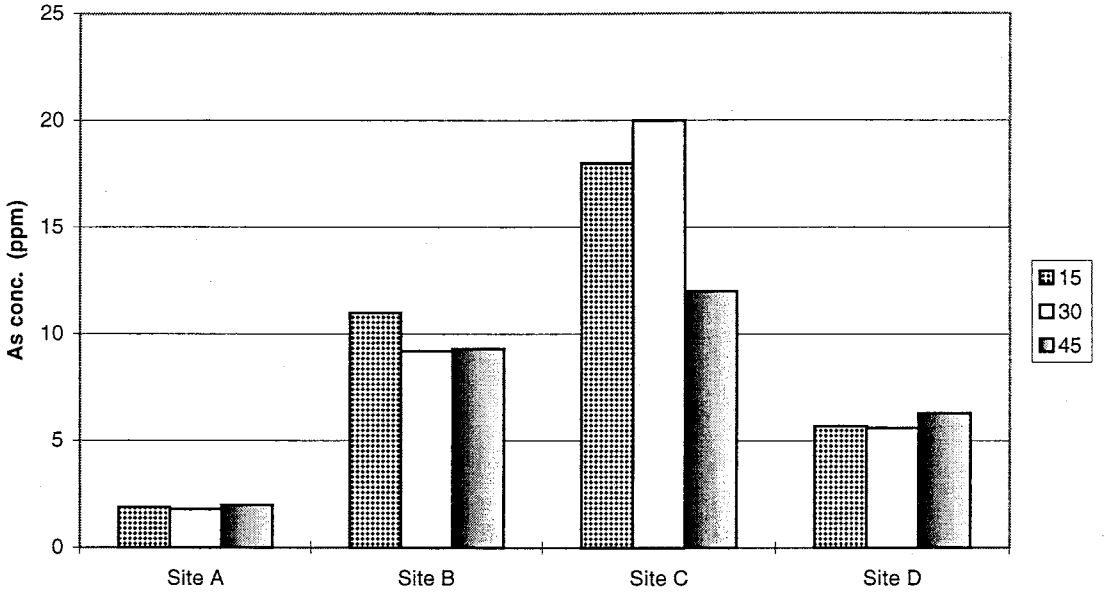


Figure 31. Arsenic concentrations (ppm) of homogenized samples representing three sampling densities (15, 30, 45) for Sites A-D. Note that typically the highest metal concentrations are obtained with 15 or 30 samples per sampling grid pattern.

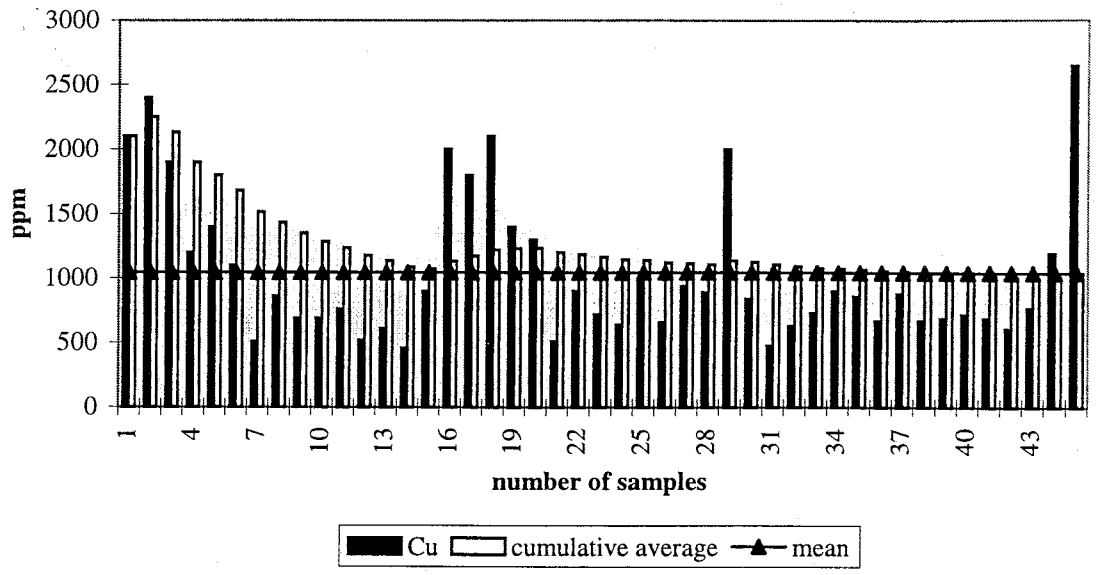


Figure 32. 45 samples from the Laramide polymetallic vein waste rock pile (Site B) individually analyzed for copper. Individual samples are plotted versus cumulative average and mean. Note that 15 or 30 samples coincide with the cumulative average and mean of the samples is approximately equal.

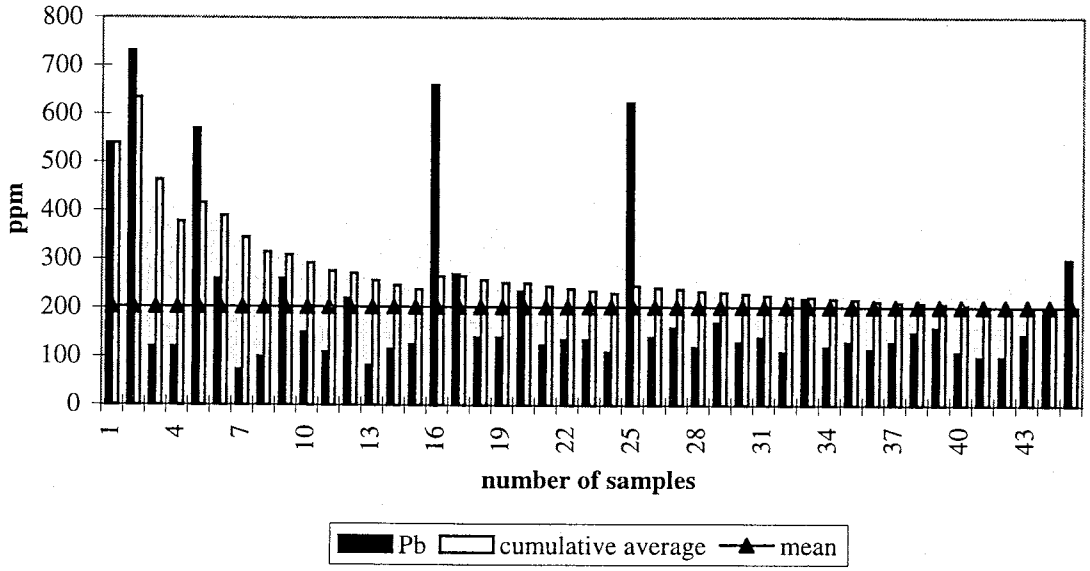


Figure 33. 45 samples from the Laramide polymetallic vein waste rock pile (Site B) individually analyzed for lead. Individual samples are plotted versus cumulative average and mean. Note that 45 samples instead of 15 or 30 coincide with a cumulative average and mean of the samples that is approximately equal.

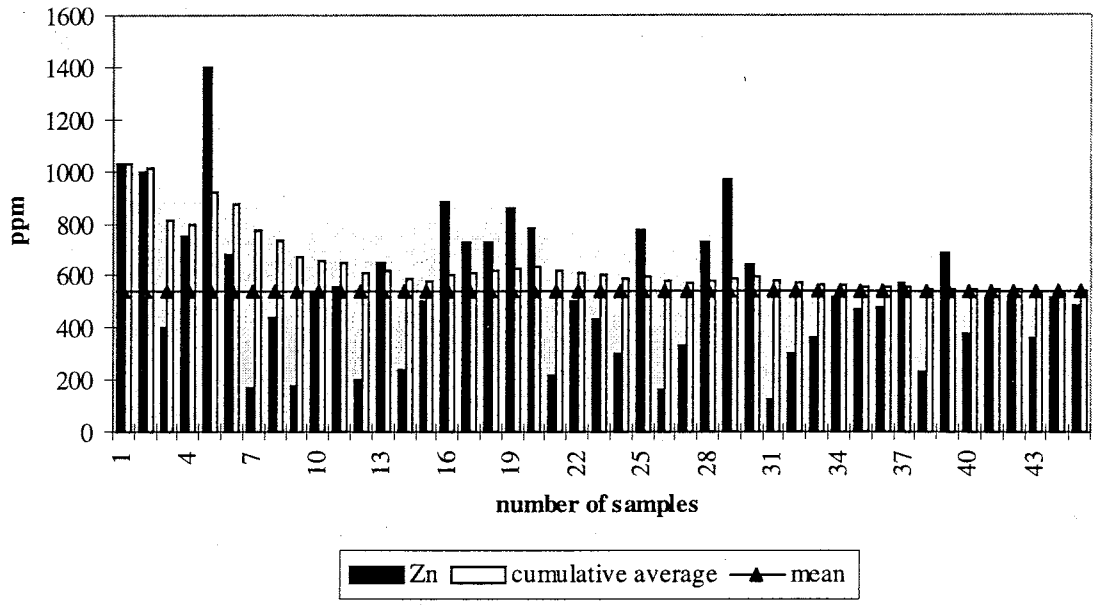


Figure 34. 45 samples from the Laramide polymetallic vein waste rock pile (Site B) individually analyzed for zinc. Individual samples are plotted versus cumulative average and mean. Note that 15 or 30 samples coincide with a cumulative average and mean of the samples that is approximately equal.

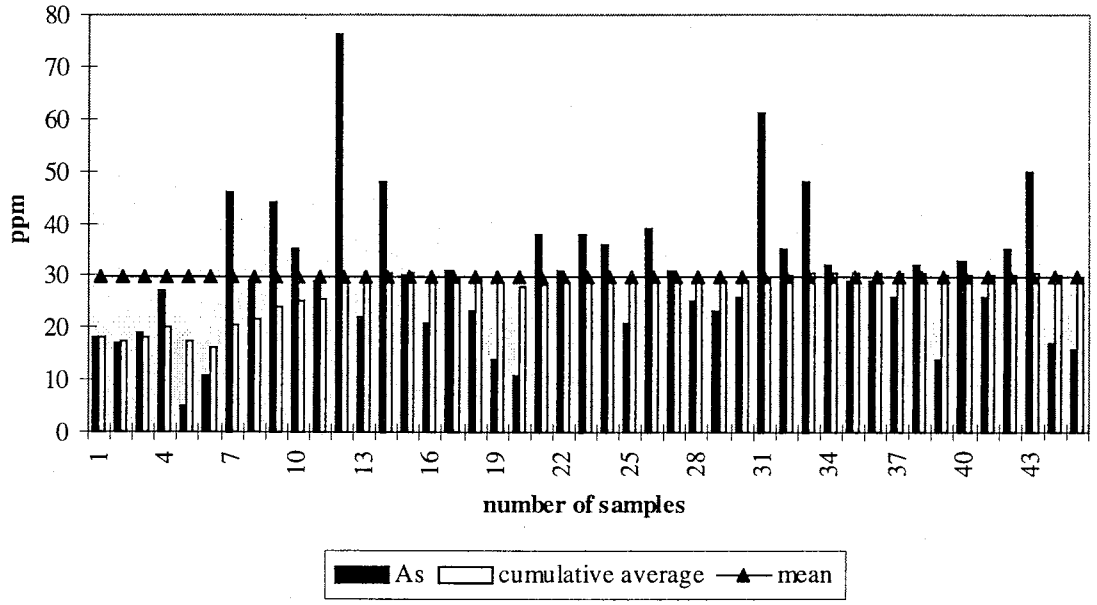


Figure 35. 45 samples from the Laramide polymetallic vein waste rock pile (Site B) individually analyzed for arsenic. Individual samples are plotted versus cumulative average and mean. Note that 15 or 30 samples coincide with a cumulative average and mean of the samples that is approximately equal.

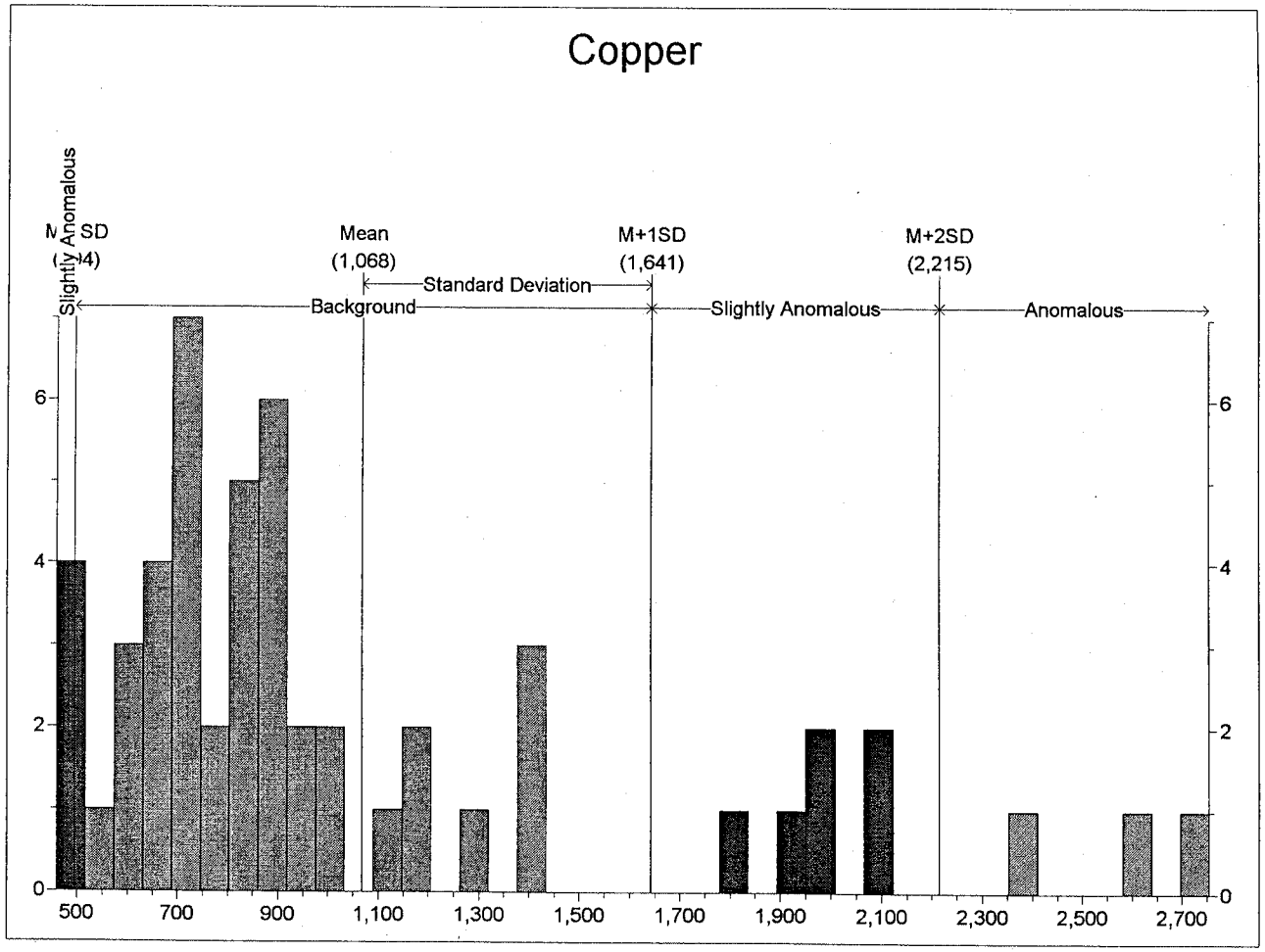


Figure 36. A histogram plot of copper concentrations (ppm) for 45 samples from a Laramide polymetallic vein waste rock pile (Site B). Concentration in ppm is plotted vs. the frequency. "Background" values fall within one standard deviation of the mean and represent the majority of the samples.

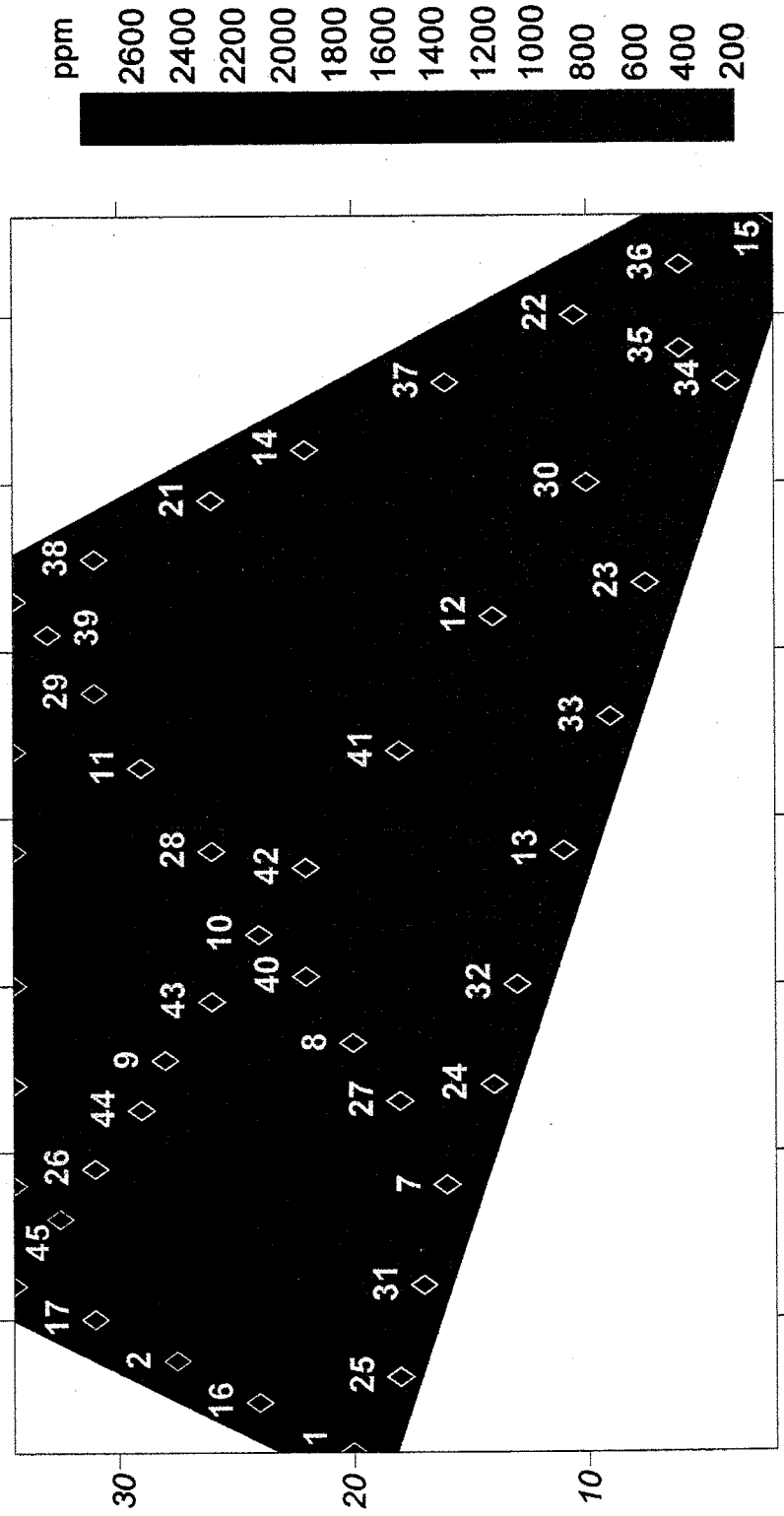


Figure 37. Copper concentrations for 45 samples from the Laramide polymetallic vein waste rock pile (Site B). Red color represents the high concentrations while blue represents the low concentrations. The waste rock pile grid sampling locations (Fig. 3) have been superimposed onto the map of metal concentrations. The x and y axes represent the width and length of the waste rock pile grid in increments of 10 meters.

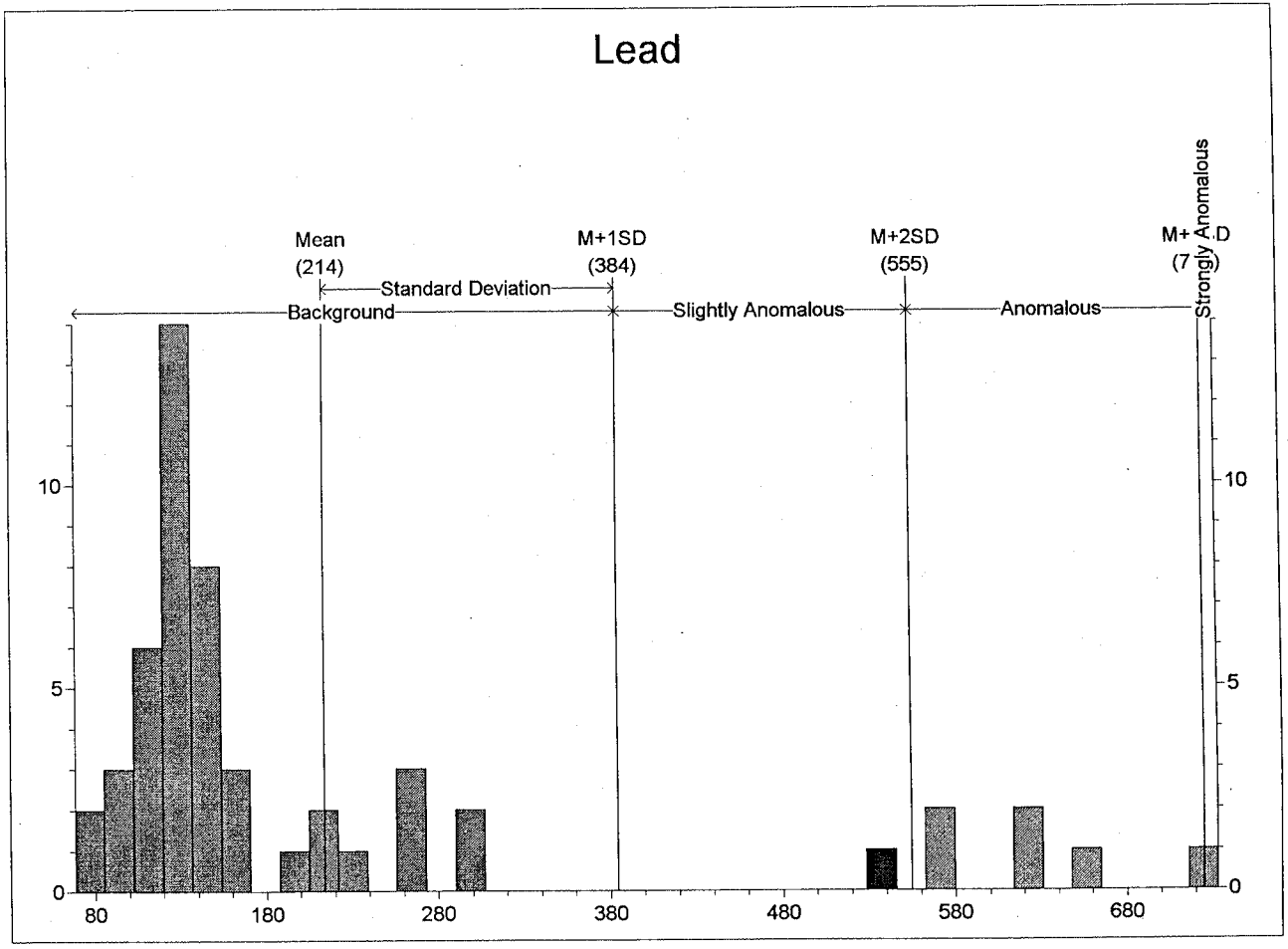


Figure 38. A histogram plot of lead concentrations (ppm) for 45 samples from a Laramide polymetallic vein waste rock pile (Site B). Concentration in ppm is plotted vs. the frequency. "Background" values fall within one standard deviation of the mean and represent the majority of the samples.

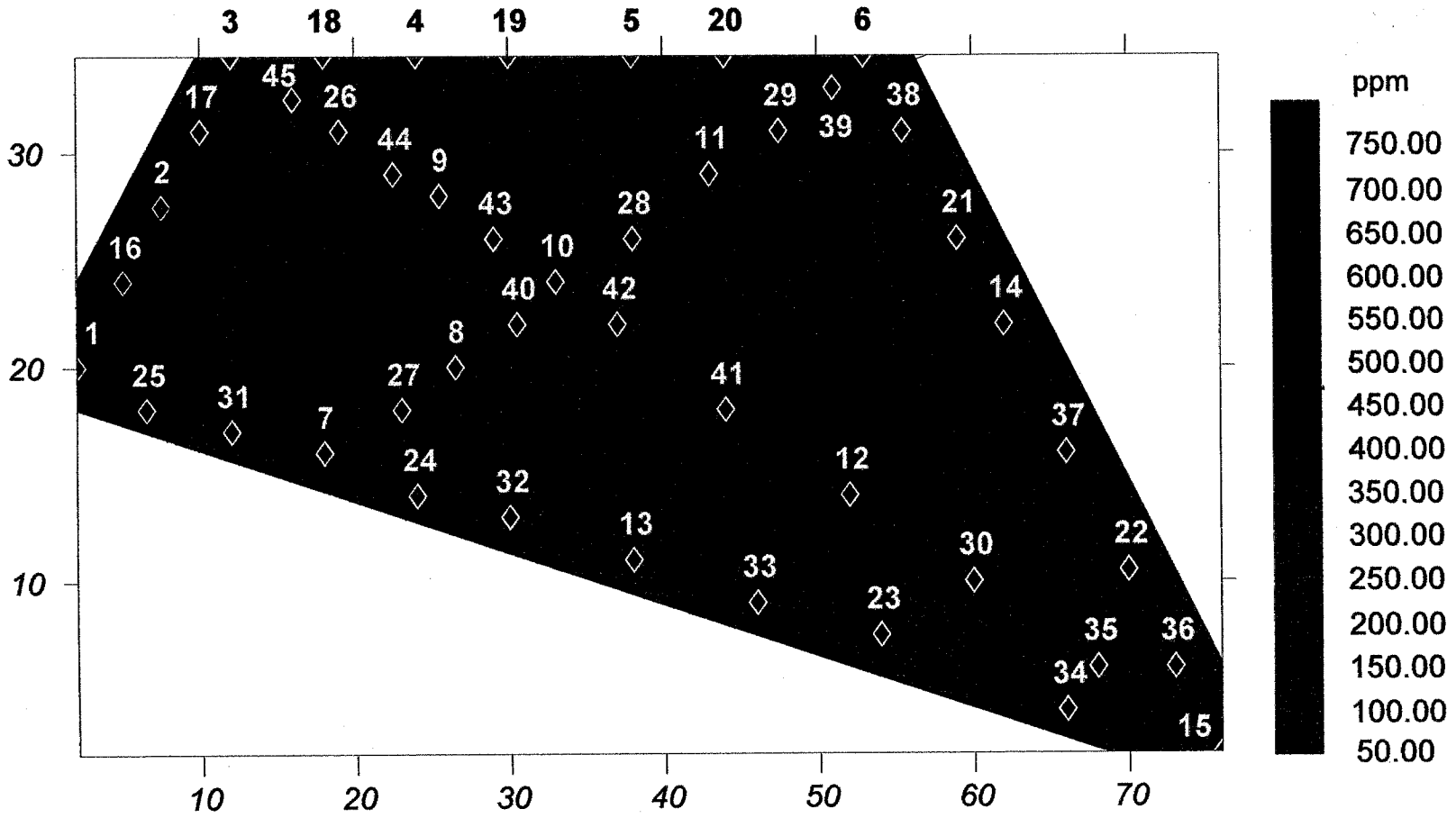


Figure 39. Lead concentrations for 45 samples from the Laramide polymetallic vein waste rock pile (Site B). Red color represents the high concentrations while blue represents the low concentrations. The waste rock pile grid sampling locations (Fig. 3) have been superimposed onto the map of metal concentrations. The x and y axes represent the width and length of the waste rock pile grid in increments of 10 meters.

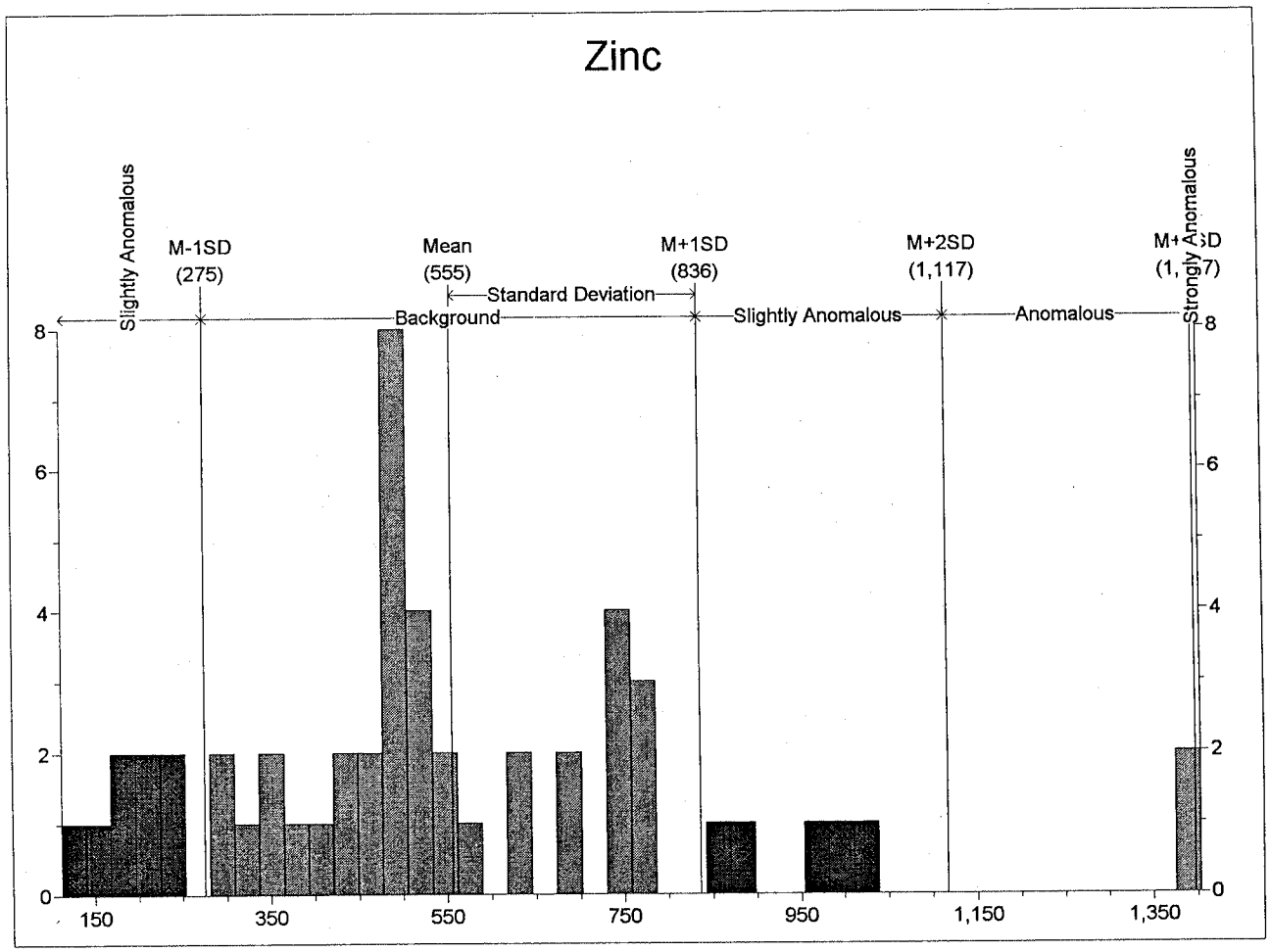


Figure 40. A histogram plot of zinc concentrations (ppm) for 45 samples from a Laramide polymetallic vein waste rock pile (Site B). Concentration in ppm is plotted vs. the frequency. "Background" values fall within one standard deviation of the mean and represent the majority of the samples.

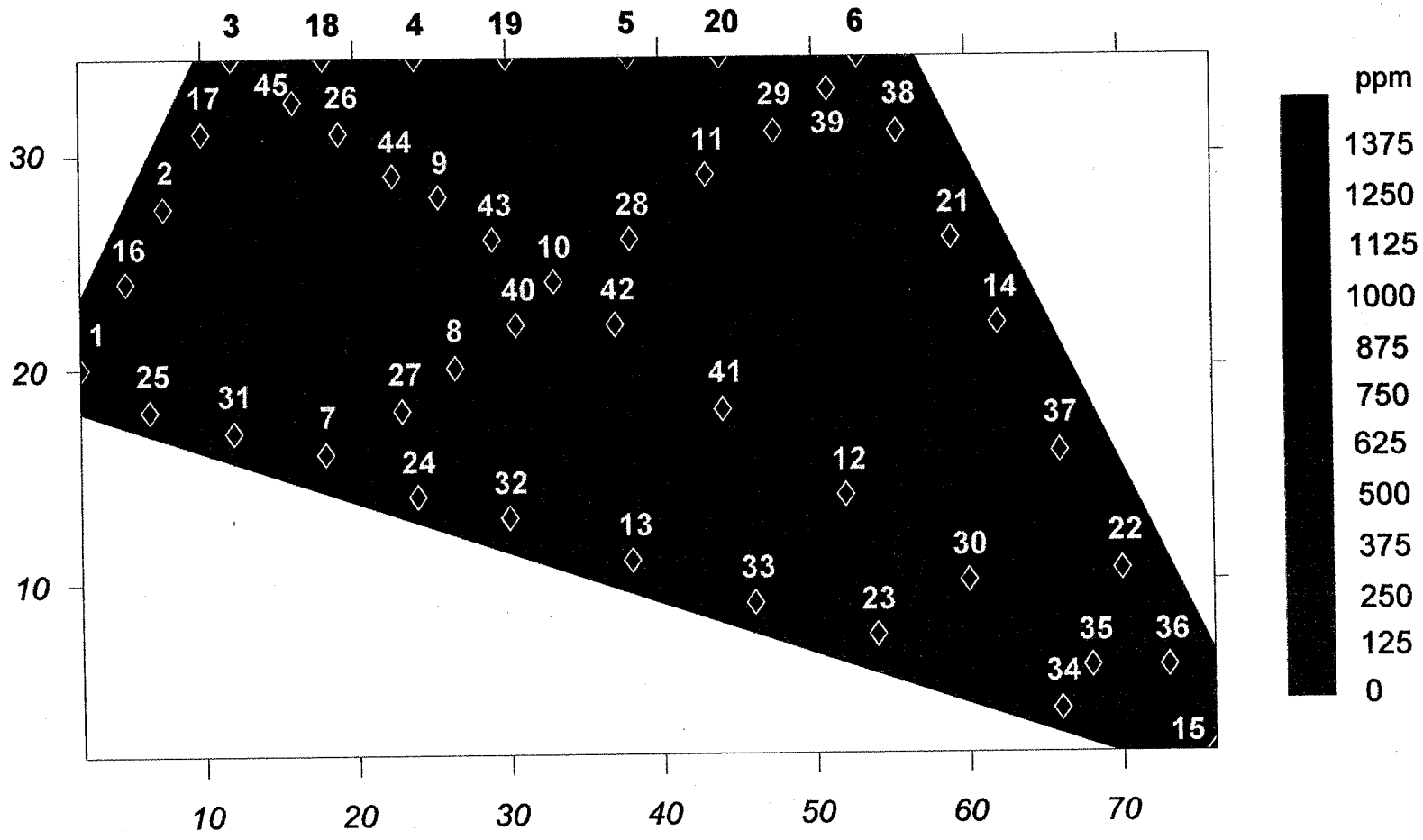


Figure 41. Zinc concentrations for 45 samples from the Laramide polymetallic vein waste rock pile (Site B). Red color represents the high concentrations while blue represents the low concentrations. The waste rock pile grid sampling locations (Fig. 3) have been superimposed onto the map of metal concentrations. The x and y axes represent the width and length of the waste rock pile grid in increments of 10 meters.

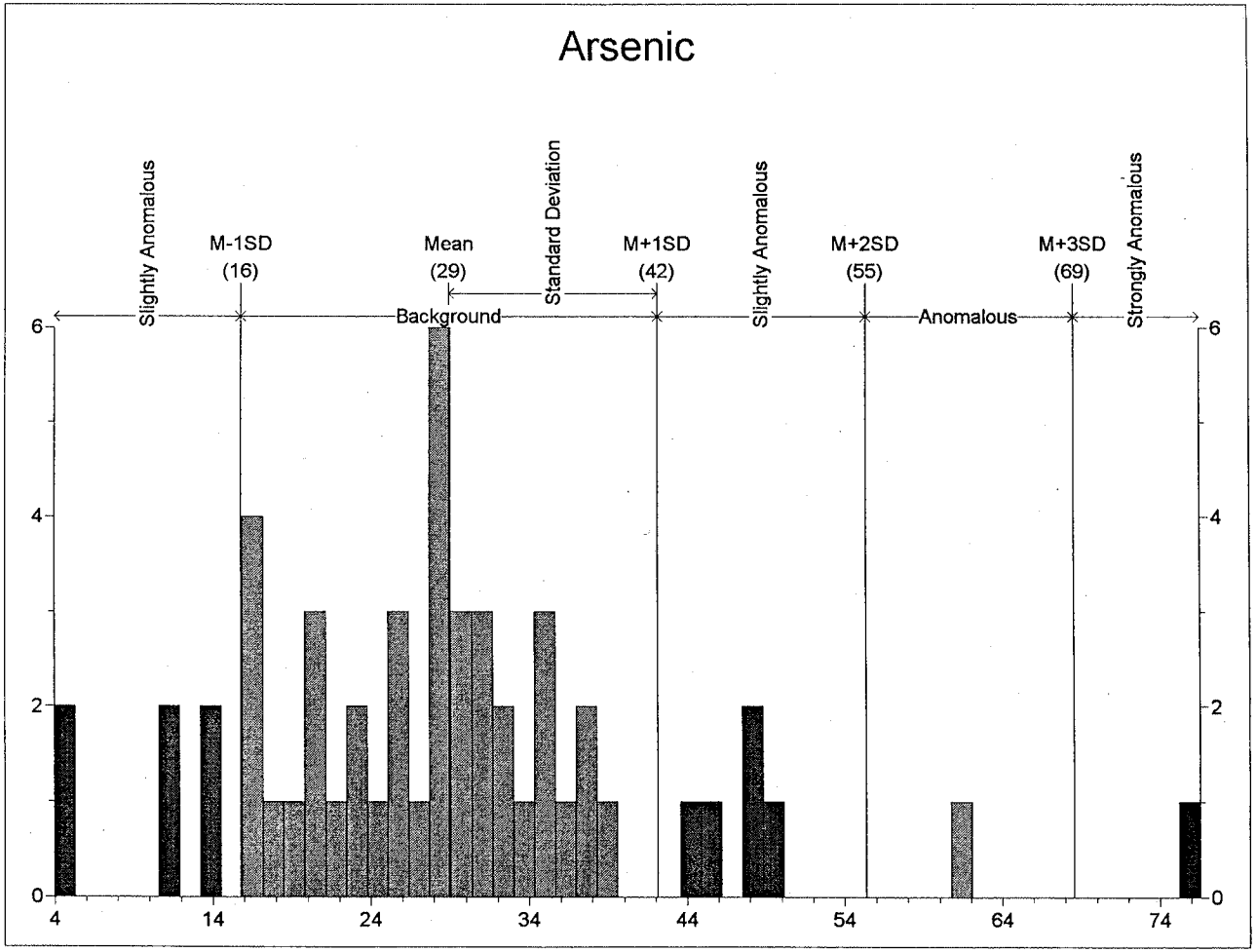


Figure 42. A histogram plot of arsenic concentrations (ppm) for 45 samples from a Laramide polymetallic vein waste rock pile (Site B). Concentration in ppm is plotted vs. the frequency. "Background" values fall within one standard deviation of the mean and represent the majority of the samples.

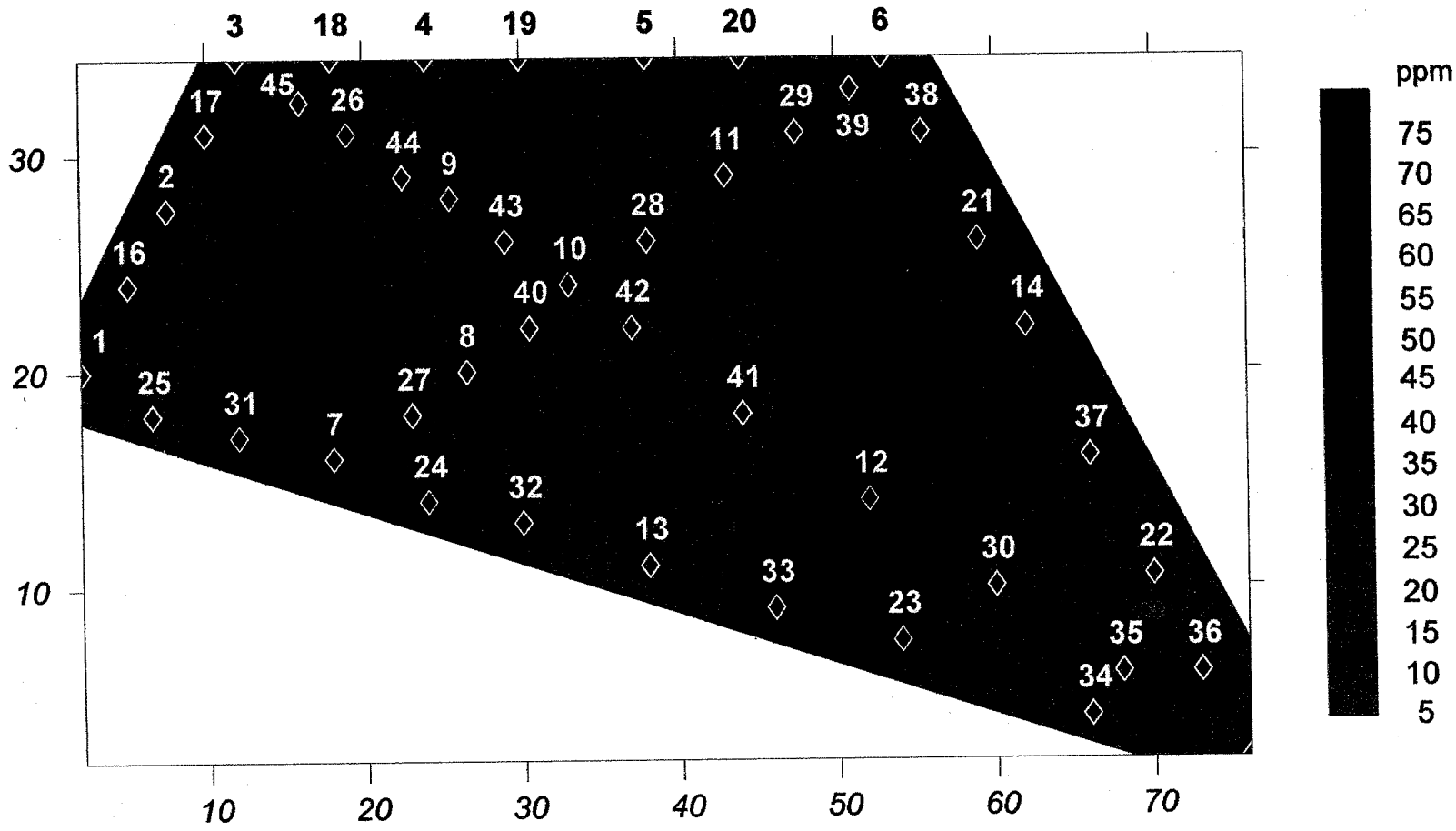


Figure 43. Arsenic concentrations for 45 samples from the Laramide polymetallic vein waste rock pile (Site B). Red color represents the high concentrations while blue represents the low concentrations. The waste rock pile grid sampling locations (Fig. 3) have been superimposed onto the map of metal concentrations. The x and y axes represent the width and length of the waste rock pile grid in increments of 10 meters.

## 8.5 STREAM SEDIMENT MINERALOGY

Stream sediment samples were collected downstream of the waste rock piles (Site A-D). The mineralogy of each of the samples reflect the mineralogical content of the waste rock pile and the surrounding country rock (Table 13). Stream sediment mineralogy can help determine the amount of physical movement of material from the waste rock pile as well as the approximate acid buffering capacity of the stream sediments.

Table 13. Stream sediment mineralogy. Identification of less than 2 mm material through binocular microscope and supplemented by XRD for select samples. EAM 1798, 198, 998, and 1298 are downstream from Site A, B, C, D respectively. EAM 1798 is located in Figure 10, EAM 198 is located in Figure 8, and EAM 998 and 1298 are located in Figure 9.

| Stream Sediment sample | Mineralogy |
|---|---|
| EAM 1798 | igneous and limestone rock fragments, quartz, plagioclase, calcite, hematite, cuprite |
| EAM 198 | igneous rock fragments, quartz, albite, sericite, sanidine, cuprite, muscovite, minor pyrite |
| EAM 998 | limestone and jasperoid rock fragments, calcite, microcystalline quartz, iron oxides |
| EAM 1298 | igneous rock fragments, manganese oxides, quartz, muscovite, calcite, iron oxides |

### 8.5.1 Stream sediment geochemistry

Stream sediment samples were collected in order to determine the level of metal mobility away from the waste rock piles sampled. Metal ratios were plotted to determine whether the elements are physically or chemically moved from the waste rock piles into the stream sediments (Fig. 44, 45, 46, 47). Metal ratios were chosen because of the high metal concentration gradient between some of the waste rock piles and the closest stream sediment. Metal concentrations from the stream sediments for this study are one to two orders of magnitude less than those concentrations determined by Alminas et al. (1978) and Watts et al., (1978; Table 2, 14). Differences in the data are due to analytical methods used, the grain size sampled, and type of fraction used (light vs. heavy fraction). Metal concentrations may be higher in the light fraction that contains clays. Not only do the metal ratios indicate beginning waste rock pile compositions but they also show the trends of stream sediment metal constituents in an ephemeral stream.

Table 14. Stream sediment chemical analyses by XRF and FAAS.

| Stream Sediment Sample | Associated with | Cu (ppm) | Pb (ppm) | Zn (ppm) | As (ppm) |
|---|---|---|---|---|---|
| | Site A | | | | |
| EAM 1698 | | 210.0 | 23.0 | 80.0 | 6.0 |
| EAM 1798 | | 160.0 | 23.0 | 74.0 | 4.0 |
| | Site B | | | | |
| EAM 598 | | 360.0 | 90.0 | 230.0 | 11.0 |
| EAM 198 | | 49.0 | 29.0 | 114.0 | 4.0 |
| EAM 298 | | 35.0 | 24.0 | 92.0 | 2.0 |
| EAM 398 | | 31.0 | 29.0 | 90.0 | 4.0 |
| | Site C | | | | |
| EAM 998 | | 23.0 | 48.0 | 91.0 | 7.0 |
| EAM 1598 | | 13.0 | 19.0 | 55.0 | 7.0 |
| EAM 1098 | | 47.0 | 25.0 | 92.0 | 6.0 |
| | Site D | | | | |
| EAM 1198 | | 0.7 | 5.2 | 2.6 | 0.3 |
| EAM 1298 | | 0.5 | 2.6 | 2.3 | 0.2 |
| EAM 1398 | | 0.6 | 3.9 | 2.5 | 0.2 |
| EAM 1498 | | 0.5 | 2.1 | 2.2 | 0.1 |

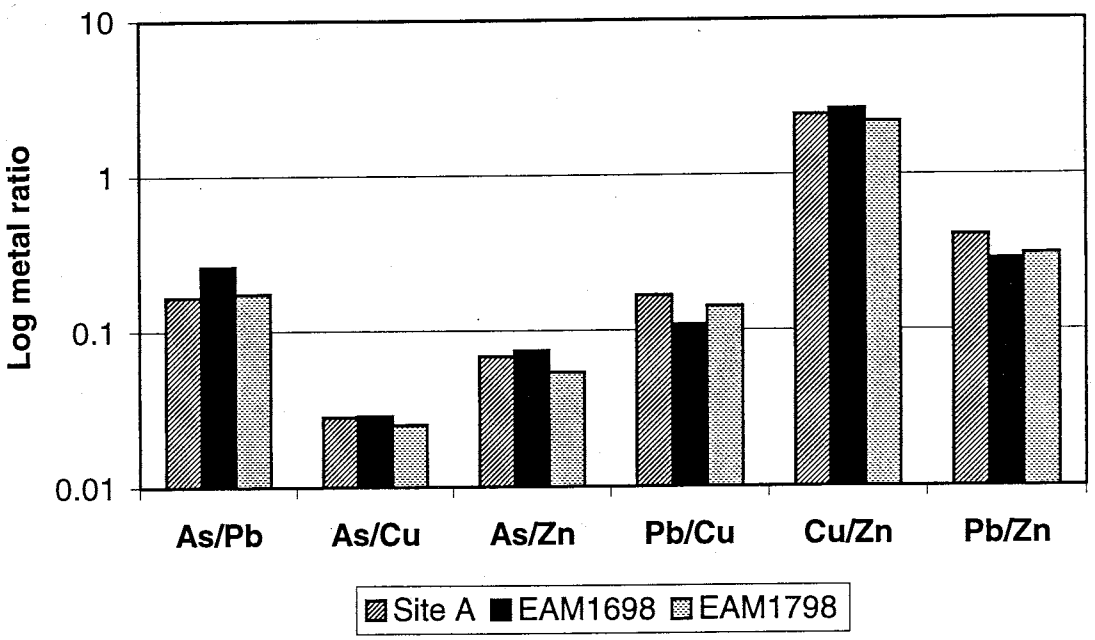


Figure 44. XRF analysis of the placer gold waste rock pile (Site A) with stream sediment samples downstream of the site. EAM stream sediment samples are graphed with increasing distance away from Site A from left to right per metal ratio.

Metal ratios show very minor decreases such as Pb/Cu from Site A to the two stream sediment samples indicating an increase in Cu concentration while Pb remains constant. This arroyo is the main drainage for the Copper Flat open pit area along with other mineralized dikes. Deposits or mineralized areas may introduce metals into the arroyo which can increase the metal concentrations immediately downstream. It is difficult to determine if there is metal mobility from the waste rock pile to the stream sediments due to the mineralized nature of the drainage area. The metal ratios indicate that the stream sediments and the waste rock pile are approximately the same mineralogy.

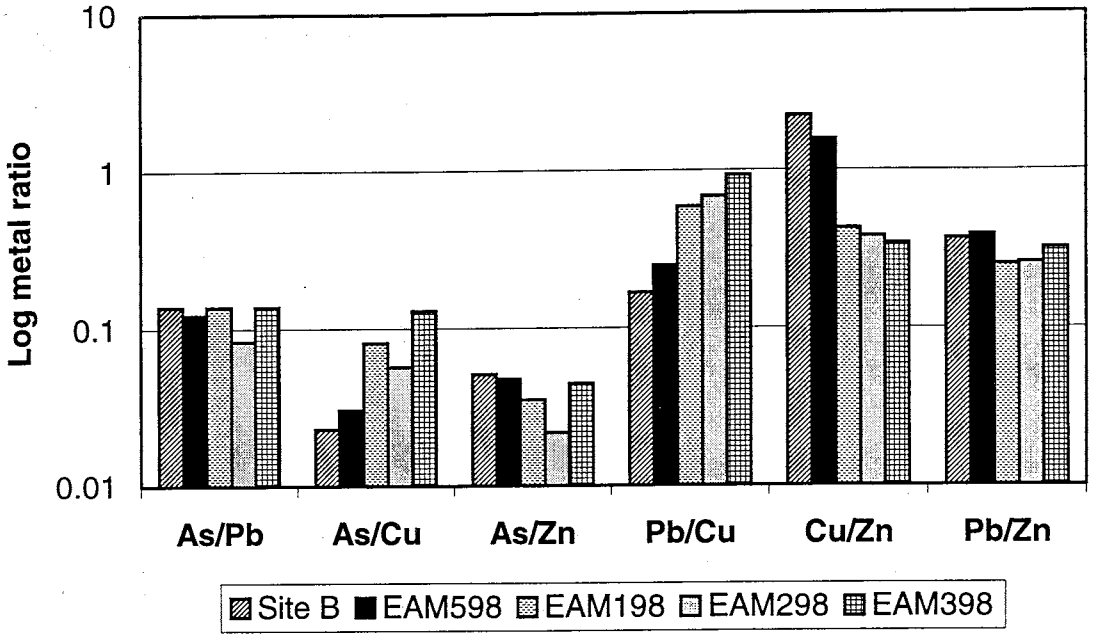


Figure 45. XRF analysis of the Laramide polymetallic vein waste rock pile (Site B) with stream sediment samples downstream of the site. EAM stream sediment samples are graphed with increasing distance away from Site B from left to right per metal ratio.

The Pb/Zn ratio remains relatively constant for Site B (Fig. 45). Assuming Pb remains constant, a Pb/Cu increase indicates Cu concentration is decreasing with increasing distance from Site B. This trend signifies greater breakdown of chalcopyrite (the main copper bearing mineral) in the waste rock pile relative to galena as well as chemical transport of copper away from Site B. Cu concentration decreases rapidly from the first to second stream sediment downstream from the waste rock pile. This further supports chemical mobility in the environment (Table 14). The drainage basin is closed to any new metal input until the intersection of an arroyo at sample location EAM 398, originating one valley to the northwest, which drains another mined Laramide polymetallic vein deposit (Fig. 8).

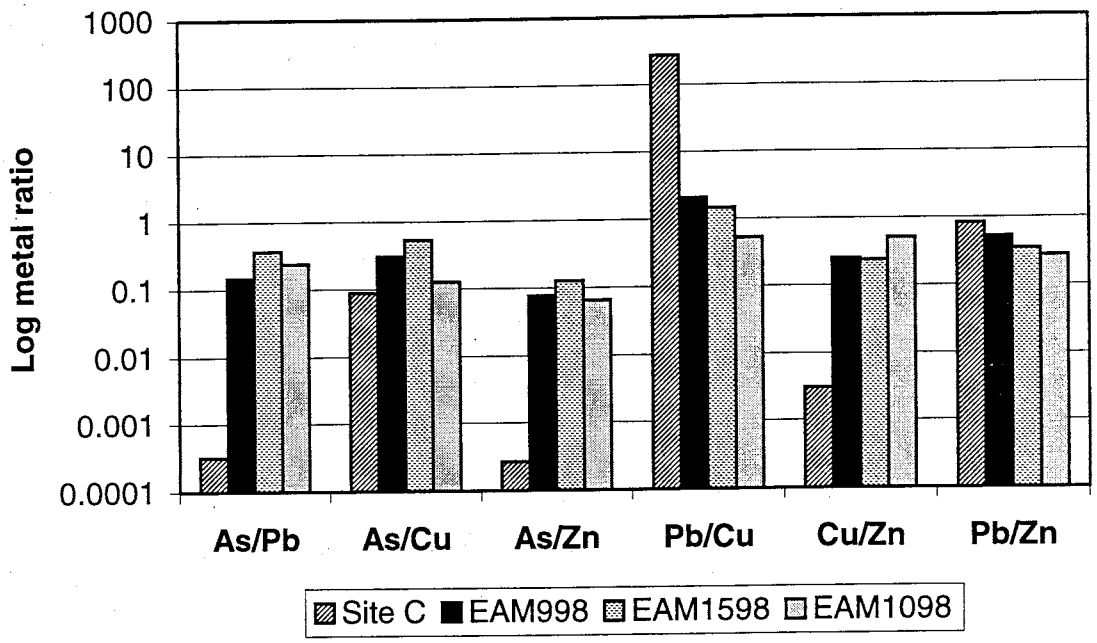


Figure 46. FAAS analysis of the carbonate-hosted Pb-Zn waste rock pile (Site C) with stream sediment samples downstream of the site. EAM stream sediment samples are graphed with increasing distance away from Site C from left to right per metal ratio.

As/Pb, As/Zn, and Cu/Zn ratios of samples from Site C waste rock pile are very low due to high lead and zinc concentrations (Fig. 46). The stream sediment samples contain a much lower concentration of zinc and lead relative to the waste rock pile. Pb/Zn slowly decreases away from the waste rock pile. Pb/Cu precipitously decreases from Site C to the first stream sediment sample indicating lead initially is high in concentration and is highly immobile perhaps due to the mineralogical composition of the lead-bearing minerals.

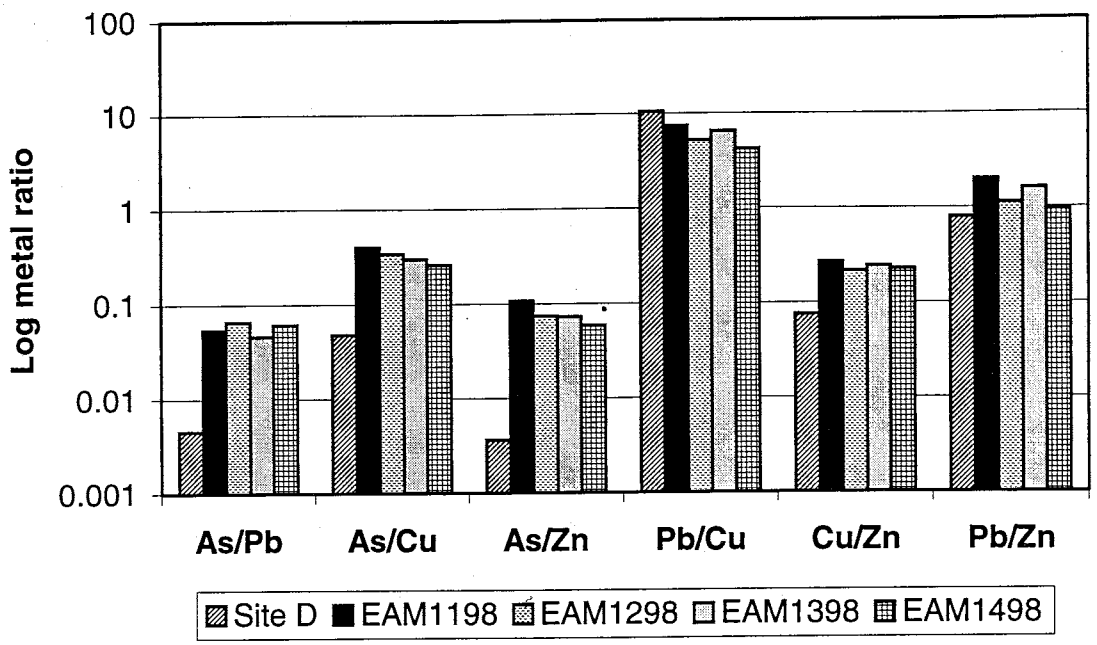


Figure 47. FAAS analysis of the carbonate-hosted Ag-Mn waste rock pile (Site D) followed by subsequent stream sediment samples downstream of the site. EAM stream sediment samples are graphed with increasing distance away from Site D from left to right per metal ratio.

As/Pb and As/Zn are disproportionately low in comparison to the stream sediments because of the high amount of lead and zinc relative to arsenic. The majority of the total lead present in the waste rock pile may be contained in lead-bearing amorphous manganese oxide mineral phases. Like Site C, the lead is preferentially kept in the mineral lattice due to the relative low chemical reactivity with the environment. Therefore, As/Pb and Pb/Zn indicate the relatively low chemical mobility of lead in the environment and constitute a physical movement of lead-bearing manganese oxides (coronadite) away from the waste rock pile.

## 8.6 WATER CHEMISTRY

Water samples were collected from four locations in the Hillsboro district to determine major and trace element chemistry (Table 15): the pit lake at the Copper Flat

open pit, water from an adit on the Bonanza vein, water from an inclined adit on the Rattlesnake vein, and a natural spring west of the Copper Flat volcano (Fig. 8, 10). Water samples were collected because background geochemistry is vital to the understanding of what elements are present in an area prior to anthropogenic disturbances such as mining. Samples were collected in May and November of 1998.

Table 15. Hillsboro district water samples from four different locations taken during the spring and fall of 1998. Four types of samples were collected at each sampling site: samples with "A" suffix are unfiltered, unacidified and used to analyze for dissolved major elements, ionic compounds, and colloidal material in water; samples with a "B" suffix are unfiltered, acidified and used to analyze for dissolved trace metal components and suspended material in water; samples with "C" suffix are filtered, acidified and used to analyze for dissolved trace metal components in water; and samples with "D" suffix are filtered, unacidified and used to analyze for dissolved major elements and ionic compounds. Copper Flat Pit Lake samples are located in Figure 10, Adit on Bonanza Vein, Natural Spring, and Adit on Rattlesnake Vein samples are located in Figure 8.

| Site | May, 1998 | November, 1998 |
|---|---|---|
| Copper Flat Pit Lake | 5/198 A, B, C, D | 11/199 A, B, C, D |
| Adit on Bonanza Vein | 5/298 A, B, C, D | 11/299 A, B, C, D |
| Natural Spring | 5/498 A, B, C, D | 11/499 A, B, C, D |
| Adit on Rattlesnake Vein | 5/598 A, B, C, D | 11/599 A, B, C, D |

The Cu, Pb, and Zn concentrations were analyzed for all district water samples (Appendix E). Chemical analyses were compared to the New Mexico water standards for irrigation and livestock watering because resultant run-off in the Hillsboro area is typically utilized in this manner. With the exception of one sample from the Bonanza vein adit, all samples were below the water standard concentrations suggested for irrigation: Cu ≤ 0.2 mg/l, Pb ≤ 5.0 mg/l, Zn ≤ 2.0 mg/l (State of New Mexico Water Standards, 1994). All samples were below the water standard concentrations suggested for livestock watering: Cu ≤ 0.5 mg/l, Pb ≤ 0.1 mg/l, Zn ≤ 25.0 mg/l (State of New Mexico Water Standards, 1994).

High $SO_4$, low $CO_3$ and $HCO_3$, and moderate Mg, Na, K, and Ca characterize the Copper Flat pit lake samples (Fig. 48). Major element chemistry remained stable from spring to fall 1998. The two water samples from the adits also contained high $SO_4$ with moderate concentrations of $CO_3$, $HCO_3$ , and Cl. The samples from the Rattlesnake adit changed chemical composition from spring to fall by a decrease in $SO_4$, and an increase in Ca, $CO_3$, and $HCO_3$. This may be a result of chemical equilibrium which is consistent with a lowering of the water level from spring to fall. The natural spring water contains much lower Ca, $SO_4$, $CO_3$, and $HCO_3$ concentrations than the pit lake and the two adit water samples. The natural spring water chemistry remains constant during the spring to fall and also contains higher Mg, Na, and K concentrations than all other samples. Comparison of pit lake water samples from BLM (1996) and Bakkom and Salvas (1997) (Table 3) indicate several trends in the pit lake history. The pH, $HCO_3$, and $SO_4$ all increase while Cu and Zn decrease in concentration from 1993 to 1997. Relative to Bakkom and Salvas (1997), and this report; the pit lake site pH, $HCO_3$, and $SO_4$ have

remained constant up to fall 1998. Cu and Pb concentrations decreased from 1996 to 1997 while Zn increased slightly (Bakkom and Salvas, 1997). Relative to Bakkom and Salvas (1997), Cu, Pb, and Zn concentrations decreased up to fall 1998. Trace metal concentrations in the pit lake water, during the period 1995 – 1998, appear to fluctuate between 0.01 – 0.71 ppm Cu, < 0.01 – 0.03 ppm Pb, and 0.17 – 0.18 ppm Zn depending on the season (BLM, 1996; Bakkom and Salvas, 1997).

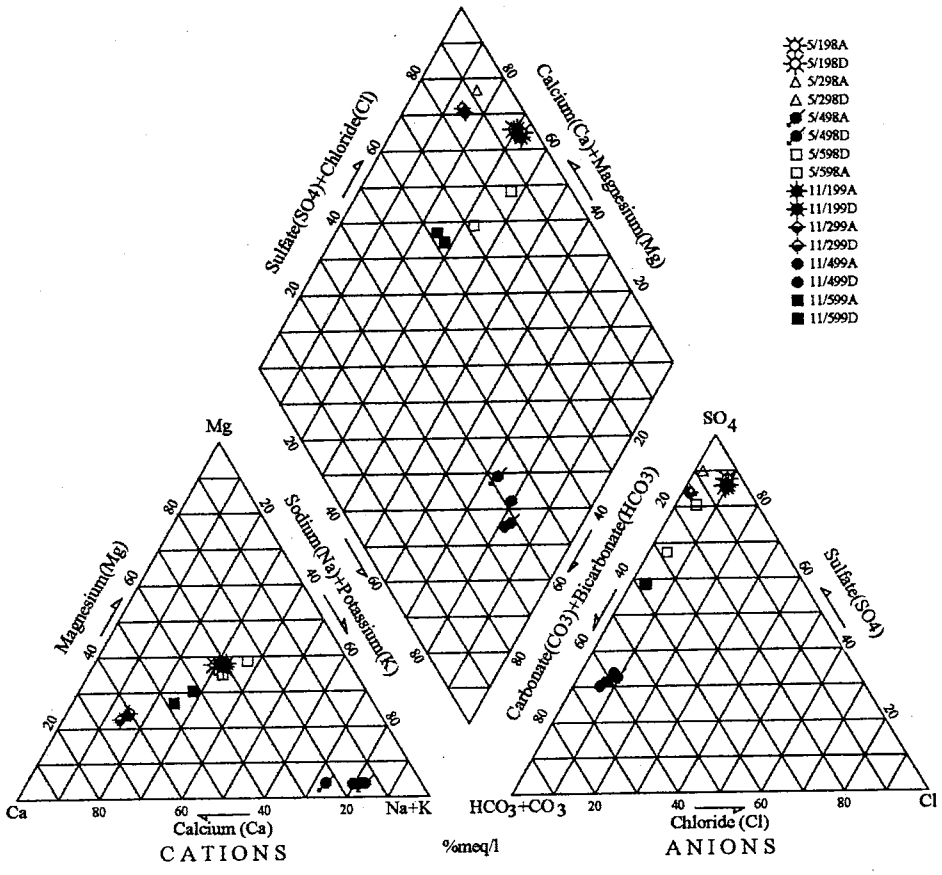


Figure 48. Piper diagram of major element chemistry of waters from the Hillsboro mining district. Samples were taken from the pit lake, an adit on the Bonanza vein, a natural spring, and an adit on the Rattlesnake vein. High $SO_4$ is present in the pit lake and Bonanza vein adit water samples. High to moderate $SO_4$ concentrations are present in the Rattlesnake vein adit while low $SO_4$ concentrations typify the natural spring water. District water sample locations are in Figure 8 and 10.

Comparison of the Hillsboro trace metal ratios from water samples indicate several trends. The pit lake sample group shows a stable relationship from spring to fall with the "B" sample consistently containing higher metal ratios compared to the "C" samples (Figs. 49, 50). In the Bonanza vein adit, water samples indicate the colloidal material in the sample "B" is the controlling factor in metal movement because the metal ratios in sample "C" remain constant. Metal ratios of dissolved and colloidal constituents in the natural spring waters appear to decrease from spring to fall (Figs. 49, 50). In the Rattlesnake adit the Cu/Zn ratio increases from spring to fall and from sample "B" to sample "C" indicating possible evaporation/concentration effects or less water input to the system.

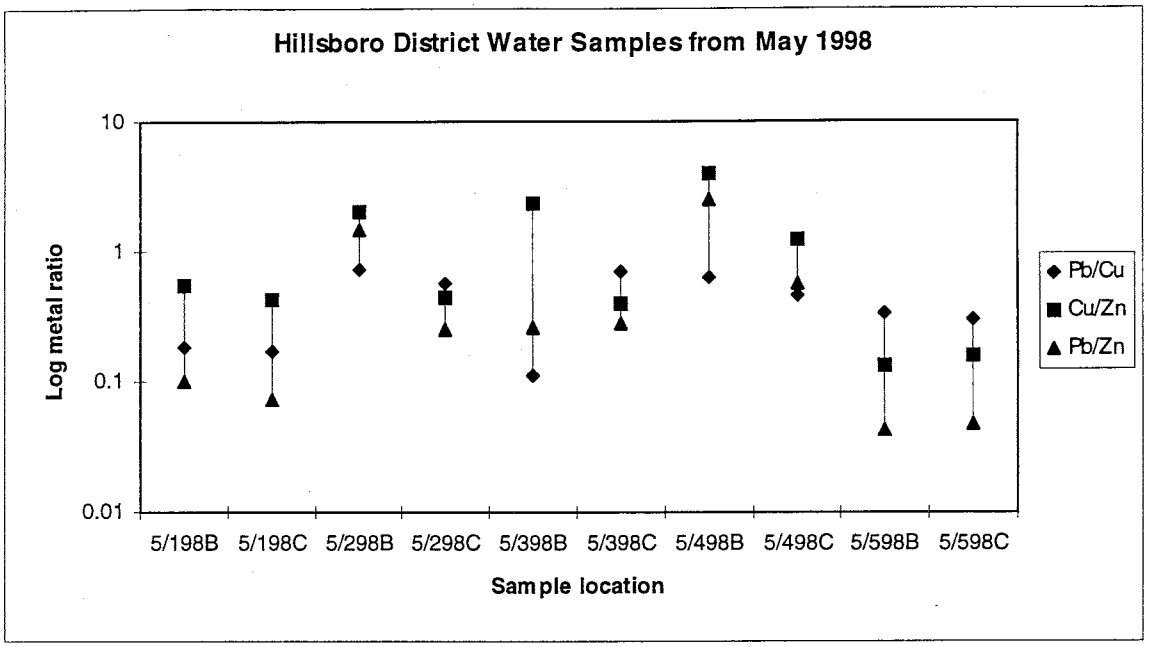


Figure 49. Log metal ratio plot of Hillsboro district water samples in May 1998. Samples with a "B" suffix are unfiltered and acidified while samples with a "C" suffix are filtered and acidified. The comparison of metals adsorbed onto grains in suspension plus dissolved metals "B" vs. dissolved metals "C" can be made.

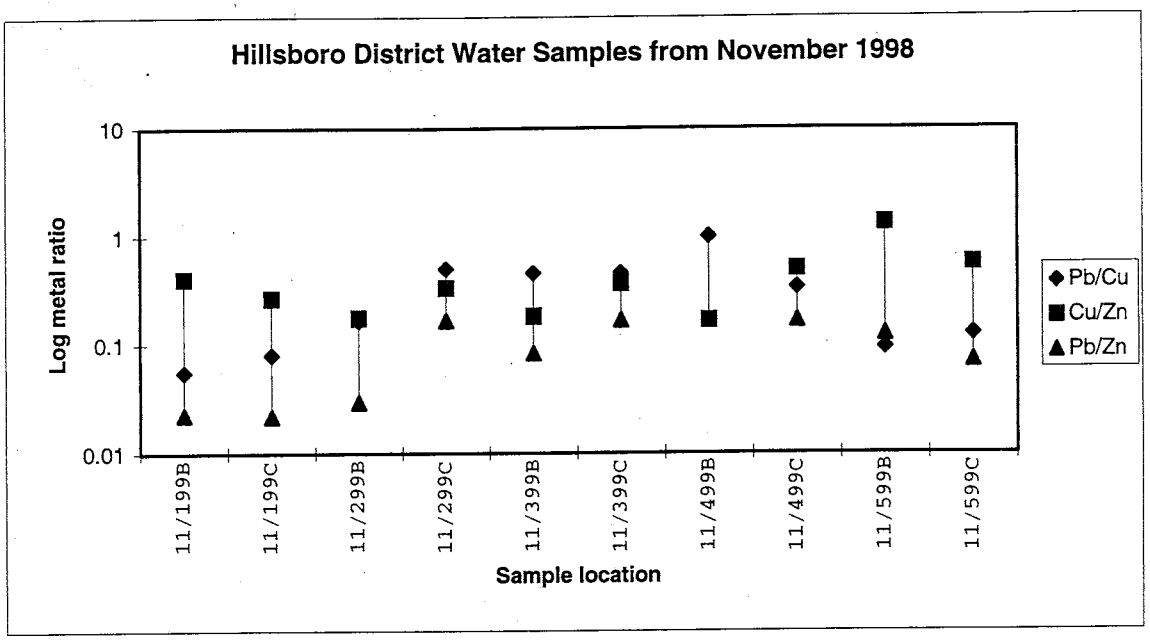


Figure 50. Log metal ratio plot of Hillsboro district water samples in November, 1998. Samples with a "B" suffix are unfiltered and acidified while samples with a "C" suffix are filtered and acidified. The comparison of metals adsorbed onto grains in suspension plus dissolved metals "B" vs. dissolved metals "C" can be made.

## 8.7 AGITATION TESTS

Agitation tests were conducted on five waste rock piles and four stream sediments. Representative solid samples less than 2 mm from the waste rock piles and the stream sediments were mixed with deionized water, pH ranging between 5 and 6, for twenty minutes. This amount of time was chosen to mimic a short-duration, high intensity precipitation event during which the sample material was inundated with water. Rain events of different intensities are suspected of increasing the probability of metal transport. The pH was measured throughout the duration of the tests. Initially, pH readings of the deionized water were taken. During the experiment, pH values changed depending on the amount and type of mineral/water interaction (Fig. 51, 52, 53, 54). Figure 55 shows the pH change comparison between Sites B and E. Waste rock pile and

stream sediment samples were each run with 100, 400, and 800 ml of deionized water respectively. Procedure and sample preparation is in Appendix D.

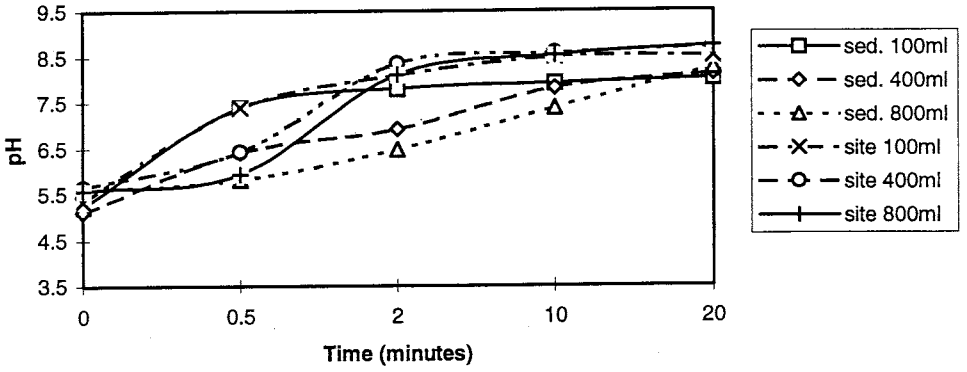


Figure 51: pH readings during a 20 minute agitation test of Site A and a nearby stream sediment.

NMBMMR metallurgical laboratory procedures were modified from standard metallurgical leach test techniques (I. Gundelier, personal communication, November, 1998). Site A and stream sediment runs for 400 and 800 ml required more time to equilibrate with the water than did the 100 ml run. This is explained by the ratio of sample material to water. A higher sample to water ratio creates a quicker pH adjustment.

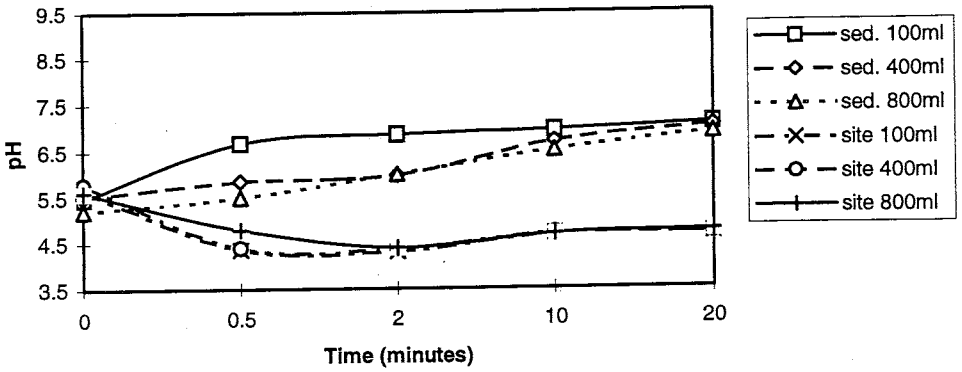


Figure 52: pH readings during a 20 minute agitation test of Site B and a stream sediment downstream from the disturbed area.

Differences in the stream sediment and Site B runs indicate the stream sediment contains minerals that contribute to neutralizing acid effluents which may come from the waste rock pile. In addition, this trend supports the idea that the waste rock pile is heterogeneous due to the fact that the stream sediment shows a different pH line. Therefore, the mineralogical compositions must be different and possibly only parts of the upper layer of the waste rock pile have been eroded and transported into the arroyo stream sediments.

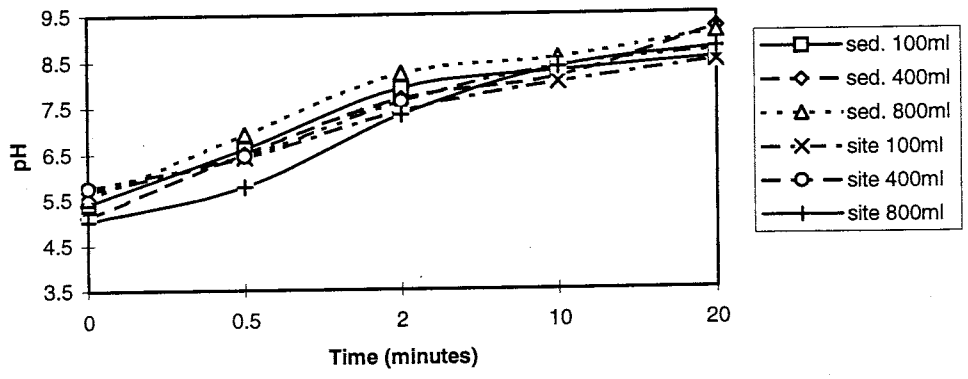


Figure 53: pH readings during a 20 minute agitation test of Site C and a stream sediment downstream from the disturbed area.

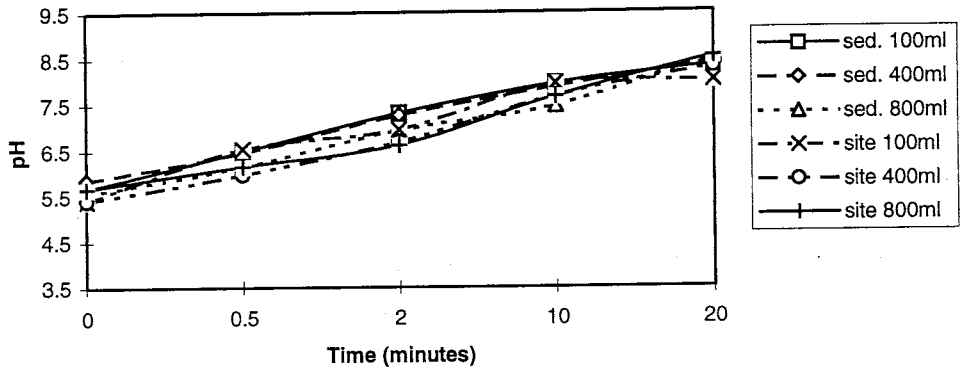


Figure 54: pH readings during a 20 minute agitation test of Site D and a stream sediment downstream from the disturbed area.

Site C and stream sediment runs showed primarily the same pH trend during the course of the experiment. Site D and stream sediment runs showed similar trends. This indicates that the waste rock pile and the surrounding lithology (limestone and dolomite)

are similar enough in gangue mineralogy to the waste rock piles that any volume of water per given sample will yield a similar pH trend.

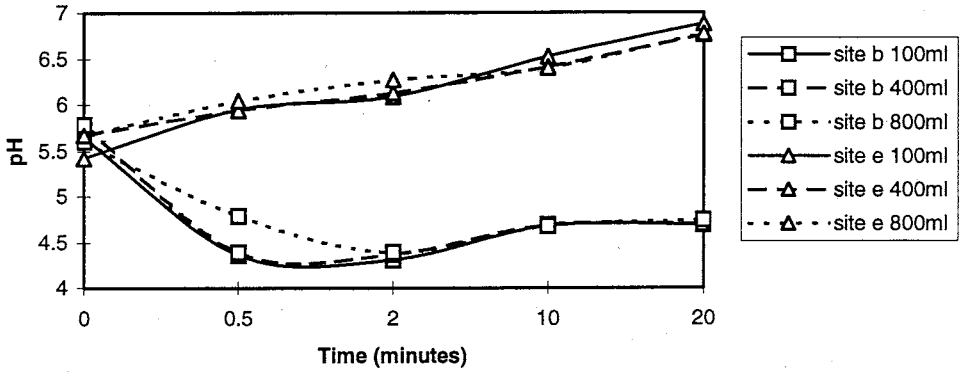


Figure 55: Comparison of pH readings during a 20 minute agitation test of the two Laramide polymetallic vein waste rock piles (Site B and Site E).

Site B created acidic waters while Site E created near-neutral waters during the agitation experiment. This is a function of the portion of the waste rock pile that was sampled. Data has shown Site B to be geochemically heterogeneous. Therefore, the same can be inferred about Site E because of the same mineralogical constituents that typically comprise a Laramide polymetallic vein deposit. In addition, waste rock piles Site B and E were created in the same manner due to the same type of mining and dumping of waste rock nearby.

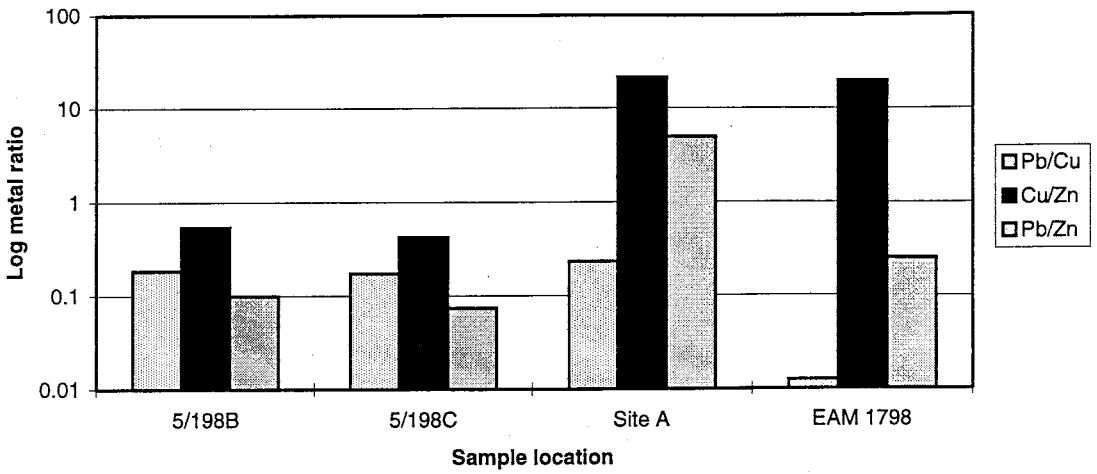


Figure 56. Comparison of Hillsboro district pit lake water sample (Table E.10) and agitation test water samples for Site A and a stream sediment down gradient (Table E.12).

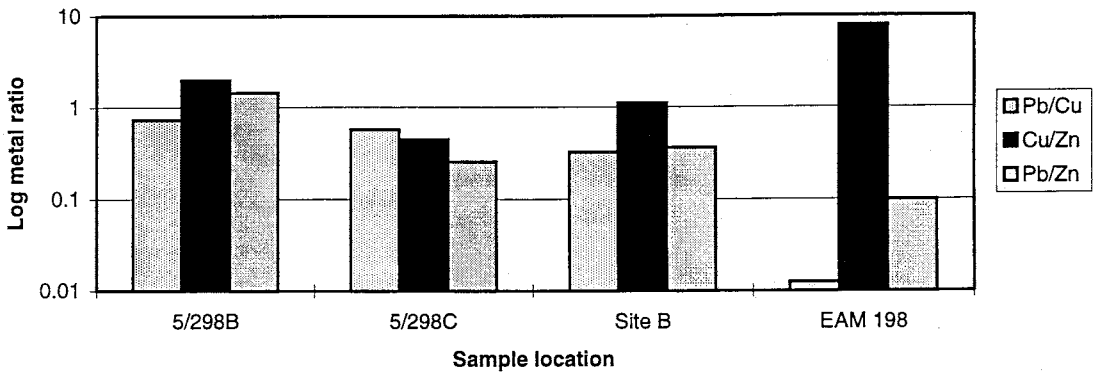


Figure 57. Comparison of Bonanza vein adit water (Table E.10) and agitation test water samples for Site B and a down gradient stream sediment (Table E.12).

Figure 56 shows the metal concentrations are higher in the agitation test water samples while in general the opposite trend is true in Figure 57. Higher metal ratios in the adit water samples than Site B and EAM 198 show that given time metals will be

released to the environment. Exception was found in the Cu/Zn ratio that is higher in the stream sediments than in the background district water samples. This indicates the likelihood that copper is in a mineralogical form more readily available to the environment (i.e. $Cu(OH)_2$ and copper sulfates).

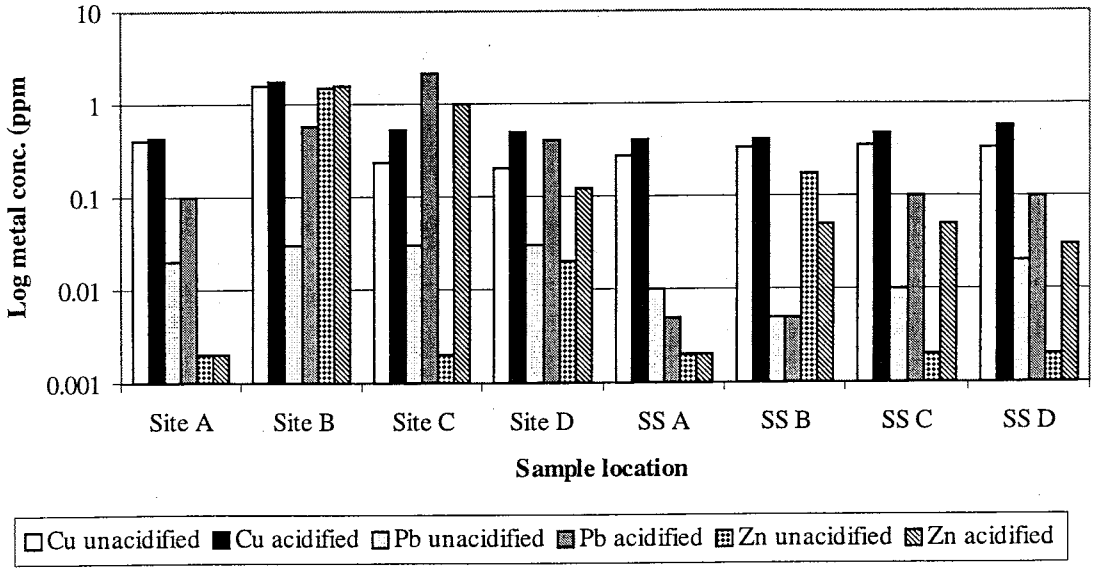


Figure 58. Unacidified vs. acidified agitation test water samples for Sites A-D and four select stream sediment samples. Unacidified samples represent the solution chemistry of laboratory prepared samples while the acidified samples represent the solution and adsorbed ions to material in suspension.

From figure 58, the acidified samples were determined to have higher metal concentrations than their unacidified counterparts. For this reason, the acidified samples were used for comparison in the metal ratios in Figure 60.

Water from agitation tests of the waste rock piles and the stream sediments typically contained higher metal concentrations than in the district water samples (Appendix E). All samples failed to meet the 0.2 mg/l irrigation cutoff for copper, but passed the lead and zinc standards. Site B continued to fail the 0.5 mg/l livestock watering cutoff for copper while the rest of the samples complied. Nearly all the

acidified samples analyzed for lead failed to meet the 0.1 mg/l livestock watering cutoff while the unacidified samples complied. All samples complied with the zinc standard of 25.0 mg/l. Arsenic was detectable only at Site C and EAM 998 and was below the acceptable limit for livestock watering of 0.2 mg/l (State of New Mexico Water Standards, 1994). Any acidified samples present in the natural environment will quickly become neutralized due to the moderate to high alkalinity of the sediments and the moderate to high acid buffering capacity of the country rock. This may drop metals out of solution and create a secondary mineral precipitate.

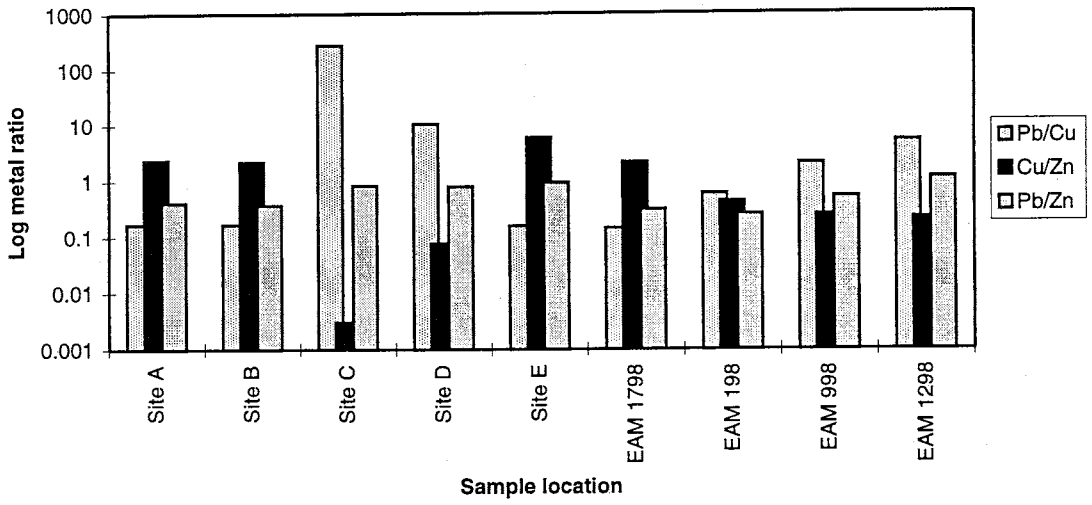


Figure 59. Waste rock pile and stream sediment solid sample metal ratios. Log metal ratio is plotted vs. the sample location. Sites A-E represent waste rock piles while samples with EAM designation are stream sediments. Sites A, B, C, and D are matched with downstream stream sediment samples EAM 1798, 198, 998, and 1298 respectively.

Metal ratios Pb/Cu, Cu/Zn, and Pb/Zn show little change from Site A to EAM 1798. This trend is expected because the material at the Site A waste rock pile came from the same arroyo bed as EAM 1798. The Pb/Cu ratio in Site C is very high in comparison to EAM 998. Lead mobility from the waste rock pile is much lower than that of copper.

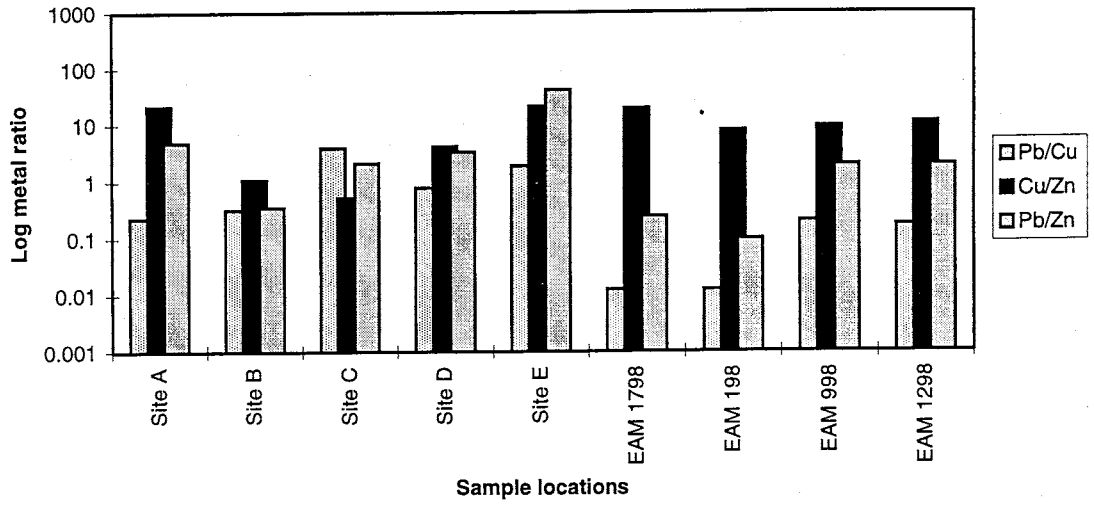


Figure 60. Waste rock pile and stream sediment agitation test water sample metal ratios. Log metal ratio is plotted vs. the sample location. Sites A-E represent waste rock piles while samples with EAM designation are stream sediments. Sites A, B, C, and D are matched with downstream stream sediment samples EAM 1798, 198, 998, and 1298 respectively.

Overall metal ratios in Site A and Site E appear to increase in comparison to solid samples in Figure 59. Apparent in all stream sediment samples is a decreasing Pb/Cu trend and an increasing Cu/Zn and Pb/Zn trend from solid to agitation test water samples (Figs. 59, 60). Metal ratio increases in the stream sediment water agitation test samples support the concept of metal movement during and after a precipitation event.

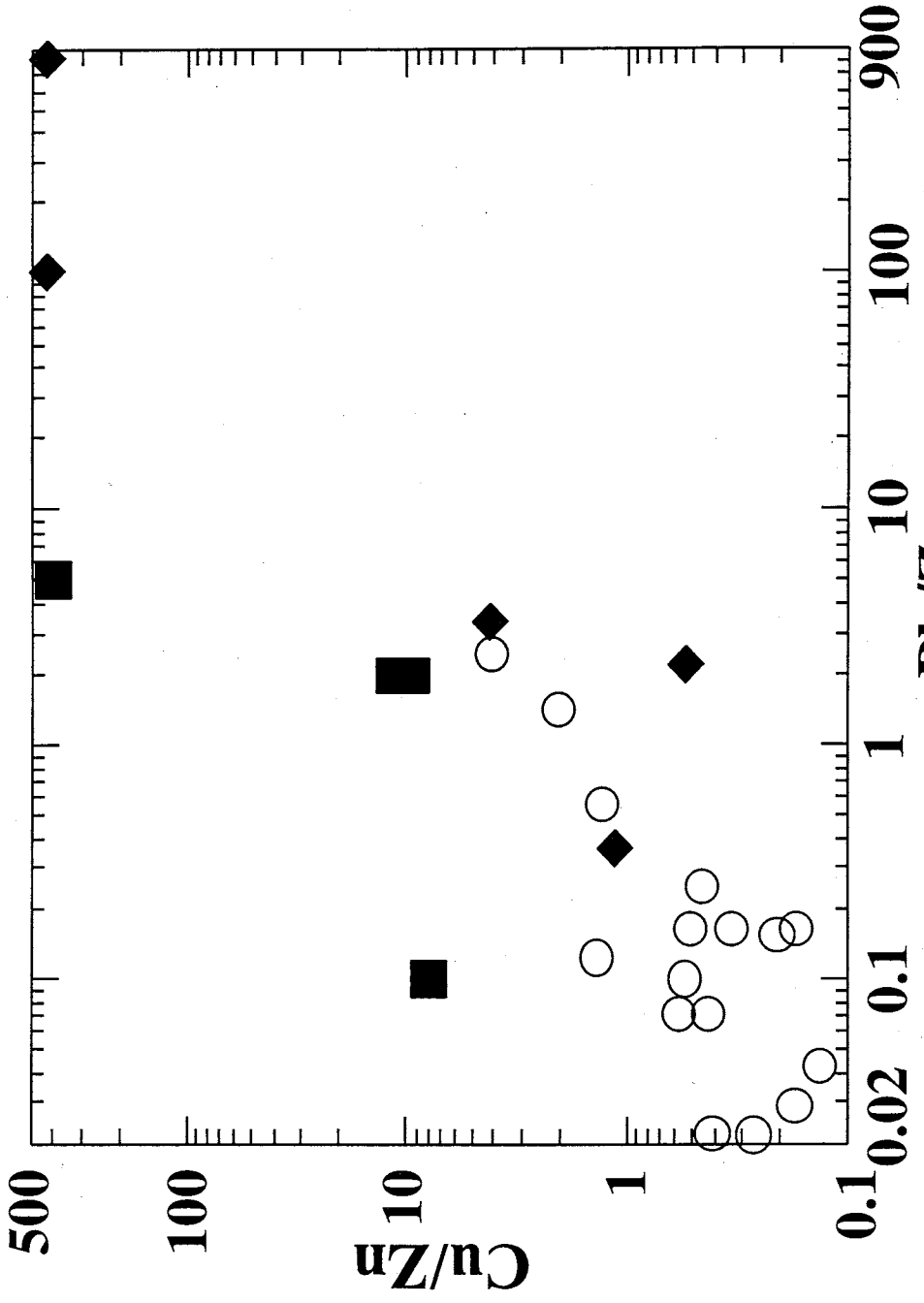


Figure 61. Binary plot of log Cu/Zn vs. log Pb/Zn for water samples. Open circles designate water samples from the Hillsboro district, closed squares represent stream sediment agitation test water samples, and closed diamonds represent waste rock pile agitation test water samples.

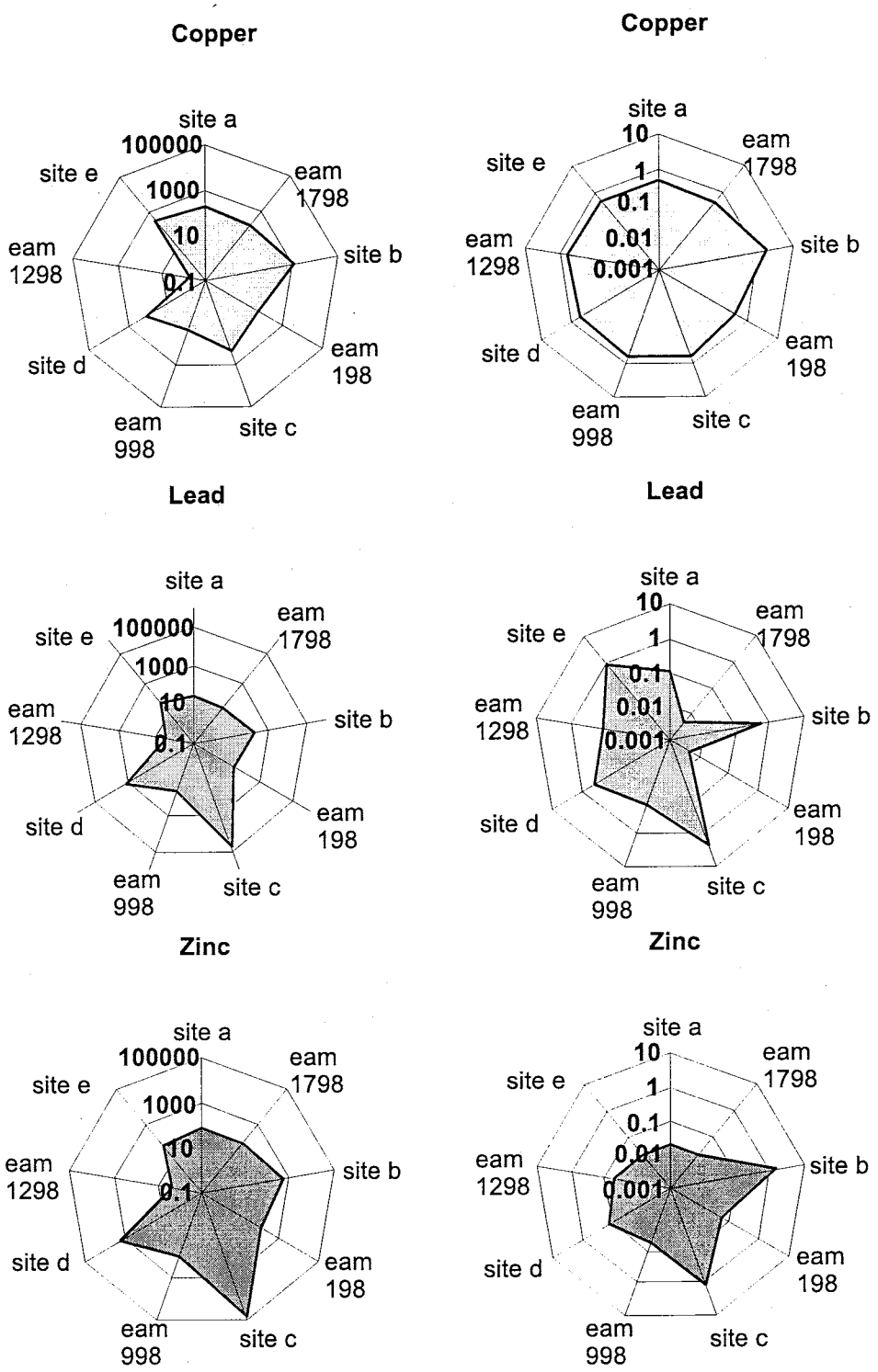


Figure 62. Log scale metal concentrations from Sites A-E and stream sediments eam 1798,198, 998, and 1298. The left three graphs are Cu, Pb, and Zn concentrations for solid samples measure by XRF and FAAS. The right three graphs are Cu, Pb, and Zn concentrations in solution and absorbed to material in suspension.

Figure 61 represents all the water samples plotted together on a log Cu/Zn versus log Pb/Zn. Generally, the stream sediment and waste rock pile agitation test water samples plot higher in overall metal ratios than the Hillsboro district water samples. The agitation test samples probably showed higher metals in solution because the acid buffering capacity as it is related to mineral / rock interaction is decreased with decreasing residence time of water from precipitation events. The differences are due possibly to the longer residence time and relative quiescence the district samples have undergone, therefore increasing chances for buffering reactions to occur. The stream sediment and waste rock pile water samples were agitated which may mechanically break down chemical rinds that may influence the fluid chemistry. Copper, lead, and zinc concentrations in Sites A-E and EAM 1798, 198, 998, and 1298 were plotted on spider/radar diagrams to compare solid sample versus water agitation sample results (Fig. 62).

# 9.0 INTERPRETATIONS

## 9.1 SAMPLING PROTOCOL

The sampling strategy appeared to be sufficient to geochemically characterize most of the waste rock piles due to their relative geochemical and mineralogical homogeneity compared to the Laramide polymetallic vein waste rock piles. Heterogeneities that are deeper than 25 cm in the waste rock piles may exist but were not quantified in this study. Caution is advised using a sampling depth of 25 cm, because mineralogical and geochemical heterogeneities exist in some of the waste rock piles examined (Table 9). Although a 25 cm sampling depth appeared to geochemically characterize some waste rock piles, the coverage was found to be incomplete for Site B. Evidence for heterogeneities was found during the sampling of the Laramide polymetallic vein waste rock pile (Site B) where different layers of waste rock could be observed from rilling features that were present. Due to the high amount of geochemical heterogeneity found in the waste rock pile (Fig. 36-43), a 25 cm sampling depth was insufficient to correctly characterize the waste rock pile.

### 9.1.1 Sampling densities

Sampling densities of 15, 30, and 45 were used to determine the level of sampling necessary to geochemically characterize a waste rock pile. Sites A-D were sampled with densities of 15, 30, and 45 in grid patterns tailored to the waste rock pile's dimensions. Waste rock piles can be adequately characterized by a sampling density of 15 or 30 samples per sampling grid pattern. This study shows that 15 or 30 samples typically yield the highest metal concentrations. As an initial geochemical characterization, 15 to 30 sample cells per given sampling grid pattern were typically adequate (Fig. 28 - 31; Table

E.3, E.4). Lower metal concentrations were found in some of the waste rock piles as the sampling density increased from 30 to 45. Effectively, this higher sampling density better characterizes the waste rock piles but the cost for sampling to that density is higher. Sampling densities of 15 or 30 per sampling grid are justified by the same metal concentration present in the cumulative average and in the mean of all 45 samples analyzed separately for Site B (Fig. 32-35). However, for some metals 45 sample cells per sampling pattern better characterized the waste rock pile (Fig. 32-35). When metal concentrations were approximately equal between sampling densities, the least number of samples was chosen not only to characterize the waste rock pile best but also to be cost effective. Ideally the samples should be analyzed in small batches to lower costs and to be able to discontinue sampling once the desired level of characterization is reached (Runnells et al., 1997). The desired level of sampling can be approached once the cumulative average of the samples is within a certain accepted standard deviation of the mean of those samples.

## 9.2 METAL MOBILITY

### 9.2.1 Local scale metal mobility

Metal mobility of trace metals from the waste rock piles into the environment was quantified by stream sediment geochemistry. According to Ficklin et al. (1994), the composition of waters draining diverse mineral deposits is a function of: the acid-buffering capacity of mineral deposit host rocks and gangue material, the types and abundance of metal bearing sulfide minerals in the deposits, the exposure of the sulfides to weathering, and the availability of dissolved oxygen for the sulfide oxidation process. Any water present in the arroyo during or after a precipitation event is short lived.

Therefore, any chemical changes incurred by the water after flowing from the waste rock pile to the stream sediment are "imprinted" on the location where the water ultimately evaporates (or percolates into the ground) with the deposition of secondary mineral precipitates. In the case of the agitation tests conducted on the waste rock piles and select stream sediments, the suspended materials less than 11 μm contained greater concentrations of copper, lead, and zinc than the same samples with dissolved species filtered through a 0.45 μm filter (Fig. 54). The suspended material is probably composed of clay (Moore and Reynolds, 1997). Therefore, clays (such as illite/smectite and smectite) eroded and transported during a flash flood event carry more base metals adsorbed to their surface than are dissolved in the water. In Figure 60 all of the stream sediment samples have the highest increase in Cu/Zn which means copper is higher in concentration relative to zinc in solution and is preferentially adsorbed on to clay surfaces (Table 12, E.12).

The placer gold waste rock pile (Site A) material was probably derived from the Grayback Arroyo about 100 meters north of the site. Even though the material was processed for gold and electrum, it has the same bulk mineralogy as the nearby arroyo sediment. This is consistent with the metal ratio trends that show little to no change between the site and the stream sediment (Fig. 44). The agitation tests showed that Cu/Zn and Pb/Zn increased in Site A and in the stream sediment sample EAM 1798 (Figs. 59, 60). This change reflects the mineralogical similarities between the two samples.

The Laramide polymetallic vein waste rock pile (Site B) and down gradient stream sediment samples showed different trends for different metal ratios. The primary

copper mineral present in the Laramide polymetallic vein deposit is chalcopyrite. Initial high Cu/Zn in the waste rock pile demonstrates the presence of chalcopyrite with minor sphalerite. Progressively decreasing Cu/Zn and a decreasing Cu concentration in the stream sediments indicate chemical metal mobility of Cu away from the waste rock pile (Fig. 45). This is due to the movement of Cu from the waste rock pile and into the stream sediments with progressively decreasing metal concentration with increasing distance from the source. An increasing Pb/Cu trend dominates the waste rock pile samples downstream to the distal stream sediment sample. Cu/Zn increases in the solid versus water sample of EAM 198, after agitation tests (Fig. 57). In addition to the prevalent mechanical or physical movement of material in the streambed, this evidence suggests there is a chemical component for metal movement away from Site B (Fig. 57). Cu/Zn may have decreased in Site B from solid to agitation water samples due to the coarse-grain size of pyrite and chalcopyrite in the waste rock pile and the relatively lower amount of surface area available for chemical reaction and transport of copper (Fig. 60, 22). Pyrite is suspected to be the primary arsenic contributor to the waste rock pile geochemical composition (as shown by electron microprobe data).

The chemical composition of the carbonate-hosted Pb-Zn waste rock pile and associated down gradient stream sediments are shown in Figure 46. Pb/Cu in Site C decreases approximately 100 times to the first stream sediment sample. This is a result of the high concentration of lead in the form of minerals such as galena, wulfenite, vanadinite, cerussite, and anglesite. This precipitous change is the result of relative immobility of lead away from the waste rock pile. Galena is rimmed by cerussite, while the vanadates (vanadinite and endlichite) and molybdates (wulfenite) have no weathering

rind. Oxidation from late-stage hydrothermal fluids are likely to be the primary source of the "armoring" of galena by cerussite because of the pervasive nature of the rind and the low acid producing potential present in the waste rock pile to warrant rind formation by weathering (Fig. 15). Comparison of the solid versus water samples from the agitation tests reveals a marked Pb/Cu decrease in Site C and the stream sediment sample EAM 998 (Figs. 59, 60). This suggests the possibility that lead-bearing minerals present in the stream sediments are mainly physically removed from waste rock pile detritus. However, Cu/Zn and Pb/Zn increase from the waste pile and the stream sediments indicating physical or chemical metal mobility (Figs. 59, 60). This indicates that copper, lead, and zinc sulfates and/or salts may form from dissolution/re-precipitation reactions with the application of moisture.

The carbonate-hosted Ag-Mn waste rock pile and associated stream sediment geochemistry is shown in Figure 47. The solid samples show a decreasing Pb/Cu trend away from Site D. This trend is most likely the result of continually decreasing detrital lead-bearing manganese oxides (coronadite) present in the stream sediments. This is further supported by the Pb/Cu decrease in EAM 1298 (Fig. 59, 60). Chemical composition of Site D and EAM 1298 indicates Cu/Zn and Pb/Zn increases from solid to water samples from the agitation test. Once again this demonstrates metals move in solution and/or solution plus suspended material. Adsorption of metals to clay surfaces is typical of smectite and illite/smectite mixed layered clays and which may be easily carried downstream.

The northern Laramide polymetallic vein waste rock pile (Site E) was sampled only to compare the mineralogy and geochemistry with Site B. No stream sediment

samples were taken. Pb/Cu, Cu/Zn, and Pb/Zn increased from the solid to the water samples from the agitation tests, perhaps as a result of evaporite rinds on the surface of sulfides which were dissolved or put into suspension during the laboratory created precipitation event (Figs. 59, 60).

Gangue mineralogy of the mineral deposits and mineralogy of the host rocks in the district is important to overall acid neutralizing capacity. As with acid production, acid neutralization rates are affected by host rock lithologies, temperature, pH, surface area, and grain size. For example, a fine-grained igneous rock will tend to have a higher capacity to neutralize acid than a coarse-grained igneous rock, providing all other factors remain static. Ritchie (1994b) describes the slow dissolution of minerals such as muscovite, biotite, albite, anorthite, and K-feldspar by acid, and the consequent neutralization of acid. Streams running through limestone or dolomite will tend to have the quickest and highest incidence of acid neutralization, thus creating possible metal bearing secondary mineral precipitates.

### 9.2.2 Oxidation by hydrothermal alteration versus weathering

Oxidation rinds on the minerals analyzed varied in thickness, shape, degree of crystallinity and geochemical composition. Sources of the mineral oxidation rinds are hydrothermal fluids or surficial weathering. Larger mineral rind crystals as well as thicker rinds are interpreted to result from hydrothermal oxidation because the grains have been affected by fluids for a longer period of time than those in the surficial weathering environment which show microcrystalline or amorphous thinner rinds. Thin clay rinds may also form on oxide grains that are another type of thin weathering rind. Weathering rinds on embayed or pitted grains in Site E may be due to high local acid

concentrations because of preferential etching from a longer acidic solution residence time (Fig. 19). The pyrites at Site E (Fig. 18) show more, and in some cases thicker, oxidation rinds than Site B (Fig. 12). Pyrite at Site B is brecciated and has been re-cemented by iron oxides and iron hydroxides. Oxidation of the pyrite grain has occurred as well as re-precipitation of iron oxides, iron hydroxides, iron oxyhydroxides, and iron sulfates, with a relative increase of sulfur, in the outer rind (Fig. 12). This occurrence is consistent with intermittent wetting and drying events. Dissolution followed by evaporation is characteristic of mineral weathering in an arid environment. Hydrothermal alteration is indicated by brecciation and grain re-cementation by iron hydroxides and iron sulfates while the pristine grain has only a secondary mineral rind (Fig. 12). In the case of sulfide minerals and rinds associated with them; supergene alteration / hydrothermal alteration cannot always be distinguished from weathering rinds (Fig. 12). In Figure 12 there is evidence for both processes. Secondary mineral rinds of the chalcopyrite grain from Site B support the hypothesis that the secondary mineral mode of formation was by dissolution and re-precipitation reactions during weathering (Fig. 14). The bladed / tabular crystal growth on the exterior of a cerussite grain and the mineralogical nature of the waste rock pile (low acid producing potential) indicates the source of the cerussite rind may have been supergene oxidation by late stage hydrothermal fluids (Fig. 16). Hydrothermal fluids have the capacity to deposit and / or re-distribute minerals to create well formed crystals. This can be further supported by the cerussite rind around a majority of the galena grain (Fig. 15). Clay rinds are interpreted to form due to surficial weathering and slow break down of oxide mineral grains relative

to sulfide grains (Figs. 11, 17). Clays can also adhere to the surface of a chemically inert oxide grain that may also create a rind.

### 9.2.3 Primary and secondary mineralogy

Sulfide weathering in a semi-arid environment may create weathering rinds due to metal complex dissolution, re-distribution, evaporation, and re-deposition effects. Mineral rinds surrounding pyrite, galena, and chalcopyrite were examined using the electron microprobe. Quantitative results indicate the presence of many secondary minerals that may preferentially concentrate metals. The rate of oxidation of pyrite is the main contributing factor for acid production in a disturbed mining area. Pyrite oxidation can be described by the following reactions (Borek, 1994):

$$FeS_2 + 7/2\ O_2 + H_2O \ ===> Fe^{2+} + 2\ SO_4^{2-} + 2\ H^+ \quad (1)$$

$$4\ Fe^{2+} + O_2 + 4\ H^+ \ ===> 4\ Fe^{3+} + 2\ H_2O \quad (2)$$

$$Fe^{3+} + 3\ H_2O \ ===> Fe(OH)_3 + 3\ H^+ \quad (3)$$

$$FeS_2 + 14\ Fe^{3+} + 8\ H_2O \ ===> 15\ Fe^{2+} + 2\ SO_4^{2-} + 16\ H^+ \quad (4)$$

Other iron species are possible products of pyrite oxidation. Hematite may have formed by the following dehydration reaction that would follow Equation 3:

$$Fe(OH)_3 \ ===> FeOOH + H_2O \quad (5)$$

$$2\ FeOOH \ ===> Fe_2O_3 + H_2O \quad (6)$$

Iron sulfate products can also aid in further oxidation of pyrite to perpetuate sulfuric acid generation (Ritchie, 1994a):

$$4\ FeSO_4 + 2\ H_2SO_4 + O_2 \ ===> 2\ Fe_2(SO_4)_3 + 2\ H_2O \quad (7)$$

$$FeS_2 + Fe_2(SO_4)_3 + 2\ H_2O + 3\ O_2 \ ===> \ 3\ FeSO_4 + 2\ H_2SO_4 \quad (8)$$

Pyrites examined were altered by chemical weathering in the environment as well as late stage hydrothermal fluid alteration. Like pyrite, chalcopyrite is a producer of sulfuric acid. The amount of acid per mole of sulfide mineral produced from oxidation reactions is, however, less than that of pyrite (Park and MacDiarmid, 1975):

$$2CuFeS_2 + 17/2\ O_2 + 2H_2O \ ===> Fe_2O_3 + 2\ Cu^{2+} + 4\ SO_4^{2-} + 4\ H^+ \qquad (9)$$

$$CuFeS_2 + 4\ Fe^{3+} + 2\ H_2O + 3\ O_2 \ ===> Cu^{2+} + 5\ Fe^{2+} + 2SO_4^{2-} + 4\ H^+ \qquad (10)$$

Chalcopyrite may chemically weather to iron oxide and an acidic solution of copper sulfate (Eq. 9), or an iron sulfate solution may be created (Eq. 10).

Although the rate of pyrite oxidation may be over-estimated by more than two times (Fennemore et al., 1998) in an arid environment; it remains a factor in metal mobility. Secondary mineral formation occurs at very low pH values resulting from the production of $H_2SO_4$ (Eq. 1, 4, 8, 10, 12, 13) (Murad et al., 1994). After a precipitation event, freshwater enters the system thereby diluting the $SO_4^{2-}$ concentration and increasing the pH. This change leads to precipitation of $Fe^{3+}$ oxides and oxyhydroxides of extremely small particle size (Murad et al., 1994). Arsenic, copper, and zinc partitioning may occur due to adsorbtion onto $Fe^{3+}$ oxyhydroxysulfate precipitates (Webster et al., 1994). Hydrothermal fluids can also create mineral rinds that exist prior to the onset of surficial weathering processes. Supergene or hydrothermal fluid oxidation processes were observed in at least one site (Fig. 15, 16) and surficial weathering in at least two sites analyzed (Fig. 11, 17). Rinds resulting from oxidizing fluids in some cases produce an armoring effect, especially on galena, which prohibits lead from chemically entering the environment.

Samples from Site C contained galena that contained cerussite oxidation rinds and anglesite replacement. Anglesite is the direct oxidation product of galena:

$$PbS + 2O_2 \text{ ===> } PbSO_4 \qquad (11)$$

Oxidation (Eq. 12) can also occur with the reaction of galena with ferric sulfate and sulfuric acid produced by oxidation of associated minor iron sulfides (Park and MacDiarmid, 1975). This reaction is an unlikely culprit due to the minor amounts of pyrite present at the waste rock pile site.

$$PbS + 2Fe^{3+} + 3SO_4^{2-} + 3/2O_2 + H_2O \text{ ===> } PbSO_4 + 2Fe^{2+} + 2H^+ + 3SO_4^{2-} \qquad (12)$$

The more common oxidation reaction, however, is that of galena to cerussite (Ramdohr, 1969). This reaction is especially common in the presence of calcareous rocks (i.e. limestone and dolomite) (Park and MacDiarmid, 1975).

$$PbS + H_2O + CO_2 + 2O_2 \text{ ===> } PbCO_3 + SO_4^{2-} + 2H^+ \qquad (13)$$

This process may have two steps with anglesite formation (Eq. 11) as an intermediate form before oxidizing further to cerussite (Eq. 14):

$$PbSO_4 + H_2O + CO_2 \text{ ===> } PbCO_3 + SO_4^{2-} + 2H^+ \qquad (14)$$

Typically oxidation reactions occur more rapidly in sulfide minerals relative to those in oxide and silicate minerals. Minor amounts of pyrite suggest a relatively low acid generation potential of the waste rock pile. The pervasive nature of the cerussite rind and replacement of cerussite along fractures in the galena crystal lattice, indicate a likely origin of oxidation by hydrothermal fluids. Although sphalerite is not present in the

samples analyzed, smithsonite will also "armor" the sphalerite grain in the same way cerussite armors galena due to the same supergene oxidation process (Ramdohr, 1969; Williams, 1990). Smithsonite ($K_{sp} = 1.46 \times 10^{-10}$), however, is more soluble than cerussite ($K_{sp} = 7.40 \times 10^{-14}$) and will chemically break down quicker (Lide, 1999). Lead mobility is relatively low in comparison to the mobility of zinc which is moderately high (Rose et al., 1979). In arid or semiarid environments zinc may also be retained in the oxidized zone as hydrozincite, hemimorphite, or other carbonate and silicate minerals (Park and MacDiarmid, 1975). These minerals will prohibit lead and zinc movement away from the rock pile due to their chemical stability in the surficial weathering zone.

The typical Laramide polymetallic vein is characterized by sericitic and propylitic alteration produced from hydrothermal fluids (Hedlund, 1985). Laboratory experiments from Bhatti et al. (1994) indicate jarosite is the sink for $K^+$ released during mica (sericite) weathering. In Figure 12, the interior rind is predominantly jarosite and the outer rind is a phase of hematite/ iron sulfate. The chalcopyrite grain has an interior rind that appears to be $Fe(OH)_3$ (ferric hydroxide) while the nodule and second rind appears to be $Fe_5HO_8 \bullet 4H_2O$ (ferrihydrite) (Fig. 14). I speculate that the third rind is the same as the first due to similar mean atomic number contrast on the electron microprobe. This would support the hypothesis of a precipitation event with subsequent evaporation.

Site E contains some pyrites with a much thicker weathering rind, perhaps due to its longer residence time on the waste rock pile relative to the material at Site B (Fig. 18). Mining at Site E ended in the early part of the 20$^{th}$ century while mining at Site B continued until the early 1970's. The interior rind in Figure 18 is a phase of iron sulfate while the exterior rind at point #5 is $Fe_8O_8(OH)_6SO_4$ (schwertmannite). Additional

weathering rinds are present in Figure 18, but it appears that some have been overprinted by subsequent dissolution/re-precipitation. Figure 19 displays an angular, hackly edge of the grain. The core iron and sulfur percentages are nearly identical in comparison to the pyrite grain (Fig. 18). The difference between the two pyrites may be their location in the waste rock pile (closer to the surface or deeper in the pile), type and amount of grain contact (mineralogy and grain packing), and different history of acid attack and/or production. These are all possible factors controlling the amount of water as well as the water's residence time on the pyrite grain. Therefore, the pyrite oxidation rind thickness may be a function of the location within the waste rock pile. Jagged edge morphology of the pyrite grain may form during surficial weathering (Fig. 19). One iron sulfate rind is present on the pyrite grain (Fig. 19). This rind is very thin in comparison to other pyrites at Site E. Preferential pyrite grain degeneration history and subsequent grain morphology may be due to different hydrothermal fluid influences between the two pyrites (Figs. 18, 19).

# 10.0 CONCLUSIONS

Typically, the smallest grain size fractions contain higher concentrations of metals due to the mineralogical nature of the material such as clays which have a high cation exchange capacity due to the higher surface area available for adsorption of ions. Of the six size fractions analyzed (2-1 mm, 1-0.5 mm, 0.5-0.25 mm, 0.25-0.125mm, 0.125-0.063 mm, and < 0.063 mm) in this study, higher metal concentrations were typically found in the three smallest size fraction ranges (Table 12, Figs. 20-27). In order to obtain the highest metal concentrations; the less than 0.25 mm (250 microns) size fraction was sampled for this study.

Geochemical and mineralogical heterogeneity exists in the Laramide polymetallic vein waste rock piles Site B and E. Vertical mineralogical variation was observed in Sites B and E as well as chemical variation in the surface sampling grid pattern of Site B (Figs. 36-43). These variations have important implications for future sampling strategies that may involve specific interval sampling or specific mineralogical layer sampling. Sampling densities continue to be difficult to determine for future sites because each site may have different history of construction and can be mineralogically different.

Using grid patterns unique to each of the waste rock piles, three homogenized samples were obtained using sampling densities of 15, 30, and 45 sample cells. Surficial samples may in some cases (Sites A, C, and D) obtain an adequate geochemical representation of the overall content of the waste rock pile. Waste rock piles can be adequately chemically characterized by homogenizing samples collected from a grid containing 15-30 sample cells (Figs. 28-31). However, this sampling strategy does not take into account for vertical heterogeneities present at depth in Site B and Site E. The

sampling strategy in this study needs to be supplemented by appropriate drilling methods with a specific grid pattern to adequately geochemically characterize high volume waste rock piles.

Metals are moving as mineral grains, suspended material, and dissolved material (Fig. 44-47). Rinds in galena may prevent lead movement geochemically but not movement physically as a mineral grain. Dissolved material may precipitate to form soluble salts onto grains in the waste rock pile and the stream bed. Agitation tests indicate copper and zinc are preferentially partitioned in the suspended material during the simulated precipitation event (Fig. 58). Primary clays present in the stream sediments were smectite, illite, and illite/smectite mixed layer clays (Table 13).

Metal mobility is higher in the Laramide polymetallic vein waste rock piles (Site B and Site E) relative to the carbonate-hosted replacement waste rock piles (Site C and Site D). This may be a result of pyrite-bearing waste rock piles generating sulfuric acid that increase metal availabilty to the environment. Iron sulfate, iron oxide, and iron oxyhydroxide form rinds on the chalcopyrite and pyrite (Figs. 12-14, 18, 19; Table 10). Pyrite oxidation rinds preferentially partition arsenic (Table 10). Weathering rind thickness varies depending on mineralogy, residence time in the waste rock pile, and hydrothermal activities associated with the different deposits. Strong precipitation events may flush out metals partitioned in the outer rinds of oxidized sulfide grains. This would create a larger concentration of metals released into the environment than if it were constantly flushed such as in a more temperate climate. Conversely, oxidation by hydrothermal fluids of some mineral grains like galena may be "armored" by cerussite

(Fig. 15). This leads to a sufficient decrease in the lead concentration available for chemical transport in the environment.

# 11.0 RECOMMENDATIONS

Although many different questions were answered in this study, many more were created. Some suggestions to answer specific questions are enumerated below.

1) Develop different sampling procedures that account for vertical mineralogical and geochemical heterogeneities within a mine waste rock pile. Other sampling procedures may entail sampling of different layers as they are apparent and extrapolating the results into what is unable to be seen.

2) Sample the layers of different mineralogies or specific intervals regardless of mineralogy. This may give insight into new methods for sampling waste rock piles with or without a mineralogical sampling bias.

3) Determine the arsenic source in the mine waste rock piles. Trace amounts of arsenic are found in the pyrite and chalcopyrite in Site B and E. Arsenic is concentrated in the rinds of the pyrites. Is this due to dissolution from the core with a concentration effect in the rind? Or is the arsenic coming from another mineral and in the dissolved form adsorbing to the surface of the sulfide grains?

4) Determine the speciation of arsenic to better understand its mobility in the mine waste rock pile and in the stream sediment environment. What arsenic complexes form in this type of environment and how do they effect the availability of arsenic to the environment?

5) Make thin sections of crusts that occur on the waste rock pile to gain insight into mineral formation from wetting and drying events. This will help quantify the amount of interaction the mine waste rock pile has had in the past and may have in the future with the environment. Identify the mineralogical and chemical composition of the crust

present on mine waste rock piles. It is recommended to impregnate the sample in situ with epoxy containing a low viscosity.

6) Determine mineralogy of clays and colloids present in the less than 11 μm fraction of the agitation test water samples to better understand metal movement in mine waste rock piles and stream sediments. Once the type of clay and/or colloid is identified, the amount of metal movement can be better quantified.

## 12.0 REFERENCES

Alminas, H.V. and Watts, K.C., 1978. Interpretive Geochemical Map of the Hillsboro And San Lorenzo Quadrangles Exclusive of the Black Range Primitive Area, Sierra and Grant Counties, New Mexico, U.S. Geological Survey Miscellaneous Field Studies Map MF-900 G;1:48000 scale.

Alminas, H.V., Watts, K.C., Siems, D.F., and Kraxberger, V.E., 1978a. Map Showing Anomalous Zinc Distribution in Stream Sediment Concentrates, Hillsboro and San Lorenzo Quadrangles, Exclusive of the Black Range Primitive Area, Sierra and Grant Counties, New Mexico. U.S. Geological Survey Miscellaneous Field Studies Map MF-900F; 1:48000 scale.

Alminas, H.V., Watts, K.C., Siems, D.F., and Kraxberger, V.E., 1978b. Map Showing Anomalous Silver Distribution in Stream Sediment Concentrates, Hillsboro and San Lorenzo Quadrangles, Exclusive of the Black Range Primitive Area, Sierra and Grant Counties, New Mexico. U.S. Geological Survey Miscellaneous Field Studies Map MF-900C; 1:48000 scale.

Alminas, H.V., Watts, K.C., Siems, D.F., and Kraxberger, V.E., 1978c. Map Showing Anomalous Copper Distribution in Stream Sediment Concentrates, Hillsboro and San Lorenzo Quadrangles, Exclusive of the Black Range Primitive Area, Sierra and Grant Counties, New Mexico. U.S. Geological Survey Miscellaneous Field Studies Map MF-900D; 1:48000 scale.

Alta Gold Company, 1999. Form 10K.

Bakkom, E. and Salvas, S., 1997. Copper Flats Reclamation Plan: Phase I. Department of Mineral and Environmental Engineering, Senior Thesis, New Mexico Institute of Mining and Technology, 56 p.

Banks, D., Younger, P.L., Arnesen, R.T., Iversen, E.R., and Banks, S.B., 1997. Mine-water chemistry: the good, the bad and the ugly. Environmental Geology, vol. 32, no. 3, p. 157-174.

Bauer, H.L. Jr., 1950. Radioactive Ilmenite, Virginia Claim, Hillsboro Mining District, Sierra County, New Mexico. U.S. Geological Survey Trace Elements Memorandum Report 139.

Bhatti, T.M., Bigham, J.M., Vuorinene, A., and Tuovinen, O.H., 1994. Alteration of Mica and Feldspar Associated with Microbial Oxidation of Pyrrhotite and Pyrite. in C. N. Alpers and D. W. Blowes, Environmental Geochemistry of Sulfide Oxidation, American Chemical Society Symposium Series 550, Washington D.C., p. 90-105.

Borek, S. L., 1994. Effect of Humidity on Pyrite Oxidation. in C. N. Alpers and D.W. Blowes, Environmental Geochemistry of Sulfide Oxidation, American Chemical Society Symposium Series 550, Washington D.C., p. 31-44.

Boulding, J. R., 1994. Description and Sampling of Contaminated Soils: A Field Guide, 2nd Ed. Boulding Soil-Water Consulting; Lewis Publishers, Ann Arbor; 146 p.

British Columbia Acid Mine Drainage Task Force, 1992. Field QA/QC Protocols for Monitoring and Predicting Impacts of Acid Mine Drainage. Norecol EnvironmentalConsultants Ltd., 68 p.

Browning-Ferris Industries, 1991. Comparison of Procedures for TCLP Extract Digestion; Conventional vs. Microwave. U.S. Environmental Protection Agency Seventh Annual Waste Testing and Quality Assurance Symposium; Washington D.C., 1991, 10 p.

Bureau of Land Managment, 1996. Copper Flat Project: Environmental Impact Statement Department of the Interior, Bureau of Land Managment, Las Cruces, New Mexico. 256 p.

Dunn, P.G., 1982. Geology of the Copper Flat porphyry copper deposit, Hillsboro, Sierra County, New Mexico; in S.R.Titley, ed., Advances in Geology of the Porphyry Copper Deposits: University of Arizona Press, p. 313-326.

Dunn, P.G., 1984. Geologic Studies During the Development of the Copper Flat Porphyry Deposit. Mining Engineering, p. 151-159.

Ebdon, L., 1982. An Introduction to Atomic Absorption Spectroscopy: A Self-teaching approach. Mackays of Chatham Ltd., London, 137 p.

Fennemore, G.G., Neller, W.C., Davis, A., 1998. Modeling Pyrite Oxidation in Arid Environments. Environmental Science and Technology, vol. 32, no. 18, p. 2680-2687.

Ficklin, W.H., Plumlee, G.S., and Smith, K.S., 1994. Geologic and Geochemical Controls on the Composition of Water Draining from Diverse Mineral Deposits; in L.M.H. Carter, M.I. Toth, and W.C. Day eds., U.S.Geological Survey Research on Mineral Resources, Part A: Ninth V.E. Mckelvey Forum on Mineral and Energy Resources. U.S. Geological Survey Circular 1103-A, p. 34-35.

Fowler, L.L., 1982. Brecciation, Alteration, and Mineralization at the Copper Flat Porphyry-Copper Deposit, Hillsboro, N.M. M.S. Thesis, University of Arizona, Tucson, 133 p.

Gold Express Corporation, 1992. Environmental Assesment for Re-establishing the Copper Mine, Copper Flat, New Mexico. Gold Express Corp., Denver, CO, 74 p.

Green, G.N. and O'Neill, J.M. eds., 1998. Digital Earth Science Database Caballo Resource Area, Sierra and Otero Counties, South-central New Mexico. U.S. Geological Survey, Open File Report 98-780.

Harley, G.T., 1934. The Geology and Ore Deposits of Sierra County, New Mexico. New Mexico Bureau of Mines and Mineral Resources, Bulletin 10, 220 p.

Hedlund, D.C., 1977. Mineral Resources Map of the Hillsboro and San Lorenzo Quadrangles, Sierra and Grant Counties, New Mexico. U.S. Geological Survey Miscellaneous Field Studies Map MF-900 B, Sheets 1 and 2; 1:48000 scale.

Hedlund, D.C., 1985. Economic Geology of some selected mines in the Hillsboro and San Lorenzo Quadrangles, Grant and Sierra Counties, New Mexico. U.S. Geological Survey, Open File Report 85-0456, 43 p.

Hedlund, D.C., Watts, K.C., Alminas, H.V., and Wynn, J.C., 1979. Background Information to Accompany Folio of Geologic, Mineral Resource, Geochemical, Aeromagnetic, and Gravity Maps of the Hillsboro and San Lorenzo Quadrangles, Sierra and Grant Counties, New Mexico. U.S. Geological Survey Circular 808, 26 p.

Herring, J.R. and McLemore, V.T., in press, Geochemistry of mine dump samples from the Lake Valley mining district of Sierra County, south-central New Mexico: U.S.Geol. Surv. Prof. Paper, 20 pp.

Hood, M., Pena, F., Avelar, J.T., and Bailey, J., 1983. Quintana Minerals Corporation Copper Flat Project. Society of Mining Engineers of AIME, Preprint no. 83-98, 18 p.

Korzeb, S.L. and Kness, R.F., 1994. Mineral Investigation of Areas of Critical Environmental Concern in part of the Caballo Resource Area, Sierra County, New Mexico. U.S. Bureau of Mines, Mineral Land Assessment Open File Report MLA 12-94, p. 1-27.

Korzeb, S.L., Kness, R.F., Geroyan, R.I., Ward, D.A., 1995. Mineral Resources Assessment of the Caballo Resource Area, Sierra and Otero Counties, New Mexico. U.S. Bureau of Mines, Mineral Land Assessment Open File Report MLA 5-95, 172 p.

Kuellmer, F.J., 1955. Geology of a Disseminated Copper Deposit near Hillsboro, Sierra County, New Mexico. New Mexico Bureau of Mines and Mineral Resources Circular, 34, 46 p.

Lawrence, R.W., 1990. Prediction of the Behavior of Mining and Processing Wastes in the Environment. in F.M. Doyle ed. Proceedings of Western Regional Symposium on Mining and Mineral Processing Wastes, Society for Mining, Metallurgy, and Exploration Inc., Littleton, Colorado, p. 115-121.

Lide, D.R., ed., 1999. CFC Handbook of Chemistry and Physics, 79th Edition. CRC Press, New York, 2378 p.

Lindgren, W., Gordon, C.H., and Graton, L.C., 1910. The Ore Deposits of New Mexico. U.S. Geological Survey, Professional Paper 68, 361 p.

Lone Tree Mine, 1996. Meteoric Water Mobility Procedure: Standardized Column Percolation Test Procedure. Nevada, 5 p.

Lovering, T.G., and Heyl, A.V., 1989. Mineral Belts in Western Sierra County, New Mexico, Suggested by Mining Districts, Geology, and Geochemical Anomalies. U.S. Geological Survey Bulletin 1876. 49 p.

Marcus, W.A., 1987. Copper Dispersion in Ephemeral Stream Sediments. Earth Surface Processes and Landforms, vol. 12, p. 217-228.

McLemore, V.T., Heizler, M.T., and Munroe, E.A., 1999. Geochemistry of Host Rocks, Veins, Replacements, and Jasperoids in the Hillsboro Mining District, Sierra County, New Mexico. NMGS abstract, New Mexico Geology, vol. 21, no. 2, p. 45.

Moore, M.M. and Reynolds, R.C., 1997. X-ray Diffraction and the Identification and Analysis of Clay Minerals, 2nd ed. Oxford University Press, New York, 378 p.

Murad, E., Schwertmann, U., Bigham, J.M., and Carlson, L., 1994. Mineralogical Characteristics of Poorly Crystallized Precipitates Formed by Oxidation of $Fe^{2+}$ in Acid Sulfate Waters. in C.N. Alpers and D.W. Blowes, eds, Environmental Geochemistry of Sulfide Oxidation, American Chemical Society Symposium Series 550, Washington D.C., p. 190-200.

Norman, D.I., Kyle, P.R., and Baron, C., 1989. Analysis of Trace Elements Including Rare Earth Elements in Fluid Inclusion Liquids. Economic Geology, vol. 84, p. 162-166.

Norrish, K. and Chappel, B., 1977. An Accurate X-ray Fluorescence Spectrographic Method for the Analysis of a wide range of Geologic Samples. Geochimica Cosmochimica Acta. vol. 33, p. 67-76.

Odor, L., Wanty, R.B., Horvath, I., and Feugedi, U., 1998. Mobilization and Attenuation of Metals Downstream from a Base-Metal Mining Site in the Matra Mountains, northeastern Hungary. Journal of Geochemical Exploration, vol. 65, p. 47-60.

Park, C. F., Jr. and MacDiarmid, R. A., 1975. Ore Deposits. 3rd edition, W.H. Freeman and Co., San Francisco, 239p.

Ramdohr, P.,1969. The Ore Minerals and Their Intergrowths. Pergamon Press, London, 1174 p.

Rampe, J.J. and Runnells, D.D., 1989. Contamination of water and sediment in a desert stream by metals from an abandoned gold mine and mill, Eureka District, Arizona. Applied Geochemistry, vol. 4, p. 445-454.

Reeves, C.C. Jr., 1963. Economic Geology of a Part of Hillsboro, New Mexico, Mining District. Economic Geology, vol. 58, p. 1278-1284.

Ritchie, A. I. M., 1994a. Rates of Mechanisms that Govern Pollutant Generation from Pyritic Wastes. in: C.N. Alpers and D.W. Blowes, eds, Environmental Geochemistry of Sulfide Oxidation, American Chemical Society Symposium Series 550, Washington D.C., p. 108-122.

Ritchie, A.I.M., 1994b. The Waste Rock Environment. in J.L. Jambor, D.W. Blowes, eds., Short Course Handbook on Environmental Geochemistry of Sulfide Mine-Wastes. Mineralogical Association of Canada, Waterloo, Ontario, p. 131-161.

Rock Ware, Inc., 1995. Rockware Utilities: A collection of geological applications for Microsoft windows. Golden, CO.

Rose, A.W., Hawkes, H.E., and Webb, J.S., 1979. Geochemistry in Mineral Exploration. Pennsylvania State University Press, 657 p.

Runnells, D.D, Shields, M.J., and Jones, R.L., 1997. Methodology for adequacy of sampling of mill tailings and mine waste rock. in Proceedings of Tailings and Mine Waste. Balkema, Rotterdam, p. 561-563.

Salomons, W., 1995. Environmental impact of metals derived from mining activities: Processes, predictions, prevention. Journal of Geochemical Exploration, vol. 52, p. 5-23.

Sanden, P., Karlsoon, S., Duker, A., Ledin, A, and Lundman, L., 1997. Variations in Hydrochemistry, trace metal concentration and transport during a rain storm event in a small catchment. Journal of Geochemical Exploration, vol. 58, p. 145-155.

Segerstrom, K., and Antweiler, J.C. III, 1975. Placer Gold Deposits of the Las Animas district, Sierra County, New Mexico. U. S. Geological Survey Open File Report, 39 p.

Sidle, R. C., Chambers, J. C., and Amacher, M. C., 1991. Fate of Heavy Metals in an Abandoned Lead-Zinc Tailings Pond: II. Sediment. Journal of Environmental Quality, vol. 20, p. 752-758.

Smith, M. L. and Williams, R. E., 1996. Examination of Methods for Evaluating Remining a Mine Waste Site. Part I. Geostatistical Characterization Methodology. Engineering Geology, vol. 43, p. 11-21.

State of New Mexico: Standards for Interstate and Intrastate Streams. 1994. New Mexico Water Quality Control Commision, Record 20 NMAC 6.1, Santa Fe, NM.

Stollenwerk, K.G., 1994. Geochemical interactions between constituents in acidic Groundwater and alluvium in an aquifer near Globe, Arizona. Applied Geochemistry, vol. 9, p. 353-369.

Trainor, T.P., Fleisher, S., Wilderman, T.R., Goldfarb, R.J., and Huber, C.S., 1996. Environmental Geochemistry of the McKinley Lake Gold Mining District, Chugach National Forest, Alaska. U.S. Geological Survey Bulletin, vol. 2152, p. 47-57.

U.S. Department of Agriculture, Weather Bureau, 1932. Climatic Summary of the United States of America, Section 29: Southern New Mexico, p. 13-23.

U.S. Environmental Protection Agency, 1986. Test Methods for Evaluating Solid Waste Vol II: Field Manual Physical/Chemical Methods. SW-846 3rd Ed., 230 p.

U.S. Environmental Protection Agency, 1994. Technical Document: Acid Mine Drainage., EPA 530-R-94-036, 45 p.

Ward, D., 1993. Deposit Summary Update: Copper Flat Deposit, Sierra County, New Mexico. U.S. Bureau of Mines, 21 p.

Watts, K.C., 1978a. Map Showing Anomalous Tungsten and Gold Distribution in Stream Sediment Concentrates, Hillsboro and San Lorenzo Quadrangles Exclusive of the Black Range Primative Area, Sierra and Grant Counties, New Mexico. U.S. Geological Survey Miscellaneous Field Studies Map MF-900I; 1:48000 scale.

Watts, K.C., Alminas, H.V., Nishi, J.M., Crim, W.C., 1978. Map Showing Anomalous Lead Distribution in Stream Sediment Concentrates, Hillsboro and San Lorenzo Quadrangles, Exclusive of the Black Range Primitive Area, Sierra And Grant Counties, New Mexico. U.S. Geological Survey Miscellaneous Field Studies Map MF-900J; 1:48000 scale.

Watts, K.C., Alminas, H.V., Nishi, J.M., Crim, W.C., 1978b. Map Showing Anomalous Bismuth Distribution in Stream Sediment Concentrates, Hillsboro and San Lorenzo Quadrangles, Exclusive of the Black Range Primitive Area, Sierra And Grant Counties, New Mexico. U.S. Geological Survey Miscellaneous Field Studies Map MF-900K; 1:48000 scale.

Webster, J.G, Nordstrum, D.K., and Smith, K.S., 1994. Transport and Natural Attenuation of Cu, Zn, As, and Fe in the Acid Mine Drainage of Leviathan and Bryant Creeks. in C. N. Alpers and D. W. Blowes, Environmental Geochemistry of Sulfide Oxidation, American Chemical Society Symposium Series 550, Washington D.C., p. 244-260.

Wells, E.H., 1918. Manganese in New Mexico. Bulletin of the New Mexico School of Mines, Bulletin 2, 85 p.

Whiting, K.S. and Olsen, R.L., 1997. Identification of sources of metals in stream Sediments using Electron Microprobe techniques. Proceedings from Tailings and Mine Waste Conference, p. 519-528.

Williams, P.A., 1990. Oxide Zone Geochemistry. Ellis Horwood Ltd., London, 286 p.

Wynn, J.C., 1978. Parallel-Surface-Continued Aeromagnetic Map of the San Lorenzo And Hillsboro Quadrangles, Grant and Sierra Counties, New Mexico. U.S. Geological Survey Miscellaneous Field Studies Map MF-900L; 1:48000 scale.

Zhixun, L. and Herbert, R.B. Jr., 1997. Heavy Metal Retention in Secondary Precipitates From a Mine Rock Dump and Underlying Soil, Dalarna, Sweden. Environmental Geology, vol. 33, no. 1; p. 1-12.

# 13.0 APPENDICES

## 13.1 APPENDIX A - Procedure for water sampling

Items needed for water sampling: suction/vacuum pump, metal rod, filter paper (0.45 micron filter paper), filter mechanism, 3 rubber hoses with rubber stoppers, clamps, plastic erlynmeyer flask for filtered water, plastic bottle with bottom cut out, zip lock bags for spent filter paper, kim wipes, extra water bottles, 3 plastic beakers (small, medium, and large), squirt bottle (for deionized water), alkalinity kit, 3 buffer solutions (ph 4, 7, 10), small dropper bottle of ultrapure nitric acid, pH kit (field meter), large container of deionized water. **Note:** Set up entire sampling apparatus prior to going into the field!

1) To setup: (Fig. A1) Place vacuum pump on a flat surface and connect metal rod to wooden platform by threading it into position. Place plastic erlynmeyer flask (approx. 2 liter volume) on wooden platform.

2a) Tighten clamp to the top of the metal rod and attach the plastic bottle with the bottom cut out upside down into the clamp.

2b) Unscrew the top of the filter mechanism, place one filter paper onto the wire mesh screen, wet the filter paper with deionized water taking caution not to create air bubbles under the paper, and screw the top of the filter mechanism back onto the top (Fig. A.1).

2c) Attach rubber hose #1 from the vacuum pump to the side of the plastic erlynmeyer flask. Attach rubber hose #2 from the throat of the plastic bottle with the bottom cut out to the top of the filter mechanism. Finally, attach rubber hose #3 from the bottom of the filter mechanism to the top of the plastic erlymeyer flask (Fig. A.1).

2d) To sample: Using plastic beakers and sample bottles, collect water. Prime the filtration system with sampled water and discard. Continue filtering until desired amount of filtered water is obtained. **Note**: If water is murky or muddy the filter paper may need to be changed. This will be apparent if the pumping of the vacuum mechanism becomes resistant or too slow.

2f) Once the desired amount of water is filtered, pour into sample bottles (soaked in 5% $HNO_3$ prior to field excursion) and label appropriately. Ultra pure $HNO_3$ was added to those samples which needed to be acidified. 24 drops were sufficient to acidify 250 ml of sample.

3) The pH, temperature, alkalinity, and conductivity of the water is measured.

4) After the sample is taken the filtration system should be dismantled. The parts should be rinsed with deionized water to keep contamination to a minimum for the next sample.

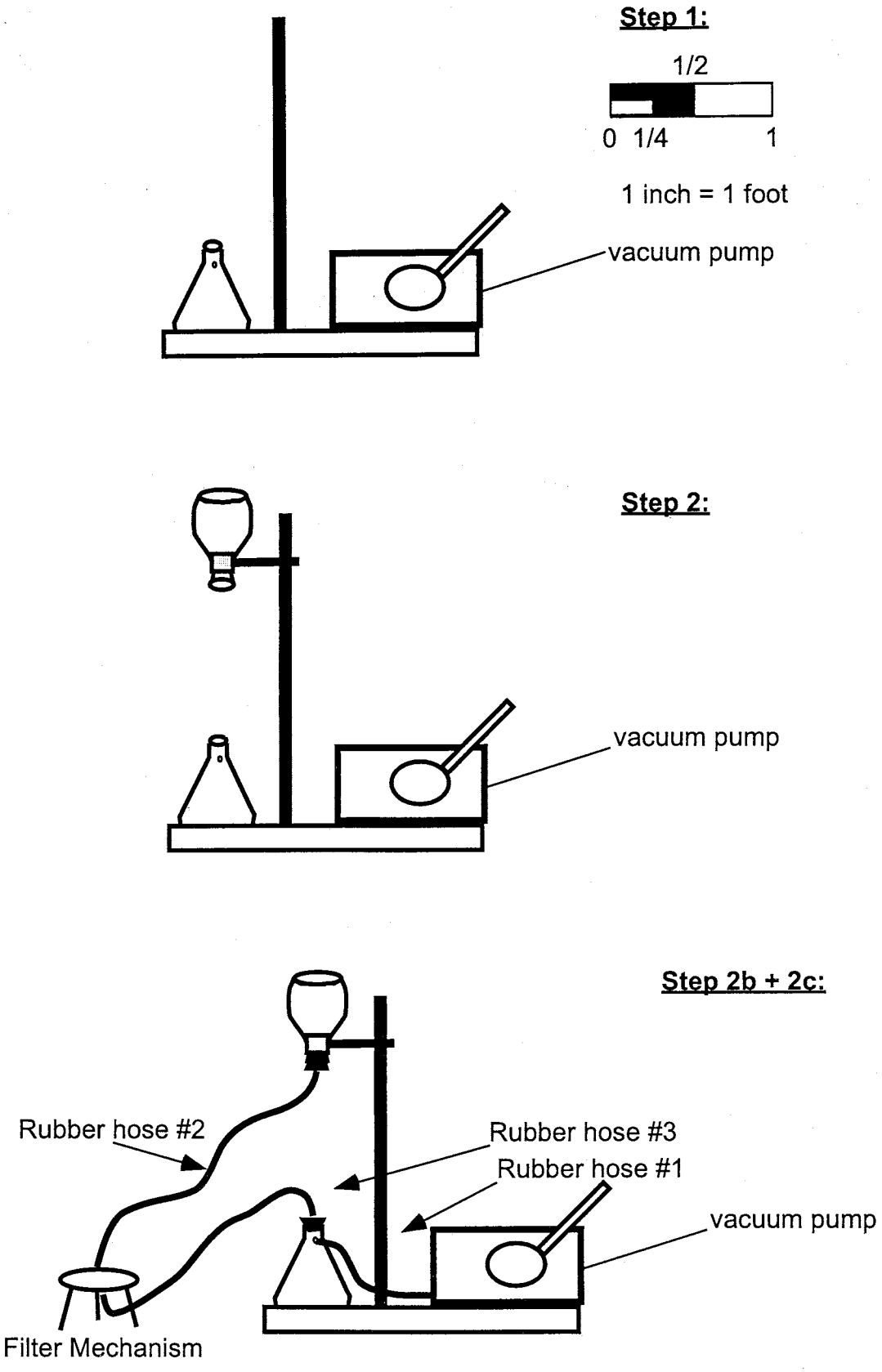


Figure A.1 Filtration system apparatus setup for water sampling

## 13.2 APPENDIX B - Procedure for preparation of oriented clay mineral aggregates

1) Place a small sample (20-25 grams) in a 100 ml beaker with deionized water. Mix and wait 5 minutes. Remix, wait 15 seconds, and pour suspension into another 100 ml beaker.

2a) If the clay flocculates or settles out, pour off clear water, add more water and remix. If the clay does not disperse, repeat this step several times.

2b) If the clay still flocculates, wet grind a sample in deionized water in a mortar until slurry is developed. Place the slurry in a 100 ml beaker and fill with deionized water.

2c) If the clay still settles, centrifuge, wash it with deionized water and cetrifuge again.

2d) If the clay still does not disperse, add a few drops of concentrated ammonium hydroxide ($NH_4OH$) and remix. If the clay flocculates, repeat step 2a.

2e) If the clay still flocculates, add a few drops of a dilute solution (50 gm/liter) of sodium hexametaphosphate (Calgon). Remix. If the clay does not disperse, repeat step 2a.

2f) If the clay is still flocculated, split sample to 10 or 15 g, and repeat the entire procedure.

3) Once the clay is in a dispersed state, allow the beaker and its contents to remain undisturbed for 10 minutes. At the end of the ten-minute period, touch eyedropper to the surface of the suspension and draw off enough material to cover a glass slide completely. This decanted fraction is less than 2-micrometer in size. It is generally desirable to prepare two or three slides of each sample at this time. Slides should be allowed to air-dry.

4) Use petrographic slides or flat, porous ceramic plates having a high melting point. The

latter will not warp at temperatures over 350° to 600° C. If desired, exchange of the saturated cations may also be accomplished with clay minerals mounted on porous plates.

This procedure generally yields a strongly oriented sample with the c axes perpendicular to the slide's surface thus giving intense basal x-ray reflections. Rarely the clay slurry will floculate on the slide surface during drying and preferred orientation of the clays will be absent. If it does, remake slide; this time, washing clay several times with deionized water before placing the suspension on the slide.

5) Run the slide of oriented clay on x-ray diffractometer at 2° 2θ/minute from 2° to 38° 2θ with monochromatic or Ni-filtered Cu radiation. Subsequent runs will vary depending on the mineralogy and nature of the information needed.

**Ethylene Glycol Treatment:**

Oriented aggregate is placed in a desicator above ethylene glycol overnight. Smectite will expand and absorb the glycol between the layers, thus changing the basal spacing. Ethylene glycol is also absorbed by smectite layers within mixed-layer clay minerals thus aiding in their identification. The container may be heated to speed up the process, making glycolation of the sample possible in about 30 minutes.

**Heat Treatment:**

The original or second oriented slide may be heat treated to help differentiate the various clay minerals. However, response of a mineral to heat treatment varies with composition, crystallinity, heating time, and temperature. If mineral's response to heat treatment appears anomalous, heat another slide in stages (375° C, 450° C, etc.) and examine the X-ray diffractogram after each state.

## 13.3 APPENDIX C - Quality Control / Quality Assurance

A standard procedure was used for sample collection and preparation for laboratory analysis. Whole rock samples were crushed and then pulverized in a tungsten carbide disc grinder. Samples already in the < 2 mm size were only pulverized in the steel disc grinder. Samples were analyzed by XRF and FAAS at New Mexico Bureau of Mines and Mineral Resources. Commercial certified standards, in house standards, and duplicates and triplicates were used to monitor analytical quality.

Understanding precision and accuracy of the data is important in order to determine quality of the data. Accuracy is how close to the real concentration the analysis is. Analyzing certified reference standards as unknown samples and comparing with know certified values monitors accuracy. Precision is a function of the total amount of error produced in the laboratory, sample collection, and sample preparation. Precision is monitored through the analysis of duplicate and triplicate samples. For the most part, analyses gathered in this study are in accord with certified values from reference standards.

Differences in results arose in samples prepared and analyzed using different analytical techniques. XRF and FAAS techniques invoke different preparation methods to measure elemental concentrations. XRF analyses involve the solid sample pressed into a pellet (trace elements) or fused into a disc (major elements). FAAS, however, involves a solid sample digestion with an acid solution mixture of hydrochloric and nitric acid. The resultant acid solution is measured by FAAS. In some cases, a portion of the sample may not be digested and therefore can't be measured by the machine. In general, samples

run by XRF analytical technique yielded a higher element concentration than did those run by FAAS.

Duplicate and triplicate samples by FAAS technique are in Table C.1. Duplicate and triplicate samples by XRF technique are in Table C.2. Results from reference standards analyzed by FAAS are in Table C.3. Comparison of XRF and FAAS techniques are summarized by data selected to show typical trends (Table C.4).

Table C.1. Duplicate and triplicate samples analyzed by FAAS technique

| FAAS ANALYSES: | | | | | |
|---|---|---|---|---|---|
| sample | Cu (ppm) | Pb (ppm) | Zn (ppm) | As (ppm) | |
| Water samples | | | | | |
| 5/398B | 0.26 | 0.11 | 0.029 | 1.228 | |
| 5/398C | 0.04 | 0.1 | 0.028 | 0.281 | |
| 5/398C | 0.05 | 0.06 | 0.042 | 0.281 | |
| | | | | | |
| 11/399B | 0.011 | 0.06 | 0.005 | 0.286 | |
| 11/399C | 0.011 | < 0.03 | 0.005 | 12.38 | |
| | | | | | |
| | Cu (ppm) | Pb (ppm) | Zn (ppm) | Fe % | Cd (ppm) |
| Site A | | | | | |
| 958 | 170 | 30 | 70 | 5.5 | 1 |
| 958 | 170 | 30 | 70 | 5.6 | 1 |
| 958 | 170 | 30 | 80 | 6 | 1 |
| | | | | | |
| Site B | | | | | |
| 967 | 1300 | 200 | 560 | 4.2 | 4 |
| 967 | 1260 | 210 | 570 | 4.1 | 4 |
| | | | | | |
| Site C | | | | | |
| 976 | 210 | 57240 | 63990 | 1.5 | 160 |
| 976 | 200 | 56830 | 63650 | 1.5 | 160 |
| | | | | | |
| Site D | | | | | |
| 985 | 110 | 1090 | 1520 | 2 | 10 |
| 985 | 120 | 1160 | 1430 | 2.1 | 10 |
| 985 | 120 | 1230 | 1530 | 2.2 | 10 |
| | | | | | |
| Site E | | | | | |
| 998 | 170 | 20 | 70 | 4.5 | 1 |
| 998 | 180 | 20 | 60 | 4.9 | 1 |
| | | | | | |
| standard 1 | | | | | |
| EM7697-1 | 190 | 20 | 40 | 2.7 | 1 |
| EM7697-2 | 190 | 20 | 50 | 2.9 | 1 |
| EM7697-3 | 190 | 30 | 40 | 2.8 | 1 |

Table C.2. Duplicate and triplicate samples analyzed by XRF technique

| XRF ANALYSES: | | | | |
|---|---|---|---|---|
| **samples** | **Cu (ppm)** | **Pb (ppm)** | **Zn (ppm)** | **As (ppm)** |
| **Site A** | | | | |
| psd1e-1 | 99 | 26 | 101 | 4 |
| psd1e-2 | 100 | 22 | 101 | 5 |
| | | | | |
| **Site C** | | | | |
| psd3c-1 | 290 | > 7000 | > 5500 | nd |
| psd3c-2 | 283 | > 7000 | > 5500 | nd |
| psd3c-3 | 283 | > 7000 | > 5500 | nd |
| | | | | |
| **Site B** | | | | |
| bzgd-5 | 1400 | 570 | 1400 | 5 |
| bzgd-5b | 1400 | 570 | 1400 | 4 |
| | | | | |
| bzgd-15 | 900 | 120 | 500 | 29 |
| bzgd-15b | 900 | 125 | 500 | 30 |
| bzgd-15c | 920 | 125 | 500 | 30 |
| | | | | |
| bzgd-25 | 1000 | 630 | 770 | 21 |
| bzgd-25b | 1000 | 620 | 780 | 21 |
| | | | | |
| bzgd-35 | 860 | 140 | 470 | 28 |
| bzgd-35b | 860 | 130 | 470 | 30 |
| bzgd-35c | 840 | 130 | 480 | 29 |
| | | | | |
| bzgd-45 | 2700 | 300 | 490 | 16 |
| bzgd-45 | 2600 | 300 | 490 | 16 |
| | | | | |
| **standard 1** | | | | |
| EM7697-1 | 197 | 37 | 49 | 48 |
| EM7697-2 | 189 | 36 | 48 | 74 |
| EM7697-3 | 194 | 37 | 49 | 75 |
| | | | | |
| **standard 2** | | | | |
| EM7297-1 | 123 | 22 | 84 | 4 |
| EM7297-2 | 124 | 22 | 85 | 4 |
| EM7297-3 | 124 | 22 | 85 | 4 |

Table C.3. Results from reference standards analyzed by FAAS. Error was calculated to be ± 15% for the waste rock piles analyzed.

| Known standards: | | | | | |
|---|---|---|---|---|---|
| sample | Cu (ppm) | Pb (ppm) | Zn (ppm) | Fe % | Cd (ppm) |
| VTM 154S - Orogrande stream sediment | | | | | |
| | 310 | 30 | 40 | 37651 | 1 |
| in house | 234 | 28 | 30 | 94400 | 4 |
| difference | 76 | 2 | 10 | -56749 | -3 |
| % diff | 32.47863 | 7.142857 | 33.33333 | | |
| | | | | | |
| RTC #2 | 660 | 1410 | 80430 | 178687 | 10 |
| certified | 753.3 | 5194.8 | 3021.7 | 191645 | 20.8 |
| difference | -93.3 | -3784.8 | 77408.3 | -12958 | -10.8 |
| | | | | | |
| RTC #2 | 670 | 3180 | 2850 | | |
| % diff | -11.05801 | -38.78494 | -5.682232 | | |
| | | | | | |
| RTC #3 | 4730 | 221285.1 | 630 | | |
| certified | 4792.4 | n/a | 526.4 | | |
| % diff | -1.302062 | | 19.68085 | | |

Table C.4. Comparison of XRF and FAAS data from chemical analyses of six size fractions from the northern Laramide polymetallic vein waste rock pile (Site E).

| XRF vs. FAAS | | | | | | | | |
|---|---|---|---|---|---|---|---|---|
| | Cu (ppm) | Cu (ppm) | Pb (ppm) | Pb (ppm) | Zn (ppm) | Zn (ppm) | Fe% | Fe% |
| sample | XRF | AA | XRF | AA | XRF | AA | XRF | AA |
| 991 | 152 | 150 | 23 | 30 | 37 | 30 | 6.5 | 3.1 |
| 992 | 161 | 180 | 26 | 30 | 40 | 30 | 7.51 | 3.3 |
| 993 | 201 | 200 | 36 | 30 | 45 | 40 | 8.87 | 3.6 |
| 994 | 232 | 140 | 41 | 40 | 52 | 40 | 9.94 | 4 |
| 995 | 278 | 170 | 56 | 50 | 60 | 60 | 11.22 | 4.2 |
| 996 | 357 | 170 | 91 | 70 | 78 | 70 | 14.42 | 6.5 |

## 13.4 APPENDIX D - Laboratory procedure for Agitation Test

1) Preparation - all sample bottles were soaked with 5% $HNO_3$ prior to use.

2) Weigh 75 grams ± 2 grams of sample into 3 small beakers (400 ml beakers used)

3) Measure 100, 400, 800 ml of distilled water

4) After measuring the initial pH of the distilled water, place weighed material from one beaker into a dry 1000 ml beaker and set magnetic stirrer at the bottom

5) Add distilled water (100, 400, and 800 ml for three samples respectively)

6) Run magnetic stirrer for 20 minutes between 4 and 4.5 speed.

Read the pH at time $T_0$, $T_{30sec}$, $T_{2min}$, $T_{10min}$, $T_{20min}$ ($T_{final}$).

7) After the run is complete, place the liquid mixture into a bruckner funnel. A Whatman qualitative filter paper #1 (medium fast filter speed) was used which has a 11μm particle retention.

8) Place filtered water into a 100ml, 500ml, and 1000ml volumetric flasks and complete the sample with deionized water to each volume respectively.

9) Place samples into sample bottles.

10) Vigorously shake sample bottle for at least 30 seconds and immediately pour 30 ml of sample into two 50 ml beakers.

11) Filter the first 30 ml sample through 0.45 μm millipore filter using a vacuum pump and store in a sample bottle. The second 30 ml sample was acidified to a pH of 2 ± 0.1, placed into a sample bottle, shaken for 2 hours on the wrist action shaker machine, and filtered with 0.45 μm millipore filter.

12) Samples were analyzed by FAAS techiques

## 13.5 APPENDIX E - Data

Table E.1. XRF trace element analysis for six grain size fractions from Sites A, B, C, and E respectively. Unless otherwise designated, element concentrations are displayed in ppm. PSD1A-F designates samples from the placer gold waste rock pile (Site A), PSD2A-F designates samples from the Laramide polymetallic vein waste rock pile (Site B), PSD3A-F designates samples from the carbonate-hosted Pb-Zn waste rock pile (Site C), GVD1-6 designates samples from the northern Laramide polymetallic vein waste rock pile (Site E).

| sample # | TiO2% | Fe2O3% | MnO% | V | Cr | Ni | Cu | Zn | Ga | As | Rb | Sr | Y | Zr | Nb | Mo | Ba | Pb | Th | U |
|---|---|---|---|---|---|---|---|---|---|---|---|---|---|---|---|---|---|---|---|---|
| | | | | | | | | | | | | | | | | | | | | |
| PSD1A | 0.64 | 6.1 | 0.12 | 104 | 34 | 11 | 80 | 71 | 18 | 5 | 180 | 553 | 32 | 211 | 9 | 1 | 993 | 20 | 12 | 3 |
| PSD1B | 0.71 | 6.82 | 0.13 | 114 | 40 | 13 | 87 | 77 | 18 | 4 | 168 | 517 | 32 | 217 | 9 | ND | 948 | 21 | 12 | 3 |
| PSD1C | 0.83 | 7.58 | 0.15 | 136 | 42 | 15 | 96 | 87 | 19 | 5 | 153 | 481 | 34 | 219 | 10 | 1 | 876 | 23 | 11 | 3 |
| PSD1D | 1.06 | 9.43 | 0.16 | 176 | 52 | 15 | 102 | 110 | 20 | 5 | 142 | 463 | 34 | 225 | 11 | ND | 800 | 25 | 12 | 3 |
| PSD1E-1 | 0.98 | 8.67 | 0.13 | 149 | 46 | 16 | 99 | 101 | 20 | 4 | 131 | 431 | 34 | 262 | 11 | 1 | 733 | 26 | 12 | 3 |
| PSD1E-2 | 0.99 | 8.65 | 0.13 | 149 | 46 | 16 | 100 | 101 | 20 | 5 | 131 | 431 | 34 | 244 | 12 | ND | 726 | 22 | 12 | 3 |
| PSD1F | 0.85 | 7.12 | 0.1 | 111 | 51 | 20 | 110 | 97 | 20 | 5 | 124 | 347 | 35 | 320 | 14 | 2 | 689 | 21 | 13 | 3 |
| | | | | | | | | | | | | | | | | | | | | |
| PSD2A | 0.37 | 7.68 | 0.21 | 62 | 41 | 4 | 860 | 462 | 22 | 15 | 279 | 141 | 25 | 244 | 12 | 11 | 551 | 73 | 23 | 5 |
| PSD2B | 0.4 | 8.71 | 0.2 | 61 | 41 | 3 | 920 | 411 | 21 | 28 | 272 | 127 | 25 | 241 | 12 | 12 | 505 | 81 | 27 | 6 |
| PSD2C | 0.44 | 8.99 | 0.19 | 62 | 46 | 3 | 790 | 392 | 21 | 34 | 259 | 120 | 25 | 249 | 14 | 15 | 481 | 94 | 30 | 7 |
| PSD2D | 0.47 | 9.28 | 0.21 | 61 | 38 | 4 | 820 | 458 | 21 | 33 | 256 | 124 | 25 | 256 | 15 | 15 | 522 | 124 | 35 | 6 |
| PSD2E | 0.5 | 9.56 | 0.22 | 67 | 21 | 5 | 810 | 464 | 23 | 35 | 266 | 146 | 28 | 256 | 16 | 18 | 530 | 160 | 40 | 7 |
| PSD2F | 0.56 | 10.94 | 0.2 | 68 | 17 | 7 | 760 | 477 | 26 | 35 | 289 | 172 | 30 | 274 | 15 | 19 | 423 | 218 | 42 | 8 |
| | | | | | | | | | | | | | | | | | | | | |
| PSD3A | 0.15 | 2.48 | 0.38 | ND | 66 | 18 | 98 | >7000 | ND | ND | ND | 111 | 39 | 89 | 2 | 450 | 574 | >5500 | 10 | ND |
| PSD3B | 0.26 | 4.76 | 0.64 | ND | 94 | 31 | 186 | >7000 | ND | ND | ND | 147 | 69 | 151 | ND | 750 | 1200 | >5500 | 14 | ND |
| PSD3C-1 | 0.33 | 7.21 | 1.05 | ND | 121 | 46 | 290 | >7000 | ND | ND | ND | 181 | 74 | 176 | ND | 860 | 2100 | >5500 | 30 | ND |
| PSD3C-2 | 0.33 | 7.32 | 1.04 | ND | 122 | 46 | 283 | >7000 | ND | ND | ND | 182 | 75 | 174 | 2 | 870 | 2000 | >5500 | 26 | ND |
| PSD3C-3 | 0.34 | 7.33 | 1.05 | ND | 122 | 46 | 283 | >7000 | ND | ND | ND | 183 | 74 | 173 | 2 | 870 | 2000 | >5500 | 23 | ND |
| PSD3D | 0.34 | 8.8 | 1.27 | ND | 130 | 51 | 365 | >7000 | ND | ND | ND | 199 | 71 | 168 | 3 | 900 | 2200 | >5500 | 18 | ND |
| PSD3E | 0.25 | 6.81 | 0.99 | ND | 92 | 31 | 308 | >7000 | ND | ND | ND | 178 | 52 | 125 | 2 | 600 | 1500 | >5500 | 23 | ND |
| PSD3F | 0.32 | 6.61 | 0.73 | ND | 62 | 28 | 294 | >7000 | ND | ND | ND | 177 | 33 | 127 | 3 | 270 | 1100 | >5500 | 15 | ND |
| | | | | | | | | | | | | | | | | | | | | |
| GVD1 | 0.57 | 6.5 | 0.11 | 98 | 40 | 8 | 152 | 37 | 21 | 31 | 324 | 599 | 25 | 255 | 8 | 3 | 889 | 23 | 17 | 6 |
| GVD2 | 0.57 | 7.51 | 0.12 | 103 | 34 | 9 | 161 | 40 | 19 | 49 | 311 | 571 | 27 | 242 | 7 | 2 | 850 | 26 | 17 | 6 |
| GVD3 | 0.59 | 8.87 | 0.14 | 108 | 33 | 10 | 201 | 45 | 20 | 72 | 288 | 543 | 27 | 221 | 7 | 3 | 752 | 36 | 17 | 6 |
| GVD4 | 0.6 | 9.94 | 0.15 | 103 | 29 | 11 | 232 | 52 | 19 | 97 | 261 | 521 | 27 | 203 | 7 | 3 | 752 | 41 | 17 | 6 |
| GVD5 | 0.65 | 11.22 | 0.18 | 120 | 30 | 12 | 278 | 60 | 20 | 122 | 246 | 507 | 29 | 194 | 7 | 4 | 778 | 56 | 19 | 6 |
| GVD6 | 0.7 | 14.42 | 0.18 | 134 | 23 | 14 | 357 | 78 | 22 | 176 | 265 | 561 | 35 | 208 | 7 | 5 | 637 | 91 | 22 | 7 |

Table E.2. FAAS chemical analyses of six grain size fractions for Sites A-E. Site A = placer gold waste rock pile, Site B = Laramide polymetallic vein waste rock pile, Site C = carbonate-hosted Pb-Zn waste rock pile, Site D = carbonate-hosted Ag-Mn waste rock pile, Site E = northern Laramide polymetallic vein waste rock pile.

| sample # | Fe % | Cu ppm | Pb ppm | Zn ppm | Cd ppm | As ppm |
|---|---|---|---|---|---|---|
| SITE A | | | | | | |
| 951 | 3.4 | 150 | 20 | 120 | 1 | 2.4 |
| 952 | 3.8 | 180 | 20 | 75 | 1 | 2.3 |
| 953 | 4.7 | 200 | 20 | 115 | 1 | 3 |
| 954 | 6.3 | 140 | 30 | 145 | 1 | 2.1 |
| 955 | 5.6 | 170 | 30 | 90 | 1 | 2.3 |
| 956 | 4 | 170 | 20 | 150 | 1 | 3.4 |
| SITE B | | | | | | |
| 960 | 3.7 | 1170 | 70 | 460 | 3 | 5.7 |
| 961 | 4.9 | 1150 | 80 | 410 | 3 | 10 |
| 962 | 4.4 | 900 | 80 | 370 | 3 | 11 |
| 963 | 4.6 | 1020 | 110 | 410 | 3 | 11 |
| 964 | 4.5 | 920 | 130 | 420 | 3 | 9.3 |
| 965 | 6 | 810 | 180 | 420 | 3 | 9.4 |
| SITE C | | | | | | |
| 969 | 0.7 | 130 | 42450 | 70210 | 240 | 20 |
| 970 | 1 | 160 | 72250 | 88780 | 220 | 33 |
| 971 | 1.3 | 190 | 75710 | 95100 | 190 | 54 |
| 972 | 1.6 | 220 | 73640 | 99170 | 200 | 83 |
| 973 | 1.6 | 240 | 51010 | 64780 | 330 | 75 |
| 974 | 1.7 | 250 | 28140 | 43470 | 450 | 52 |
| SITE D | | | | | | |
| 978 | 2.4 | 120 | 1500 | 1710 | 10 | 4 |
| 979 | 2.6 | 130 | 1700 | 1910 | 10 | 6.8 |
| 980 | 2.6 | 110 | 1840 | 1950 | 10 | 6.7 |
| 981 | 2.7 | 120 | 1770 | 1900 | 10 | 7.8 |
| 982 | 2.6 | 120 | 1800 | 1810 | 10 | 8.9 |
| 983 | 1.4 | 90 | 1470 | 1520 | 10 | 6.7 |
| SITE E | | | | | | |
| 991 | 3.1 | 210 | 30 | 30 | 1 | 16 |
| 992 | 3.3 | 220 | 30 | 30 | 1 | 30 |
| 993 | 3.6 | 250 | 30 | 40 | 1 | 56 |
| 994 | 4 | 290 | 40 | 40 | 1 | 73 |
| 995 | 4.2 | 320 | 50 | 60 | 1 | 105 |
| 996 | 6.5 | 400 | 70 | 70 | 1 | 148 |

Table E.3. XRF trace element analysis for composite samples (15, 30, 45) from Sites A and B respectively. Unless otherwise designated, element concentrations are displayed in ppm.

| sample # | TiO2% | Fe2O3% | MnO% | V | Cr | Ni | Cu | Zn | Ga | As | Rb | Sr | Y | Zr | Nb | Mo | Ba | Pb | Bi | Th | U |
|---|---|---|---|---|---|---|---|---|---|---|---|---|---|---|---|---|---|---|---|---|---|
| | | | | | | | | | | | | | | | | | | | | | |
| CFPGD1H | 1 | 8.7 | 0.14 | 161 | 46 | 16 | 110 | 95 | 18 | 5 | 134 | 465 | 34 | 254 | 8 | 2 | 760 | 21 | 1 | 14 | 4 |
| 2H | 1 | 8.7 | 0.14 | 165 | 41 | 16 | 110 | 93 | 18 | 5 | 132 | 464 | 33 | 246 | 7 | 1 | 740 | 20 | 1 | 14 | 4 |
| 3H | 0.9 | 8.4 | 0.13 | 150 | 43 | 16 | 110 | 91 | 18 | 5 | 131 | 463 | 33 | 237 | 7 | 1 | 743 | 20 | 1 | 13 | 3 |
| | | | | | | | | | | | | | | | | | | | | | |
| BZGD1H | 0.5 | 9.6 | 0.2 | 65 | 21 | 6 | 990 | 530 | 20 | 30 | 254 | 195 | 28 | 255 | 10 | 14 | 513 | 220 | 60 | 1 | 7 |
| 2H | 0.5 | 9.4 | 0.22 | 69 | 21 | 6 | 1200 | 550 | 21 | 26 | 256 | 185 | 27 | 256 | 10 | 13 | 499 | 230 | 70 | 1 | 7 |
| 3H | 0.5 | 9.4 | 0.22 | 66 | 22 | 7 | 1100 | 530 | 21 | 28 | 256 | 180 | 26 | 255 | 11 | 14 | 507 | 210 | 70 | 1 | 8 |

Table E.4. FAAS chemical analysis for composite samples (15, 30, 45) from Sites A-D.

| sample # | Fe % | Cu ppm | Pb ppm | Zn ppm | Cd ppm | As ppm |
|---|---|---|---|---|---|---|
| | | | | | | |
| SITE A | | | | | | |
| 957 | 5.6 | 190 | 30 | 80 | 1 | 1.9 |
| 958 | 5.5 | 170 | 30 | 70 | 1 | 1.8 |
| 958 | 5.6 | 170 | 30 | 70 | 1 | 1.8 |
| 958 | 6 | 170 | 30 | 80 | 1 | 1.8 |
| 959 | 5.7 | 170 | 20 | 80 | 1 | 2 |
| SITE B | | | | | | |
| 966 | 4.2 | 1083 | 200 | 510 | 4 | 11 |
| 967 | 4.2 | 1300 | 200 | 560 | 4 | 9.2 |
| 967 | 4.1 | 1260 | 210 | 570 | 4 | 9.2 |
| 968 | 4 | 1160 | 170 | 620 | 4 | 9.3 |
| SITE C | | | | | | |
| 975 | 1.8 | 240 | 63130 | 83160 | 200 | 18 |
| 976 | 1.5 | 210 | 57240 | 63990 | 160 | 20 |
| 976 | 1.5 | 200 | 56830 | 63650 | 160 | 20 |
| 977 | 1.6 | 220 | 53290 | 68860 | 200 | 12 |
| SITE D | | | | | | |
| 984 | 2.3 | 120 | 1430 | 1670 | 10 | 5.7 |
| 985 | 2 | 110 | 1090 | 1520 | 10 | 5.6 |
| 985 | 2.1 | 120 | 1160 | 1430 | 10 | 5.6 |
| 985 | 2.2 | 120 | 1230 | 1530 | 10 | 5.6 |
| 986 | 2.4 | 120 | 1050 | 1320 | 10 | 6.3 |

Table E.5A. XRF trace element analysis of stream sediment samples. Unless otherwise designated, element concentrations are displayed in ppm. Sample sites are located in Figures 8, 9, and 10.

| sample # | TiO2% | Fe2O3% | MnO% | V | Cr | Ni | Cu | Zn | Ga | As | Rb | Sr | Y | Zr | Nb | Mo | Ba | Pb | Bi | Th | U |
|---|---|---|---|---|---|---|---|---|---|---|---|---|---|---|---|---|---|---|---|---|---|
| EAM 198 | 0.75 | 7.01 | 0.18 | 120 | 38 | 10 | 49 | 114 | 20 | 4 | 153 | 334 | 34 | 237 | 10 | ND | 998 | 29 | ND | 13 | 3 |
| EAM 298 | 0.63 | 5.81 | 0.13 | 90 | 95 | 15 | 35 | 92 | 21 | 2 | 189 | 153 | 28 | 178 | 8 | ND | 744 | 24 | ND | 11 | 2 |
| EAM 398 | 0.79 | 6.82 | 0.11 | 114 | 59 | 13 | 31 | 90 | 18 | 4 | 193 | 351 | 27 | 213 | 10 | ND | 909 | 29 | ND | 15 | 3 |
| EAM 598 | 0.6 | 7.1 | 0.17 | 103 | 29 | 11 | 360 | 230 | 20 | 11 | 223 | 328 | 29 | 255 | 7 | 3 | 805 | 90 | 20 | 1 | 5 |
| EAM 698 | 0.6 | 6.3 | 0.18 | 107 | 35 | 12 | 190 | 150 | 20 | 8 | 234 | 400 | 28 | 260 | 8 | ND | 859 | 52 | ND | 21 | 5 |
| EAM 798 | 0.4 | 2.6 | 0.09 | 41 | 36 | 12 | 13 | 53 | 6 | 10 | 54 | 184 | 21 | 122 | 2 | ND | 344 | 36 | ND | 6 | 3 |
| EAM 898 | 0.5 | 4.2 | 0.09 | 56 | 52 | 18 | 19 | 130 | 11 | 5 | 96 | 169 | 23 | 175 | 5 | ND | 420 | 39 | ND | 9 | 4 |
| EAM 998 | 0.6 | 4.7 | 0.1 | 71 | 60 | 21 | 23 | 91 | 12 | 7 | 111 | 185 | 25 | 184 | 6 | ND | 451 | 48 | ND | 9 | 3 |
| EAM 1098 | 0.6 | 5.5 | 0.13 | 102 | 60 | 16 | 47 | 92 | 15 | 6 | 148 | 489 | 30 | 179 | 4 | ND | 827 | 25 | ND | 14 | 3 |
| EAM 1598 | 0.3 | 2.7 | 0.07 | 40 | 53 | 13 | 13 | 55 | 8 | 7 | 62 | 226 | 19 | 94 | 1 | ND | 353 | 19 | ND | 6 | 2 |
| EAM 1698 | 0.8 | 7.7 | 0.16 | 138 | 34 | 12 | 210 | 80 | 19 | 6 | 184 | 529 | 32 | 205 | 5 | ND | 914 | 23 | ND | 14 | 2 |
| EAM 1798 | 0.7 | 7.4 | 0.15 | 128 | 35 | 12 | 160 | 74 | 19 | 4 | 185 | 552 | 31 | 205 | 5 | 3 | 950 | 23 | ND | 13 | 3 |

Table E.5B. FAAS trace element analysis of stream sediment samples downstream from the Ag-Mn carbonate-hosted waste rock pile (Site D).

| sample | Cu (ppm) | Pb (ppm) | Zn (ppm) | As (ppm) |
|---|---|---|---|---|
| EAM 1198 | 0.70 | 5.20 | 2.60 | 0.28 |
| EAM 1298 | 0.50 | 2.60 | 2.30 | 0.17 |
| EAM 1398 | 0.60 | 3.90 | 2.45 | 0.18 |
| EAM 1498 | 0.50 | 2.10 | 2.20 | 0.13 |

Table E.6. XRF trace element analysis of 45 samples from Site B. Unless otherwise designated, element concentrations are displayed in ppm.

| sample # | TiO2% | Fe2O3% | MnO% | V | Cr | Ni | Cu | Zn | Ga | As | Rb | Sr | Y | Zr | Nb | Mo | Ba | Pb | Bi | Th | U |
|---|---|---|---|---|---|---|---|---|---|---|---|---|---|---|---|---|---|---|---|---|---|
| BZGD-1 | 0.6 | 8.4 | 0.28 | 61 | 28 | 8 | 2100 | 1030 | 23 | 18 | 253 | 204 | 30 | 232 | 10 | 11 | 495 | 540 | 50 | 1 | 6 |
| 2 | 0.5 | 8.4 | 0.28 | 62 | 29 | 7 | 2400 | 1000 | 23 | 17 | 256 | 211 | 28 | 236 | 10 | 12 | 573 | 730 | 70 | 1 | 6 |
| 3 | 0.6 | 7.9 | 0.18 | 74 | 55 | 12 | 1900 | 400 | 20 | 19 | 239 | 239 | 30 | 266 | 11 | 10 | 597 | 120 | 50 | 1 | 8 |
| 4 | 0.5 | 8.3 | 0.3 | 51 | 30 | 7 | 1200 | 750 | 20 | 27 | 252 | 176 | 27 | 250 | 9 | 9 | 469 | 120 | 50 | 1 | 9 |
| 5 | 0.5 | 8.3 | 0.37 | 60 | 16 | 8 | 1400 | 1400 | 21 | 5 | 246 | 205 | 30 | 268 | 8 | 7 | 597 | 570 | 40 | 1 | 9 |
| 5#2 | 0.4 | 8.3 | 0.38 | 61 | 19 | 8 | 1400 | 1400 | 22 | 4 | 247 | 206 | 30 | 269 | 9 | 8 | 616 | 570 | 40 | 1 | 9 |
| 6 | 0.7 | 7.9 | 0.18 | 93 | 37 | 11 | 1100 | 680 | 20 | 11 | 217 | 269 | 32 | 299 | 12 | 5 | 652 | 260 | 20 | 1 | 7 |
| 7 | 0.5 | 10.4 | 0.13 | 75 | 17 | 6 | 510 | 170 | 21 | 46 | 256 | 125 | 22 | 232 | 9 | 8 | 379 | 73 | 30 | 1 | 7 |
| 8 | 0.6 | 9 | 0.25 | 74 | 27 | 10 | 860 | 440 | 21 | 29 | 239 | 208 | 31 | 273 | 12 | 15 | 507 | 100 | 30 | 1 | 8 |
| 9 | 0.4 | 10.7 | 0.11 | 56 | 13 | 5 | 690 | 180 | 18 | 44 | 238 | 241 | 18 | 193 | 5 | 38 | 470 | 260 | 190 | 1 | 6 |
| 10 | 0.6 | 10 | 0.2 | 77 | 25 | 9 | 690 | 540 | 21 | 35 | 250 | 186 | 30 | 279 | 11 | 13 | 554 | 150 | 50 | 1 | 7 |
| 11 | 0.5 | 9.6 | 0.22 | 66 | 25 | 7 | 760 | 560 | 22 | 29 | 281 | 171 | 30 | 270 | 11 | 12 | 560 | 110 | 50 | 1 | 9 |
| 12 | 0.5 | > 11 | 0.11 | 55 | 17 | 5 | 520 | 200 | 189 | 76 | 249 | 194 | 19 | 222 | 9 | 12 | 457 | 220 | 90 | 1 | 5 |
| 13 | 0.5 | 9.3 | 0.27 | 67 | 25 | 8 | 610 | 620 | 22 | 22 | 276 | 141 | 31 | 282 | 12 | 9 | 539 | 82 | 30 | 1 | 8 |
| 14 | 0.6 | 10.6 | 0.14 | 64 | 21 | 6 | 460 | 240 | 22 | 48 | 295 | 160 | 25 | 261 | 11 | 16 | 474 | 115 | 60 | 1 | 8 |
| 15 | 0.5 | 9.3 | 0.24 | 58 | 26 | 7 | 900 | 500 | 22 | 29 | 278 | 129 | 27 | 272 | 12 | 16 | 565 | 120 | 80 | 1 | 9 |
| 15#2 | 0.5 | 9.3 | 0.24 | 54 | 20 | 6 | 900 | 500 | 21 | 30 | 277 | 128 | 27 | 268 | 12 | 16 | 579 | 125 | 80 | 1 | 7 |
| 15#3 | 0.5 | 9.3 | 0.24 | 59 | 21 | 6 | 920 | 500 | 23 | 30 | 277 | 129 | 28 | 270 | 12 | 17 | 589 | 125 | 80 | 1 | 8 |
| 16 | 0.5 | 8.5 | 0.28 | 58 | 21 | 6 | 2000 | 880 | 22 | 21 | 254 | 208 | 30 | 233 | 10 | 13 | 516 | 660 | 60 | 1 | 7 |
| 17 | 0.4 | 9.9 | 0.33 | 61 | 13 | 6 | 1800 | 730 | 20 | 31 | 255 | 179 | 26 | 247 | 9 | 14 | 439 | 270 | 200 | 1 | 7 |
| 18 | 0.5 | 9 | 0.3 | 60 | 22 | 6 | 2100 | 730 | 20 | 23 | 254 | 167 | 27 | 255 | 10 | 9 | 414 | 140 | 70 | 1 | 8 |
| 19 | 0.4 | 8.9 | 0.29 | 54 | 16 | 6 | 1400 | 860 | 22 | 14 | 269 | 150 | 27 | 259 | 9 | 7 | 559 | 140 | 70 | 1 | 8 |
| 20 | 0.6 | 7.8 | 0.26 | 72 | 27 | 8 | 1300 | 780 | 20 | 11 | 224 | 234 | 30 | 283 | 10 | 8 | 622 | 235 | 30 | 1 | 7 |
| 21 | 0.4 | 10.7 | 0.14 | 57 | 20 | 5 | 510 | 220 | 19 | 38 | 261 | 244 | 21 | 221 | 8 | 20 | 445 | 124 | 60 | 1 | 7 |
| 22 | 0.5 | 9.6 | 0.23 | 59 | 23 | 6 | 900 | 500 | 22 | 31 | 277 | 126 | 26 | 262 | 10 | 15 | 539 | 135 | 80 | 1 | 9 |
| 23 | 0.5 | 9.8 | 0.22 | 65 | 22 | 7 | 720 | 430 | 22 | 38 | 266 | 172 | 28 | 266 | 11 | 10 | 516 | 135 | 50 | 1 | 8 |
| 24 | 0.5 | 9.3 | 0.19 | 72 | 23 | 7 | 640 | 300 | 21 | 36 | 243 | 172 | 27 | 253 | 9 | 13 | 544 | 110 | 50 | 1 | 7 |
| 25 | 0.6 | 8.1 | 0.29 | 59 | 23 | 8 | 1000 | 770 | 23 | 21 | 245 | 154 | 29 | 264 | 11 | 12 | 482 | 630 | 40 | 1 | 6 |
| 25#2 | 0.6 | 8 | 0.29 | 65 | 25 | 8 | 1000 | 780 | 23 | 21 | 247 | 154 | 30 | 264 | 11 | 12 | 501 | 620 | 40 | 1 | 7 |
| 26 | 0.5 | 10.2 | 0.13 | 69 | 21 | 5 | 660 | 160 | 21 | 39 | 248 | 215 | 22 | 232 | 9 | 24 | 495 | 140 | 70 | 1 | 7 |
| 27 | 0.5 | 9.2 | 0.19 | 60 | 26 | 7 | 940 | 330 | 22 | 31 | 276 | 163 | 27 | 253 | 11 | 31 | 628 | 160 | 120 | 1 | 7 |
| 28 | 0.4 | 9.1 | 0.23 | 72 | 21 | 8 | 890 | 730 | 24 | 25 | 286 | 132 | 29 | 275 | 11 | 10 | 495 | 120 | 70 | 1 | 10 |
| 29 | 0.5 | 9 | 0.36 | 55 | 19 | 6 | 2000 | 970 | 21 | 23 | 262 | 156 | 28 | 256 | 9 | 7 | 409 | 170 | 70 | 1 | 8 |
| 30 | 0.5 | 9 | 0.27 | 59 | 28 | 8 | 840 | 640 | 23 | 26 | 281 | 136 | 28 | 278 | 12 | 13 | 508 | 130 | 60 | 1 | 8 |
| 31 | 0.6 | 10.6 | 0.1 | 58 | 20 | 5 | 480 | 120 | 22 | 61 | 278 | 88 | 21 | 243 | 10 | 9 | 389 | 140 | 60 | 1 | 8 |
| 32 | 0.5 | 9.3 | 0.19 | 76 | 28 | 9 | 630 | 300 | 21 | 35 | 239 | 176 | 28 | 259 | 11 | 12 | 543 | 110 | 50 | 1 | 8 |
| 33 | 0.5 | 10.9 | 0.2 | 65 | 24 | 7 | 730 | 360 | 21 | 48 | 246 | 165 | 25 | 250 | 10 | 11 | 506 | 220 | 60 | 1 | 8 |
| 34 | 0.5 | 9.4 | 0.27 | 58 | 19 | 5 | 900 | 520 | 23 | 32 | 287 | 122 | 28 | 272 | 12 | 14 | 470 | 120 | 70 | 1 | 9 |
| 35 | 0.5 | 9.3 | 0.24 | 59 | 21 | 5 | 860 | 470 | 22 | 28 | 277 | 134 | 26 | 269 | 12 | 16 | 565 | 140 | 80 | 1 | 8 |
| 35#2 | 0.5 | 9.3 | 0.24 | 61 | 20 | 5 | 860 | 470 | 21 | 30 | 278 | 135 | 27 | 267 | 12 | 16 | 527 | 130 | 80 | 1 | 8 |
| 35#3 | 0.5 | 9.3 | 0.24 | 55 | 22 | 6 | 840 | 480 | 22 | 29 | 279 | 134 | 27 | 267 | 12 | 16 | 533 | 130 | 80 | 1 | 8 |
| 36 | 0.6 | 9.5 | 0.2 | 63 | 18 | 6 | 670 | 480 | 23 | 29 | 282 | 165 | 27 | 270 | 13 | 16 | 533 | 115 | 60 | 1 | 9 |
| 37 | 0.5 | 9.1 | 0.25 | 60 | 22 | 5 | 880 | 570 | 22 | 26 | 279 | 135 | 27 | 269 | 11 | 14 | 542 | 130 | 70 | 1 | 8 |
| 38 | 0.4 | 10.3 | 0.18 | 56 | 16 | 5 | 670 | 230 | 20 | 32 | 253 | 145 | 21 | 235 | 9 | 14 | 527 | 150 | 80 | 1 | 7 |
| 39 | 0.5 | 7.7 | 0.34 | 53 | 18 | 6 | 690 | 690 | 21 | 14 | 255 | 158 | 28 | 262 | 11 | 7 | 507 | 160 | 40 | 1 | 9 |
| 40 | 0.6 | 9.7 | 0.2 | 73 | 22 | 7 | 720 | 380 | 23 | 33 | 273 | 173 | 28 | 272 | 11 | 13 | 515 | 110 | 50 | 1 | 8 |
| 41 | 0.6 | 8.8 | 0.24 | 72 | 30 | 9 | 690 | 520 | 22 | 26 | 261 | 158 | 30 | 286 | 11 | 12 | 615 | 100 | 40 | 1 | 8 |
| 42 | 0.6 | 9.5 | 0.22 | 78 | 30 | 10 | 610 | 510 | 21 | 35 | 241 | 208 | 30 | 275 | 11 | 14 | 565 | 100 | 30 | 1 | 9 |
| 43 | 0.6 | 10.9 | 0.19 | 69 | 22 | 8 | 770 | 360 | 22 | 50 | 277 | 155 | 28 | 262 | 12 | 18 | 518 | 145 | 60 | 1 | 6 |
| 44 | 0.4 | 8 | 0.19 | 57 | 21 | 6 | 1200 | 520 | 20 | 17 | 256 | 185 | 24 | 236 | 8 | 20 | 515 | 200 | 80 | 1 | 8 |
| 45 | 0.6 | 8.2 | 0.18 | 87 | 31 | 10 | 2700 | 490 | 20 | 16 | 219 | 294 | 28 | 246 | 10 | 8 | 625 | 300 | 130 | 1 | 6 |
| 45#2 | 0.6 | 8.2 | 0.18 | 82 | 31 | 10 | 2600 | 490 | 20 | 16 | 218 | 293 | 27 | 247 | 9 | 7 | 613 | 300 | 130 | 1 | 6 |

Table E.7. XRF major element analysis for major lithologies found in the Hillsboro mining district. Samples are from quartz latite dikes, andesite, Copper Flat quartz monzonite, Fusselman dolomite, El Paso Group, alkalai basalt, and jasperoids respectivley.

| sample # | SiO2% | TiO2% | Al2O3% | Fe2O3T% | MnO% | MgO% | CaO% | Na2O% | K2O% | P2O5% | LOI | TOTAL |
|---|---|---|---|---|---|---|---|---|---|---|---|---|
| | | | | | | | | | | | | |
| Qtz. Lat. | | | | | | | | | | | | |
| Hill 1 | 69.21 | 0.25 | 17.22 | 1.46 | < 0.01 | 0.34 | 0.14 | 4.30 | 6.67 | 0.02 | 1.04 | 100.64 |
| Hill 21 | 61.56 | 0.44 | 16.87 | 3.70 | 0.11 | 2.55 | 1.10 | 3.23 | 6.99 | 0.18 | 3.61 | 100.34 |
| Hill 43 | 59.79 | 0.29 | 16.93 | 3.73 | 0.04 | 1.78 | 0.48 | 2.69 | 8.68 | 0.09 | 3.82 | 98.32 |
| Hill 13 | 60.87 | 0.36 | 17.45 | 2.55 | 0.17 | 3.30 | 0.57 | 3.23 | 6.30 | 0.10 | 4.55 | 99.44 |
| Hill 17 | 60.23 | 0.39 | 17.64 | 4.06 | 0.24 | 2.88 | 0.58 | 3.72 | 6.24 | 0.13 | 3.52 | 99.62 |
| | | | | | | | | | | | | |
| Andesite | | | | | | | | | | | | |
| Hill 5 | 50.28 | 1.16 | 16.50 | 12.32 | 0.21 | 7.87 | 4.42 | 3.20 | 2.52 | 0.59 | 1.77 | 100.84 |
| Hill 5A | 51.83 | 0.98 | 17.09 | 9.81 | 0.20 | 6.24 | 4.24 | 3.73 | 2.99 | 0.53 | 2.07 | 99.71 |
| Hill 6 | 51.02 | 1.03 | 19.29 | 9.86 | 0.21 | 7.54 | 3.31 | 3.08 | 2.04 | 0.61 | 1.80 | 99.79 |
| Hill 14 | 54.53 | 0.70 | 15.81 | 6.67 | 0.17 | 5.30 | 2.44 | 3.39 | 4.83 | 0.45 | 5.53 | 99.82 |
| Hill 60 | 62.79 | 0.62 | 14.38 | 8.09 | 0.14 | 0.89 | 1.00 | 0.26 | 3.65 | 0.27 | 6.66 | 98.75 |
| Hill 78 | 56.54 | 0.78 | 16.39 | 7.36 | 0.15 | 5.83 | 2.62 | 3.67 | 5.26 | 0.51 | ND | 99.11 |
| | | | | | | | | | | | | |
| Qtz. Mon. | | | | | | | | | | | | |
| Hill 11 | 67.93 | 0.45 | 14.74 | 3.76 | 0.07 | 2.35 | 1.01 | 3.78 | 4.29 | 0.16 | 1.04 | 99.58 |
| Hill 15 | 60.26 | 0.81 | 15.61 | 7.05 | 0.14 | 5.28 | 2.61 | 3.26 | 3.18 | 0.41 | 1.06 | 99.67 |
| Hill 39 | 60.57 | 0.50 | 16.90 | 5.63 | 0.05 | 2.40 | 1.02 | 3.76 | 5.32 | 0.21 | 1.81 | 98.17 |
| Hill 45 | 66.61 | 0.38 | 16.55 | 3.11 | < 0.01 | 0.73 | 0.41 | 3.68 | 5.28 | 0.08 | 2.94 | 99.77 |
| | | | | | | | | | | | | |
| Fuss. Dol. | | | | | | | | | | | | |
| Hill 20 | | 0.02 | | 0.16 | 0.04 | | | | | | | |
| | | | | | | | | | | | | |
| EP Group | | | | | | | | | | | | |
| Hill 22 | | 0.79 | | 4.91 | 0.04 | | | | | | | |
| | | | | | | | | | | | | |
| Al. Basalt | | | | | | | | | | | | |
| Hill 2 | 52.61 | 0.90 | 17.97 | 9.45 | 0.12 | 7.19 | 3.11 | 3.83 | 1.39 | 0.69 | 1.61 | 98.87 |
| | | | | | | | | | | | | |
| Jasperoid | | | | | | | | | | | | |
| Hill 77 | 88.45 | 0.01 | 0.20 | 0.50 | 0.12 | 5.62 | 0.28 | 0.02 | 0.03 | 0.01 | 4.23 | 99.77 |
| Hill 80 | 92.68 | 0.02 | 0.50 | 3.07 | 0.16 | 0.71 | 0.04 | 0.09 | 0.04 | 1.30 | ND | 98.96 |
| | | | | | | | | | | | | |
| | | | | | | | | | | | | |

Table E.8. XRF trace element analysis for major lithologies found in the Hillsboro mining district. Samples are from quartz latite dikes, andesite, Copper Flat quartz monzonite, Fusselman dolomite, El Paso Group, alkalai basalt, and jasperoids respectively.

| sample # | As | Ba | Cr | Cu | Ga | Mo | Nb | Ni | Pb | Rb | Sr | Th | U | V | Y | Zn | Zr |
|---|---|---|---|---|---|---|---|---|---|---|---|---|---|---|---|---|---|
| | | | | | | | | | | | | | | | | | |
| Lat. Dike | | | | | | | | | | | | | | | | | |
| Hill 1 | 1 | 361 | 8 | 13 | 23 | 4 | 14 | 3 | 16 | 248 | 208 | 20 | 4 | 10 | 24 | 17 | 400 |
| Hill 21 | 3 | 796 | < 2 | 38 | 18 | 1 | 8 | 6 | 9 | 264 | 364 | 16 | 5 | 55 | 27 | 48 | 298 |
| Hill 43 | 5 | 768 | 38 | 237 | 17 | 5 | 9 | 7 | 46 | 382 | 291 | 22 | 3 | 32 | 23 | 175 | 337 |
| | | | | | | | | | | | | | | | | | |
| Qtz. Lat. | | | | | | | | | | | | | | | | | |
| Hill 13 | 1 | 728 | 3 | 5 | 19 | 4 | 10 | 4 | 6 | 264 | 336 | 17 | 5 | 29 | 23 | 49 | 268 |
| Hill 17 | 1 | 873 | 3 | 5 | 19 | 2 | 7 | 4 | 17 | 245 | 421 | 19 | 8 | 37 | 31 | 69 | 267 |
| | | | | | | | | | | | | | | | | | |
| Andesite | | | | | | | | | | | | | | | | | |
| Hill 5 | 3 | 686 | 17 | 19 | 21 | 2 | < 2 | 16 | 11 | 161 | 897 | 11 | 3 | 294 | 28 | 96 | 110 |
| Hill 5A | 3 | 685 | 43 | 84 | 19 | < 2 | < 2 | 14 | 12 | 183 | 899 | 9 | 2 | 215 | 25 | 82 | 109 |
| Hill 6 | 1 | 466 | 18 | 70 | 24 | 1 | 3 | 9 | 14 | 132 | 642 | 9 | 2 | 210 | 34 | 117 | 155 |
| Hill 14 | 1 | 848 | 28 | 15 | 18 | 3 | 10 | 14 | 10 | 200 | 664 | 18 | 4 | 149 | 30 | 96 | 217 |
| Hill 60 | 15 | 381 | 34 | 350 | 19 | 1 | 5 | 8 | 79 | 222 | 64 | 11 | 4 | 135 | 33 | 2200 | 210 |
| Hill 78 | 4 | 1119 | 83 | 87 | 20 | < 2 | 2 | 16 | | 189 | 1020 | 18 | 3 | 153 | 31 | 78 | 219 |
| | | | | | | | | | | | | | | | | | |
| Qtz. Mon. | | | | | | | | | | | | | | | | | |
| Hill 11 | 1 | 1121 | 18 | 7 | 17 | 2 | 7 | 10 | 13 | 185 | 450 | 23 | 4 | 45 | 35 | 35 | 178 |
| Hill 15 | 1 | 1083 | 14 | 32 | 19 | 2 | 10 | 14 | 19 | 110 | 705 | 15 | 4 | 126 | 40 | 76 | 206 |
| Hill 39 | 2 | 776 | 64 | 499 | 20 | 3 | 7 | 7 | 16 | 293 | 751 | 21 | 5 | 63 | 30 | 41 | 237 |
| Hill 45 | < 2 | 817 | 89 | 69 | 20 | 4 | 10 | 6 | 13 | 251 | 527 | 27 | 9 | 33 | 21 | 16 | 244 |
| | | | | | | | | | | | | | | | | | |
| Fuss. Dol. | | | | | | | | | | | | | | | | | |
| Hill 20 | < 2 | 5 | 5 | < 2 | < 2 | < 2 | < 2 | 3 | 3 | ND | 37 | ND | 2 | 4 | 4 | 7 | ND |
| | | | | | | | | | | | | | | | | | |
| EP Group | | | | | | | | | | | | | | | | | |
| Hill 22 | 2 | 265 | 108 | 15 | 20 | 2 | 22 | 40 | 13 | 249 | 36 | 13 | 6 | 141 | 18 | 52 | 148 |
| | | | | | | | | | | | | | | | | | |
| Al. Basalt | | | | | | | | | | | | | | | | | |
| Hill 2 | 2 | 451 | 22 | 827 | 23 | 1 | < 2 | 10 | 5 | 120 | 776 | 5 | < 2 | 167 | 28 | 74 | 124 |
| | | | | | | | | | | | | | | | | | |
| Jasperoid | | | | | | | | | | | | | | | | | |
| Hill 77 | 10 | 305 | 218 | 11 | < 2 | 2 | < 2 | 10 | | < 2 | 39 | < 2 | 1 | 23 | 5 | 20 | 2 |
| Hill 80 | 2 | 250 | 253 | 49 | 3 | 2 | < 2 | 13 | | 6 | 10 | 7 | 3 | 131 | 30 | 268 | 12 |

Table E.9. pH, alkalinity, conductivity and temperature in degrees celcius of Hillsboro water samples. 5/198 = Copper Flat pit lake (May, 1998), 5/298 = Bonanza vein adit (May, 1998), 5/498 = Natural spring (May, 1998), 5/598 = Rattlesnake adit (May, 1998). 11/199 = Copper Flat pit lake (November, 1998), 11/299 = Bonanza vein adit (November, 1998), 11/499 = Natural spring (November, 1998), 11/599 = Rattlesnake adit (November, 1998).

| sample # | pH | alkalinity | cond. (ms) | temp. C |
|---|---|---|---|---|
| 5/198 | 8.22 | 159.3 | 4.83 | 26.6 |
| 5/298 | 7.2 | 218.4 | 1.59 | 18.5 |
| 5/498 | 8.1 | 359.5 | 0.99 | 24.7 |
| 5/598 | 7.04 | 382.2 | 1.29 | 24.3 |
| 11/199 | 8.1 | 195 | 4.63 | 18.9 |
| 11/299 | 7.7 | 195 | 1.44 | 19.5 |
| 11/499 | 7.97 | 315 | 0.79 | 16.7 |
| 11/599 | 7.01 | 375 | 1.21 | 23.8 |

Table E.10. Cu, Pb, Zn and As concentrations of water samples from Hillsboro district, determined by FAAS in ppm unless otherwise denoted. Samples with a "B" suffix are unfiltered and acidified, while samples with a "C" suffix are filtered and acidified.

| sample # | Cu | Zn | Pb | As ppb |
|---|---|---|---|---|
| 5/198B | 0.14 | 0.26 | 0.026 | 0 |
| 5/198C | 0.11 | 0.26 | 0.019 | 0.408 |
| 5/298B | 0.1 | 0.05 | 0.073 | 0 |
| 5/298C | 0.04 | 0.09 | 0.023 | 0 |
| 5/398B | 0.26 | 0.11 | 0.029 | 1.228 |
| 5/398C | 0.04 | 0.1 | 0.028 | 0.281 |
| 5/398C | 0.05 | 0.06 | 0.042 | 0.281 |
| 5/498B | 0.04 | < 0.01 | 0.025 | 1.407 |
| 5/498C | 0.05 | 0.04 | 0.023 | 2.913 |
| 5/598B | < 0.03 | 0.23 | 0.01 | 0 |
| 11/199B | 0.09 | 0.22 | 0.015 | 0.32 |
| 11/199C | 0.062 | 0.23 | 0.005 | 0.306 |
| 11/299B | 0.03 | 0.17 | 0.005 | 0.846 |
| 11/299C | 0.01 | < 0.03 | 0.005 | 0.053 |
| 11/399B | 0.011 | 0.06 | 0.005 | 0.286 |
| 11/399C | 0.011 | < 0.03 | 0.005 | 12.38 |
| 11/499B | < 0.005 | < 0.03 | 0.005 | 2.209 |
| 11/499C | 0.015 | < 0.03 | 0.005 | 2.783 |
| 11/599B | 0.053 | 0.04 | 0.005 | 0.393 |
| 11/599C | 0.04 | 0.07 | 0.005 | 0.211 |

Table E.11. Major element concentrations for water samples. TDS = total dissolved solids in the sample. Samples with an "A" suffix are filtered and unacidified while samples with a "D" suffix are unfiltered and unacidified.

| sample # | TDS | $CaCO_3$ | $HCO_3$ | Cl | $SO_4$ | $NO_3$ | F | Na | K | Mg | Ca |
|---|---|---|---|---|---|---|---|---|---|---|---|
| 5/198A | 4500 | 2527 | 208 | 232 | 2850 | 1 | 20 | 471 | 22 | 328 | 471 |
| 5/198D | 4890 | 2541 | 164 | 241 | 3200 | < 0.2 | 13 | 535 | 21 | 335 | 465 |
| 5/298A | 1320 | 803 | 104 | 14 | 900 | 2.1 | 0.39 | 64 | 2 | 55 | 231 |
| 5/298D | 1370 | 896 | 180 | 14 | 870 | < 0.2 | 0.73 | 70 | 1.9 | 60 | 260 |
| 5/498A | 200 | 47 | 104 | 10 | 46 | 0.6 | 13 | 57 | 2.4 | 1.7 | 16 |
| 5/498A | 730 | 342 | 104 | 21 | 455 | 3.1 | <0.2 | 91 | 3.3 | 51 | 53 |
| 5/498D | 760 | 115 | 461 | 32 | 185 | 0.76 | 9.8 | 245 | 11 | 6.2 | 36 |
| 5/598D | 810 | 436 | 230 | 21 | 433 | < 0.2 | 0.24 | 96 | 3.6 | 55 | 84 |
| 11/199A | 4690 | 2623 | 177 | 257 | 2968 | < 0.2 | 20 | 511 | 24 | 349 | 475 |
| 11/199D | 4960 | 2579 | 211 | 260 | 3200 | < 0.2 | 14 | 550 | 25 | 351 | 454 |
| 11/299A | 1380 | 871 | 192 | 14 | 891 | 2.7 | 0.89 | 64 | 1.8 | 55 | 258 |
| 11/299D | 1310 | 859 | 180 | 14 | 830 | 0.51 | 0.72 | 70 | 1.8 | 60 | 245 |
| 11/499A | 530 | 95 | 295 | 24 | 135 | 5.3 | 11 | 167 | 7.1 | 4.3 | 31 |
| 11/499D | 560 | 88 | 353 | 21 | 132 | 5.4 | 11 | 175 | 7 | 4.5 | 28 |
| 11/599A | 970 | 631 | 370 | 20 | 448 | 1.4 | 0.5 | 94 | 3.4 | 55 | 162 |
| 11/599D | 910 | 539 | 350 | 20 | 430 | 2.6 | 0.38 | 94 | 3.4 | 55 | 125 |

Table E.12. Results of unacidified and acidified agitation tests for water samples from four waste rock piles and a select down gradient stream sediment. Concentrations are in ppm. Analyses by FAAS.

| | Site A | Site B | Site C | Site D | EAM 1798 | EAM 198 | EAM 998 | EAM 1298 |
|---|---|---|---|---|---|---|---|---|
| Cu – unacid | 0.4 | 1.57 | 0.23 | 0.2 | 0.27 | 0.33 | 0.35 | 0.33 |
| Cu – acid | 0.43 | 1.73 | 0.53 | 0.5 | 0.4 | 0.4 | 0.48 | 0.57 |
| Pb – unacid | 0.02 | 0.03 | 0.03 | 0.03 | 0.01 | 0.005 | 0.01 | 0.02 |
| Pb – acid | 0.1 | 0.57 | 2.12 | 0.4 | 0.005 | 0.005 | 0.1 | 0.1 |
| Zn – unacid | 0.002 | 1.53 | 0.002 | 0.02 | 0.002 | 0.17 | 0.002 | 0.002 |
| Zn – acid | 0.002 | 1.55 | 0.98 | 0.12 | 0.002 | 0.05 | 0.05 | 0.03 |

Table E.13. pH measurements of stream sediments and the waste rock piles from where the stream sediments originated. Samples were 100, 400, and 800 ml. Measurements were taken at time zero, 30 seconds, 2 minutes, 10 minutes, and a final pH was read at 20 minutes.

| Sample | 100 ml | 400 ml | 800 ml | 100 ml | 400 ml | 800 ml |
|---|---|---|---|---|---|---|
| EAM 198 | | | | dump ph readings for respective sites | | |
| 0 | 5.47 | 5.51 | 5.21 | 5.65 | 5.79 | 5.61 |
| 0.5 | 6.67 | 5.85 | 5.5 | 4.36 | 4.39 | 4.79 |
| 2 | 6.85 | 5.97 | 5.99 | 4.31 | 4.37 | 4.39 |
| 10 | 6.93 | 6.69 | 6.51 | 4.68 | 4.69 | 4.68 |
| 20 | 7.06 | 7.01 | 6.86 | 4.69 | 4.7 | 4.74 |
| | | | | | | |
| EAM 1798 | | | | | | |
| 0 | 5.23 | 5.11 | 5.59 | 5.35 | 5.65 | 5.58 |
| 0.5 | 7.39 | 6.41 | 5.81 | 7.39 | 6.42 | 5.93 |
| 2 | 7.8 | 6.91 | 6.47 | 8.1 | 8.35 | 8.11 |
| 10 | 7.92 | 7.81 | 7.38 | 8.49 | 8.58 | 8.53 |
| 20 | 8.01 | 8.12 | 8.25 | 8.51 | 8.71 | 8.73 |
| EAM 998 | | | | | | |
| 0 | 5.41 | 5.11 | 5.53 | 5.68 | 5.76 | 5.02 |
| 0.5 | 6.6 | 6.49 | 6.91 | 6.41 | 6.45 | 5.77 |
| 2 | 7.9 | 7.67 | 8.22 | 7.41 | 7.62 | 7.32 |
| 10 | 8.26 | 8.13 | 8.55 | 8.02 | 8.37 | 8.34 |
| 20 | 8.53 | 9.19 | 9.09 | 8.46 | 8.69 | 8.75 |
| EAM 1298 | | | | | | |
| 0 | 5.67 | 5.86 | 5.57 | 5.41 | 5.42 | 5.67 |
| 0.5 | 6.48 | 6.46 | 6.16 | 6.54 | 5.98 | 6.16 |
| 2 | 7.31 | 7.27 | 6.94 | 6.95 | 6.68 | 6.61 |
| 10 | 7.95 | 7.87 | 7.47 | 7.95 | 7.66 | 7.66 |
| 20 | 8.33 | 8.41 | 8.51 | 7.99 | 8.3 | 8.52 |

Table E.14A. Electron Microprobe data for select quantitative points

| Site | point # | MoO3 | P2O5 | SiO2 | SO2 | TiO2 | Al2O3 | V2O3 | As2O3 | Ce2O3 | MgO | CaO | MnO | FeO | CuO | ZnO | PbO | Na2O | K2O | H2O | F | Cl | total |
|---|---|---|---|---|---|---|---|---|---|---|---|---|---|---|---|---|---|---|---|---|---|---|---|
| Site A | pic10-3a | 0 | 0.084 | 30.518 | 0.013 | 34.393 | 2.611 | 1.859 | 0.001 | 0.152 | 0.022 | 27.655 | 0.058 | 1.942 | 0 | 0.056 | 0.046 | 0.023 | 0.026 | 1.47 | 0.882 | 0.01 | 101.821 |
| | pic10-4a | 0 | 1.788 | 37.849 | 0.109 | 0.258 | 19.462 | 0.049 | 0 | 0 | 9.202 | 3.046 | 0.153 | 13.299 | 0.202 | 0.545 | 0 | 0.07 | 0.74 | 1.63 | 0.319 | 0.062 | 88.783 |
| Site B | pic21-4 | 0 | 0.324 | 11.993 | 0.647 | 0 | 1.803 | 0.003 | 0.05 | 0 | 0.105 | 1.309 | 0.079 | 64.28 | 4.468 | 0.295 | 0 | 0.246 | 0.13 | 1.06 | 0.021 | 0.137 | 86.95 |
| | pic23-3 | 0 | 0.049 | 3.711 | 3.689 | 1.975 | 2.309 | 0.111 | 0.152 | 0 | 0.193 | 1.874 | 0.044 | 68.715 | 1.237 | 0.053 | 0 | 0.011 | 0.595 | 0.975 | 0.118 | 0.018 | 85.829 |
| | pic23-5 | 0 | 0.097 | 2.474 | 2.548 | 0.047 | 0.94 | 0 | 0.391 | 0 | 0.015 | 0.253 | 0.045 | 76.426 | 0.243 | 0.121 | 0.042 | 0 | 0.025 | 0.888 | 0.137 | 0.014 | 84.706 |
| Site D | pic19-1 | 0 | 0.082 | 13.401 | 0.389 | 0.466 | 6.129 | 0.094 | 0 | 0.43 | 0.972 | 1.727 | 48.444 | 1.737 | 0.172 | 0.726 | 0.067 | 0.465 | 0.644 | 1.045 | 0 | 0.162 | 77.152 |
| | pic19-2 | 0 | 0.032 | 6.225 | 0.128 | 0.355 | 1.434 | 0.041 | 0 | 0.321 | 1.539 | 2.255 | 62.517 | 1.15 | 0.071 | 0.647 | 0.053 | 0.528 | 0.776 | 0.944 | 0 | 0.035 | 79.051 |
| | pic19-5 | 0.013 | 0.022 | 0.31 | 0 | 0.115 | 0.909 | 0.029 | 0 | 0.224 | 1.987 | 2.281 | 66.998 | 0.631 | 0.052 | 0.416 | 0.081 | 0.736 | 0.621 | 0.832 | 0 | 0.009 | 76.266 |
| Site E | pic24-3 | 0 | 0.192 | 0.641 | 6.178 | 0 | 0.103 | 0 | 0.285 | 0.047 | 0 | 0.789 | 0.012 | 71.401 | 0.006 | 0.067 | 0.059 | 0 | 0 | 0.929 | 0 | 0.002 | 80.711 |
| | pic26-5 | 0 | 0.062 | 3.867 | 1.591 | 0 | 0.582 | 0 | 0.035 | 0 | 0.022 | 0.542 | 0.045 | 76.868 | 0.071 | 0.03 | 0 | 0.263 | 0.034 | 0.954 | 0 | 0.043 | 85.009 |

| Site | point # | SO2 | TiO2 | Al2O3 | V2O3 | As2O3 | MnO | FeO | CoO | CuO | ZnO | PbO | total |
|---|---|---|---|---|---|---|---|---|---|---|---|---|---|
| Site A | pic10-1 | 0.021 | 0.427 | 0.211 | 0.182 | 0.021 | 0 | 98.305 | 0.019 | 0.023 | 0.002 | 0 | 99.211 |
| | pic10-2 | 0.018 | 0.372 | 0.112 | 0.186 | 0.044 | 0 | 99.834 | 0.03 | 0.026 | 0 | 0.004 | 100.626 |
| Site B | pic21-5 | 0.45 | 0.008 | 2.251 | 0.006 | 0.069 | 0.121 | 69.999 | 0.015 | 3.973 | 0.153 | 0.013 | 77.058 |
| | pic21-6 | 0.519 | 0.038 | 2.197 | 0 | 0.061 | .0.23 | 74.74 | 0.025 | 4.264 | 0.236 | 0 | 82.103 |
| | pic23-2 | 2.674 | 0.017 | 2.612 | 0.008 | 0.114 | 0 | 85.813 | 0.001 | 1.007 | 0.012 | 0.001 | 92.259 |
| | pic23-4 | 4.047 | 0 | 0.119 | 0 | 0.585 | 0 | 90.605 | 0.04 | 0.319 | 0.051 | 0.115 | 95.881 |
| Site D | pic19-3 | 0.143 | 0.408 | 1.5 | 0.065 | 0 | 64.734 | 1.338 | 0.016 | 0.044 | 0.619 | 0.014 | 68.881 |
| | pic19-4 | 0.011 | 0.225 | 1.053 | 0.057 | 0 | 68.33 | 0.923 | 0.032 | 0.115 | 0.481 | 0.038 | 71.265 |
| | pic19-7 | 0.039 | 0.24 | 2.173 | 0.047 | 0 | 63.918 | 1.739 | 0.034 | 0.046 | 0.729 | 0.02 | 68.985 |
| | pic19-8 | 0.013 | 0.23 | 2.52 | 0.024 | 0 | 64.085 | 1.823 | 0.016 | 0.061 | 0.972 | 0.028 | 69.772 |
| Site E | pic24-4 | 7.01 | 0.019 | 0.129 | 0.007 | 0.303 | 0 | 81.726 | 0 | 0 | 0.043 | 0.076 | 89.313 |
| | pic24-5 | 6.823 | 0.081 | 2.585 | 0.009 | 0.2 | 0 | 74.401 | 0 | 0.1 | 0.029 | 0.099 | 84.327 |
| | pic26-4 | 11.713 | 0.009 | 1.946 | 1.017 | 0.042 | 0 | 87.453 | 0.017 | 0.01 | 0.065 | 0 | 101.272 |

| Site | point # | V | Mo | As | Pb | Zn | Cu | Co | Fe | Ti | S | total |
|---|---|---|---|---|---|---|---|---|---|---|---|---|
| Site C | pic13-1 | | | 0.032 | 86.826 | 0.099 | | | | | 13.211 | 99.826 |
| Site B | pic21-1 | 0 | 0 | 0 | 0.03 | 0 | 33.181 | 0.038 | 30.072 | 0 | 32.87 | 96.191 |
| | pic21-2 | 0.006 | 0 | 0.054 | 0 | 0.017 | 33.14 | 0.01 | 29.609 | 0 | 33.696 | 96.532 |
| | pic22-2a | 0 | 0 | 0.09 | 0 | 13.735 | 26.276 | 0.021 | 22.591 | 0.005 | 34.121 | 96.839 |
| | pic23-1 | 0.013 | 0 | 0.061 | 0 | 0 | 0.005 | 0.002 | 46.41 | 0 | 53.64 | 100.131 |
| Site E | pic24-1 | 0.003 | 0 | 0.154 | 0 | 0.017 | 0.051 | 0 | 46.923 | 0.017 | 53.174 | 100.339 |
| | pic24-2 | 0 | 0 | 0.086 | 0.03 | 0.025 | 0.057 | 0 | 46.538 | 0.026 | 53.275 | 100.037 |
| | pic25-1 | 0.01 | 0 | 0.014 | 0 | 0 | 0.083 | 0.037 | 47.428 | 0.003 | 52.896 | 100.471 |
| | pic25-2 | 0 | 0 | 0 | 0 | 0.011 | 0.046 | 0.001 | 47.203 | 0 | 52.798 | 100.059 |
| | pic25-3 | 0 | 0 | 0.045 | 0.019 | 0.028 | 0.013 | 0.014 | 46.854 | 0 | 52.521 | 99.494 |
| | pic26-1 | 0.006 | 0 | 0.128 | 0.002 | 0.038 | 0.121 | 0.015 | 47.03 | 0 | 52.916 | 100.256 |
| | pic26-2 | 0.013 | 0 | 0 | 0.077 | 0.398 | 18.033 | 0.011 | 29.149 | 0 | 40.017 | 87.698 |
| | pic26-3 | 0.001 | 0 | 0 | 0.032 | 0.045 | 0.078 | 0 | 47.198 | 0.001 | 52.857 | 100.212 |

Table E.14B. Electron microprobe data for select quantitative points

| Site | point # | Si | P | S | Cl | Ca | Zn | As | Pb | Total |
|---|---|---|---|---|---|---|---|---|---|---|
| Site C | pic13-1 | 0.093 | 0 | 13.211 | 0 | 0.008 | 0.099 | 0.032 | 86.383 | 99.826 |
| | pic13-1 | 0.117 | 0.008 | 13.047 | 0 | 0.019 | 0.021 | 0 | 86.645 | 99.857 |
| | pic13-1 | 0.082 | 0.008 | 13.08 | 0 | 0 | 0.092 | 0.012 | 86.212 | 99.486 |
| | pic13-4 | 0.077 | 0.004 | 6.211 | 0 | 0 | 0 | 0.022 | 65.875 | 72.189 |
| | pic13-2 | 0.117 | 0.019 | 0 | 0.105 | 1.003 | 0.035 | 0.081 | 78.945 | 80.305 |
| | pic16-1 | 0.415 | 0.956 | 0 | 0.11 | 0.67 | 0.15 | 0.061 | 77.761 | 80.123 |

| Site | point # | Mg | Al | Si | P | Ca | Mn | Fe | Zn | As | Pb | Total |
|---|---|---|---|---|---|---|---|---|---|---|---|---|
| Site C | pic16-2 | 0.002 | 0 | 0.159 | 0 | 0 | 0 | 0 | 0 | 0.05 | 79.637 | 79.848 |
| | pic16-3 | 0.003 | 0 | 0.138 | 0 | 0.009 | 0 | 0.021 | 0 | 0.004 | 71.581 | 71.756 |
| Site D | pic19-1 | 0.668 | 0.651 | 3.663 | 0.015 | 1.213 | 34.832 | 1.259 | 0.416 | 0 | 0.905 | 43.622 |
| | pic19-2 | 0.973 | 0.61 | 2.427 | 0.02 | 1.54 | 45.386 | 0.677 | 0.391 | 0 | 0.695 | 52.719 |
| | pic19-3 | 1.17 | 0.512 | 0.274 | 0.019 | 1.617 | 49.038 | 0.543 | 0.327 | 0 | 0.48 | 53.98 |
| | pic19-4 | 1.095 | 1.416 | 0.203 | 0.021 | 1.729 | 45.363 | 1.099 | 0.593 | 0 | 0.63 | 52.149 |

## 13.6 APPENDIX F – Detection Limits

### FAAS Analyses
(Ebdon, 1982)

| Element | Detection Limit | |
|---|---|---|
| | ppm | |
| Cu | 0.04 | |
| Pb | 0.015 | |
| Zn | 0.009 | |
| | | |
| Element | GFAA | |
| | Detection limit | |
| As | 2 ppb | |

### XRF Analyses

Chris McKee, personal communication, (1998)
(ppm except where noted otherwise)

| element | LLD (ppm) |
|---|---|
| | |
| As | 1 |
| Ba | 4 |
| Bi | 10 |
| Cr | 4 |
| Cu | 4 |
| Fe | 0.02% |
| Ga | 3 |
| Mn | 0.01% |
| Mo | 1 |
| Nb | 2 |
| Ni | 2 |
| Pb | 1 |
| Rb | 2 |
| Se | 10 |
| Sr | 1 |
| Th | 2 |
| Ti | 0.01% |
| U | 1 |
| V | 3 |
| Y | 2 |
| Zn | 3 |
| Zr | 4 |

## Electron Microprobe Analyses

Nelia Dunbar, personal communication, (1999)

| Element | Lower Level of Detection (%) |
|---|---|
| | |
| Al | 0.052 |
| As | 0.163 |
| Ca | 0.085 |
| Ce | 0.405 |
| Cl | 0.094 |
| Co | 0.072 |
| Cu | 0.304 |
| F | 0.836 |
| Fe | 0.162 |
| K | 0.075 |
| Mg | 0.163 |
| Mo | 0.318 |
| Mn | 0.164 |
| Na | 0.176 |
| P | 0.141 |
| Pb | 0.444 |
| S | 0.138 |
| Si | 0.069 |
| Ti | 0.121 |
| V | 0.139 |
| Zn | 0.335 |

This thesis is accepted on behalf of the faculty

of the institute by the following committee:

Advisor

August 23, 1999

Date